Mechanical Properties of F-actin Network

by

Hyungsuk Lee

Submitted to the Department of Mechanical Engineering
in partial fulfillment of the requirements for the degree of

Doctor of Philosophy in Mechanical Engineering

at the

MASSACHUSETTS INSTITUTE OF TECHNOLOGY

May 2009

Author .....
Department of Mechanical Engineering
May 31, 2009

Certified by.....
Roger D. Kamm
Professor of Mechanical and Biological Engineering
Thesis Supervisor

Accepted by .....
David E. Hardt
Chairman, Department Committee on Graduate Students

Mechanical Properties of F-actin Network
by

Hyungsuk Lee

Submitted to the Department of Mechanical Engineering
on May 31, 2009, in partial fulfillment of the requirements for the degree of

Doctor of Philosophy in Mechanical Engineering

Abstract

Cells sense, generate and respond to forces in their surroundings through cytoskeletal dynamics. Actin, the most abundant protein found in eukaryotic cells, is organized into various cytoskeletal structures that provide physical support for the cell and play important roles in numerous cellular processes. Assembly of F-actin into higher-order structures is regulated by over 100 actin binding proteins (ABPs). Although extensive measurements to estimate the mechanical properties of ABP/F-actin networks showed that they are nonlinear and viscoelastic, a full understanding of the origin of such fascinating behaviors is lacking. This thesis presents a multi-scale approach to identify the factors that determine the mechanical properties of F-actin networks from the macroscopic level to the single-molecule level.

The mechanical properties of F-actin networks were probed by *passive* and *active* methods using optical tweezers. For the *passive* approach the thermal fluctuations of colloidal spheres are monitored to estimate the frequency-dependent complex shear modulus of an F-actin network. In the *active* approach, the response of an embedded microsphere to a driving force is tracked to obtain the strain-dependent viscoelasticity. The developed methods were applied to F-actin networks cross-linked with various ABPs such as filamin and α-actinin, with and without gelsolin to control filament length. Microstructures of those networks were also characterized in terms of filament length, mesh size, and degree of bundling. Comparison between cross-linked F-actin with two different length scales of actin filament suggested that network connectivity is another critical parameter in determining mechanical properties.

To better understand how the cross-linking protein responds to an external force, a single molecule assay was used to measure the rupture force of a complex formed by an ABP filamin linking two actin filaments. Both force-induced unbinding and unfolding of filamin were observed at the critical force of 70 ± 23pN and 57 ± 19pN, respectively, although unbinding occurred more frequently. Similar pulling experiments were also performed on cross-linked F-actin networks and an abrupt transition was observed in the force trace indicating network rupture. The critical forces at transitions exhibited a similar loading-rate dependence to that observed for rupture forces in the single molecule measurements. Nonlinear behavior observed in strain-dependent microrheology was found to be irreversible. Combined results of molecular

unbinding, network rupture, and irreversible network properties suggest that unbinding rather than unfolding is a dominant mechanism governing the mechanical properties of cross-linked F-actin networks.

In addition, the mechanical behavior of F-actin networks subjected to an external prestress was investigated using a shear device. Visualization of sheared F-actin networks showed the structural evolution including mesh deformation, filament alignment, and network rupture. Measurement of mechanical properties as a function of external strain demonstrated that some regions exhibited strain-hardening while the others showed strain-softening. Aligned stretching of actin filaments observed at high strain seemed to play a role in strain-stiffening. By comparing the behaviors of an F-actin network cross-linked with wildtype and mutant FLNa, it was demonstrated how molecular structure of the ABP alters the mechanical behavior of F-actin network.

Thesis Supervisor: Roger D. Kamm
Title: Professor of Mechanical and Biological Engineering

Acknowledgments

This work would not have been possible without the contributions of many people. First of foremost, I would like to thank my advisor, Prof. Roger Kamm who has been a great mentor. His enthusiasm and intuition have always inspired me. I appreciate the patience and respect he has shown me even during tough times. I would like to thank Prof. Matthew Lang for his guidance and advice for my research. He introduced me to the field of single molecule mechanics using optical tweezers and he has inspired me to look at my projects from different aspects. I would like to thank Prof. Peter So who has provided me with regular inputs on this thesis work and has been encouraging. I would like to thank Prof. Thomas Stossel for his biological inputs on my research and his advice for my future career. I would also like to thank Prof. Richard Lee for his advice and help for my research.

I thank Jorge Ferrer for all the time he spent in the lab with me. He never hesitated to help me whenever I was faced with challenges in using optical tweezers. Fumihiko Nakamura has provided all the samples and his biological advice has provoked me to try new and creative projects. Benjamin Pelz helped me running the single molecule experiments and developing the assays.

I would like to thank Jan Lammerding who has shown interest in my research and has always been helpful with his expertise. I would like to thank Wonmuk Hwang and Mohammad Mofrad who have shown me a support and guidance since my first year in the Kamm Lab.

I would like to thank all the past and current Lab members for all their supports through years of long days and nights. They made my day-to-day life at MIT very enjoyable. Thanks to Peter Mack, Seung Lee, Belinda Yap, Helene Karcher, Aida Rahim, Taeyoon Kim, Cherry Wan, Jessie Jeon, Ted Feldman, and all of the Kamm Lab member, Ricardo Brau, David Appleyard, Carlos Castro, Mo Khalil, Yongdae Shin, Ricardo Gonzalez, and all of the Lang Lab, and James Evans, Alec Robertson, Michael Murrell, and Muhammad Zaman in the Matsudaira Lab.

Last but not least, I would never have been able to complete this PhD without constant love and support of my family. They have been a constant source of joy and happiness in my life. I would like to express my deepest thanks to my wife Sungmin for always being supportive and encouraging. I was able to complete this thesis because of her unconditional love.

Contents

List of Figures

List of Tables

1 Introduction

1.1 Actin Filament

The cytoskeleton of most eukaryotic cells is composed of three types of filaments: microfilaments, microtubules, and intermediate filaments. They are distinguished by their size and type of subunit. Microtubules are hollow polymers of α- and β-tubulin with a diameter of 25nm. Intermediate filaments have the structure of a 10nm diameter rope, consisting of a diverse family of proteins such as lamin, desmin, keratin and so on. Microfilaments are helical filamentous polymers of actin.

Actin is the most abundant and conserved protein found in eukaryotic cells. It comprises 10% by weight of total protein in muscle cells and 5% in non-muscle cells (1). Humans have six different actin genes encoding isoforms. α-actin isoforms predominate in various muscle cells while β- and γ-actin isoforms are present in non-muscle cells. Actin exists in two forms in a cell, globular monomer called G-actin and filamentous polymer called F-actin. G-actin is a 42kDa protein consisting of 375 amino acids. Promoted by local high concentrations of K^+ or Mg^{2+} cations, G-actin with bound ATP can polymerize into an F-actin through three phases: nucleation (lag phase), elongation (growth phase), and quiescence (equilibrium phase). Actin filaments exhibit a double helical structure with a diameter of 5nm and contour length up to 20μm. A filament's persistence length (ℓ_p) is the length over which tangent vectors to the filament contour are uncorrelated by the balance between thermal energy (k_BT) and bending rigidity (κ_0), and is defined as $l_p = \frac{\kappa_0}{k_BT}$. For F-actin, ℓ_p is 17μm, which is intermediate compared to that of DNA, ℓ_p ≈ 0.05μm, and microtubules, ℓ_p ≈ 1000μm. The extensional modulus (Young's modulus) and bending rigidity of F-actin is in the order of 1GPa and $10^{-26}Nm^2$, respectively (2, 3).

Actin filaments provide structural stability for the cell. The highest concentrations of F-actin are found in the cortex which is just beneath the plasma membrane. Network structures arranged by actin filaments determine cell shape and protect organelles from the cortical cytoplasm. Membrane-tethered actin bundles sometimes form fingerlike projections or microvilli. Connections between membrane and actin filaments in cytoskeleton are achieved directly through integral membrane proteins or peripheral membrane proteins that function as adapter proteins. Also certain structures of actin formed during cell migration allow a directed movement of the cell. During migration, actin filaments at the leading edge of the cell are rapidly cross-linked into either sheet-like protrusions, called lamellipodia, or fingerlike membrane projections, called filopodia. These structures are extended and then form stable contacts with the underlying structure facilitating cell locomotion. Additionally, actin and Myosin II are assembled into a contractile ring during cytokinesis. Actin filaments are accumulated at the cell cortex and contraction forces generated by myosin separate daughter cells to complete the cell division (4). According to these functional demands, actin filaments are organized into various structures in concert with a variety of actin binding proteins.

1.2 Actin Binding Proteins

Actin binds to more than 100 distinct proteins excluding their many synonyms or isoforms. Many of the identified actin binding proteins (ABPs) bind to the same loci on the surface of actin and therefore are expected to compete. The complex and dynamic properties of the actin cytoskeleton are regulated at multiple levels by a variety of ABPs. Some ABPs are membrane-associated proteins and others are membrane receptors or ion transporters. ABPs cross-link actin filaments or enable filaments to interact with other elements of the cytoskeleton. Also, a variety of lengths and spatial conformations of actin filaments are conferred by ABPs. Therefore, ABPs are essential for proper function of actin cytoskeleton. For example, cells can migrate at the speed of ~2μm/s. However, treadmilling of actin filaments has been observed to occur *in vitro* at a rate of ~2μm/h which is much slower than observed *in vivo* due to the slow exchange of ATP for ADP and dissociation of P_i from actin monomers in the filament (5). The rapid assembly of actin filaments during cell locomotion is achieved with the help of ABPs.

ABPs can be classified into several groups based on their function (Table 1.1): 1) Monomer-binding proteins sequestering G-actin and preventing its polymerization, 2) Filament-depolymerizing proteins, 3) Filament end-binding proteins capping the ends of the actin filament, 4) Filament severing proteins, 5) Cross-linking proteins forming a network or bundles structure, 6) Stabilizing proteins preventing depolymerization, and 7) Motor proteins moving along an actin filament.

However, some ABPs are not limited to one group. For example, gelsolin can interact with either G- and F-actin. Interaction of gelsolin with G-actin forms a tight complex with two actin monomers, and the complex acts as a nucleus of polymerization. Gelsolin also binds to and severs a filamentous actin. The Arp2/3 complex nucleates new actin filaments, elongates existing

filaments, and facilitates the formation of a branching site. The distinction between bundling and cross-linking is sometimes ambiguous. At low concentrations α-actinin links actin filaments to form an isotropic gel. However, at high concentrations, α-actinin assembles actin filaments into parallel or anti-parallel bundles.

Group	Function	Actin binding protein
ADF/Cofilin family	- induce the conversion of F- to G-actin - rapidly recycle actin monomers associated with membrane ruffling and with cytokinesis	porcine ADF, destrin, cofilin, acanthamoeba actophorin, twinfilin
Monomer sequestering proteins	- regulate spatial and temporal growth of actin filaments - bind to monomeric actin to inhibit polymerization - catalyze the exchange of actin-bound ADP to ATP - transmit signals between the cell membrane and the actin cytoskeleton	profilin (19kDa), thymosin (5kDa)
Gelsolin superfamily	- bind to monomeric actin to sequester - cap the barbed end of the actin filament - severing an actin filament	Gelsolin (80kDa), villin (92.5kDa), adseverin, CapG, severin, Flil
Stabilizing proteins	- bind to F-actin and stabilize it against depolymerization	Tropomyosin, nebulin (600-900kDa)
Bundling proteins	- bind to the sides of actin filaments and assemble loose or tight bundles - form the cores in microvilli and filopodia	Fascin (58kDa), fimbrin (67kDa), villin, α-actinin, 30-kd, Band 4.9
Cross-linking proteins	- cross-link actin filaments into an orthogonal network	Filamin (280kDa), 240-kd, α-actinin(100kDa), spectrin (220kDa), 120-kd
Motor proteins	- produce movement (and force) through the hydrolysis of ATP - move cargo along an actin filament	myosin
Cytoskeletal linkers & Membrane anchors	- connect actin filament to membrane or membrane proteins - connect actin filament to different cytoskeletal elements such as microtubule and intermediate filament	dystrophin(410kDa), utrophin, talin (270kDa), vinculin, annexin, plectin

Table 1.1 Actin binding proteins.

ABPs that cross-link F-actin are important for the maintenance of viscoelastic properties of the cytoplasm and for maintaining the integrity of cellular structures. In this thesis, we consider only two cross-linking ABPs: α-actinin and FLNa.

α-actinin is a dimer formed from two anti-parallel peptides, each having four spectrin-like α-helix repeats. An actin binding domain is located close to the N terminus while EF-hand (calcium binding motif) is located near the other end. α-actinin binds to the sides of actin filaments and lies between them in bundles. Due to the relatively small molecular weight of α-actinin, the separation between filaments are close < 30nm. The polarity of actin filaments bundled by α-actinin depends on the particular isoform. For example, chicken gizzard and *Dictyostelium* α-actinin tend to bundle in an anti-parallel manner while Acanthamoeba α-actinin promotes parallel bundling (6)

Filamin A (FLNa) is the most widely expressed family member of ABPs. Each subunit is ~280kDa and consists of an actin binding domain and 24 β-sheet repeats interrupted by two hinge regions. Dimerization occurs through the 24 repeat at the C terminus. Filamin assembles actin filament into a three-dimensional web-like network. By cross-linking actin filaments, filamin is essential for cellular structures, cell locomotion, fetal development, and cell signaling. The detailed structure and function of FLNa are described in Ch. 5.

1.3 Optical Trapping

Optical tweezers, also known as an optical trap, are one of the most versatile tools to investigate the forces and motions associated with biological samples. Arthur Ashkin and others demonstrated that micro-size particles could be trapped using the force of radiation pressure from visible laser light (7, 8). They showed that optical tweezers could manipulate single cells, viruses, and bacteria by choosing a proper wavelength and power of the trapping laser to minimize an optical damage to biological specimens (9-11).

An optical trap is formed by tightly focusing a laser beam with an objective lens with high numerical aperture (NA). A dielectric particle in the vicinity of the focal point experiences a force due to the radiation pressure. The resulting optical force has two components: the scattering force and the gradient force. Light impinges on the particle from one direction and is scattered in a variety of directions while some of the light may be absorbed. For isotropic scattering, the net momentum from the incident photons cancel in all but the forward direction. As a result, the scattering force is in the direction of light propagation. The gradient force arises from fluctuating electric dipoles that are induced when light passes through an object. The steep gradient of the optical field near the focus results in a force directed along the direction of the spatial light gradient. The gradient force is proportional to both the polarizability of the dielectric and the optical intensity gradient at the focus. To form a stable trap with optical tweezers, the gradient force along the optical axis must overcome the scattering force, which necessitates the very steep gradient achieved by a high NA objective. The balance between the gradient force and the scattering force locates the equilibrium position of a trapped particle at a point slightly beyond the focal point. For small displacements from the equilibrium position the force varies linearly with the displacement, and the trap can be represented as a Hookean spring (12).

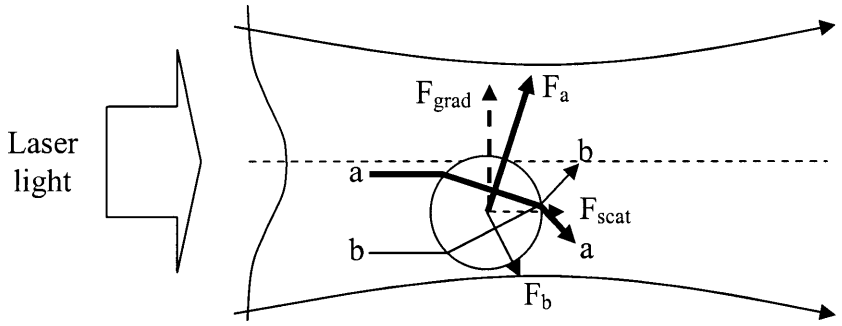

Figure 1.1 Scattering and gradient forces in optical trapping of high index sphere. Neglecting relatively minor surface reflections, most of the rays refract through the sphere. The change in the direction of the photons results in a change of their momentum giving rise to a force acting on the sphere. Since the intensity of the light close to the center of the beam (a) is higher than that of the light at the edge (b), the force F_a is greater than F_b. Taking into account all of the light striking the sphere, the net force can be resolved into two components, the scattering (F_{scat}) and gradient (F_{grad}) forces. The scattering force points in the direction of the incident light and the gradient force points transversely toward the center of the light.

Optical tweezers can exert forces in excess of 100pN (13, 14) on objects ranging in size from nanometer to micrometer objects (13-15) with sub-nanometer spatial and sub-millisecond temporal resolutions. Compared to the other force spectroscopy such as magnetic tweezers and atomic force microscopy, optical tweezers provide a non-invasive and non-contact tool.

Optical traps apply forces that are in an ideal range for exerting forces on biological systems and for detecting their responses. Therefore, optical tweezers have found a wide range of applications. They have been used to characterize the mechanical properties of cell membrane (16), colloid systems (17-19), polymers and biopolymers (20-24). Also the assays developed using optical tweezers were used to probe the binding interactions in kinesin-microtubules (25-27), dynein-microtubules (28), virus-erythrocytes (29), fibrinogen-integrin (14), actin-myosin (30, 31) systems. Recent development of the combined optical trapping and single molecule fluorescence demonstrated the simultaneous observations of force and fluorescence at the force-induced unzipping of double-stranded DNA (32).

The experiments presented in this thesis were performed using a custom-built instrument described previously (33). Briefly, a high numerical aperture objective (100X, 1.40 NA, oil IR;

Nikon, Tokyo, Japan) tightly focuses a 1064-nm laser (Coherent, Santa Clara, CA) at the specimen plane for optical trapping. The trap location is computer-controlled with a pair of orthogonally oriented acousto-optic deflectors (AODs) (Intra-Action, Bellwood, IL) and sample positioning is controlled using a piezo-stage (Polytech PI, Auburn, MA) with sub-nanometer resolution. The combination of a 975 nm laser (Corning, Corning, NY) and a position sensitive device (PSD) (Pacific Silicon, West Lake Village, CA) is employed for back-focal plane position detection (34). The 975-nm laser is operated at ~ 0.1 mW such that it forms a negligible trap with respect to the 1064-nm laser operated between 5-100 mW. The detection zone consists of a circular area with radius of ~250 nm for 0.5 μm radius beads and ~500 nm for 1.0 μm beads. A second PSD is also employed to track the position of the trapping laser if necessary. The output voltages from both PSDs are collected by an A/D board (National Instruments, Austin, TX) and a custom program coded in LabView software (National Instruments, Texas, NI) is used to control experimental runs and data acquisition. Data analysis is performed using software written in MATLAB (Mathworks, Natick, MA).

1.4 One- and Two-Particle Microrheology

The linear viscoelastic properties of a complex material can be estimated by monitoring the thermally-driven random motion of an embedded probe particle. The principle is that the thermal motion of the particle in a homogeneous material depends on the mechanical properties of the local microenvironment. A generalized Langevin equation is used to describe the force on a thermally-fluctuation particle of mass m and velocity $v(t)$ in a complex material

$$m\dot{v}(t) = f_R(t) - \int_0^t \zeta(t-\tau)v(\tau)d\tau \tag{1.1}$$

where f_R(t) represents all the force acting on the particle, and ζ(t) is a casual memory function which describes the local viscoelastic response of the isotropic and incompressible complex fluid. The force consists of both the contribution of the surrounding fluid and the interactions with any other particles in the fluid. The force is assumed to be random with a Gaussian distribution and is entirely decoupled from the past distribution of velocities. Therefore,

$$< v(0) f_R(t) > = 0\,, \tag{1.2}$$

where the angle bracket denotes an ensemble average. By taking the unilateral Laplace transform of Eq. (1.1) and using the equipartition theorem of $m<$v(0) v(0)$> = m<$v(0) v(0)$> = k_BT$,

$$\varsigma(s) = \frac{k_BT}{< v(0)v(0) >} - ms \tag{1.3}$$

The inertial term is negligible except at very high frequencies and the velocity autocorrelation is written in terms of the Laplace transform of the mean squared displacement (MSD) which is defined as

$$< \Delta\tilde{r}^2(\tau) > = < \left|\tilde{r}(t+\tau) - \tilde{r}(t)\right|^2 > \tag{1.4}$$

where r is the particle position, τ is the lag time.

The expression of the memory function in Eq. 1.3 becomes

$$\varsigma(s) = \frac{6k_B T}{s^2 < \Delta\tilde{r}^2(s) >} \tag{1.5}$$

To relate the linear viscoelasticity of the complex fluid to the memory function, the Stokes law can be used with the assumption that the complex fluid is a continuum around the particle. The frequency dependent complex viscosity is determined by (35)

$$\tilde{G}(s) = \frac{s\tilde{\varsigma}(s)}{6\pi a}. \tag{1.6}$$

By combining Eq. (1.5) and Eq. (1.6), we obtain the direct relationship between the mean-squared displacement of the particle and the shear modulus of the complex fluid.

$$\tilde{G}(s) \approx \frac{k_B T}{\pi a s < \Delta\tilde{r}^2(s) >} \tag{1.7}$$

This equation is a generalized, frequency-dependent form of the Stokes-Einstein equation for a complex fluid. If $<\Delta r^2(t)>$ is known and its Laplace transform can be evaluated, then the storage and shear modulus can be estimated from the real and imaginary parts of Eq. (1.7).

In practice, $<\Delta r^2(t)>$ is measured at discrete times over a limited duration in experiments, so computation of the transform in the frequency domain may incur errors. We use the transforms algebraically by expanding $<\Delta r^2(t)>$ around the frequency s using a power law and retaining the leading term (36), obtain

$$< \Delta r^2(\mathrm{t}) > \approx < \Delta r^2(1/s) > (st)^{\alpha(s)}, \tag{1.8}$$

where $<\Delta r^2(1/s)>$ is the magnitude of $<\Delta r^2(t)>$ and α is the power law exponent describing the logarithmic slope of $<\Delta r^2(t)>$ at $t = 1/s$.

$$\alpha(s) \equiv \left.\frac{\mathrm{d}\ln < \Delta r^2(t) >}{\mathrm{d}\ln t}\right|_{t=1/s} \tag{1.9}$$

For thermally-driven spheres, the slope is zero when the medium is purely elastic and unity when the medium is purely viscous. The Laplace transform of Eq. (1.6) leads to $s\langle\Delta r^2(s)\rangle \approx \langle\Delta r^2(1/s)\rangle\Gamma[1+\alpha(s)]$, where Γ is the gamma function.

By substituting into Eq. (1.7),

$$\tilde{G}(s) \approx \left.\frac{k_B T}{\pi a < \Delta r^2(t) > \Gamma[1 + (\mathrm{d} \ln < \Delta r^2(t) > / \mathrm{d} \ln t)]}\right|_{t=1/s} \tag{1.10}$$

where the gamma function is represented by $\Gamma[1+\alpha] \approx 0.457(1+\alpha)2\text{-}1.36\ (1+\alpha)+1.90$. While this equation is convenient to use, it fails to give an accurate estimate for the moduli when the slope of the MSD varies rapidly. Dasgupta et al. (37) have empirically modified Eq. (1.10) to account for the curvature and give a better estimate of the moduli in such curved regions of the data.

Microrheology using a single probe particle is sensitive to the local environment. If the sample is heterogeneous, one-particle microrheology probes mechanical properties of local environment rather than bulk properties. Also, an inadequate coupling between the particle and the sample can interfere a precise estimation of the mechanical properties (38). Two-particle microrheology overcomes these limitations by measuring the cross-correlated motion of pairs of particles instead of monitoring a single particle's motion (39). The correlated motion of the particles is independent of the size, shape, and even the coupling between the particle and the sample. Moreover, the length scale of measurement is the distance between the particles, which is typically 10-100μm, rather than the size of the particle itself.

In two-particle microrheology, a distinct mean squared displacement, $\langle\Delta r^2(\tau)\rangle_D$, is defined from the ensemble averaged tensor product of the trace displacements. The vector displacement of the trace bead α is defined as $\Delta r_\alpha(t,\tau) = r_\alpha(t + \tau) - r_\alpha(t)$ where t is the absolute

time and τ is the lag time. The ensemble averaged tensor product of the tracer displacements is calculated from

$$D_{\alpha\beta}(r,\tau) = \left\langle \Delta r^{i}{}_{\alpha}(t,\tau)\Delta r^{j}{}_{\beta}(t,\tau)\delta[r - R^{ij}(t)] \right\rangle_{i\neq j,t}, \tag{1.11}$$

where i and j label different particles, α and β label different coordinates, and R^{ij} is the distance between particles i and j. The average is taken over only the "distinct" terms ($i \neq j$); the "self" terms yield the one-particle mean squared displacement, $<\Delta r^2(\tau)>$. In the limit where the particle separation (r) is much greater than the particle radius (a), the two-particle correlation for particles in an incompressible continuum is computed by multiplying the one-particle mean squared displacement predicted by the generalized Stokes-Einstein relation in Eq. (1.7) by a/r and the result is

$$\tilde{D}_{rr}(r,s) = \frac{k_B T}{2\pi r s \tilde{G}(s)}, \quad D_{\theta\theta} = D_{\phi\phi} = \frac{1}{2} D_{rr}, \tag{1.12}$$

where $\tilde{D}_{rr}(r,s)$ is the Laplace transform of $D_{rr}(r,t)$ and the off-diagonal terms vanish. As shown in Eq. (1.12), $D_{\alpha\beta}(r,\tau)$ is independent of the size and shape of the probe particle. We have obtained the result for an incompressible medium. However, Eq. (1.12) can be generalized to compressible media by using a modified Stokes-Einstein relation and different strain field (40).

Comparing the longitudinal two-point correlation to the generalized Stokes-Einstein equation defines a distinct mean squared displacement $<\Delta r^2(\tau)>_D$.

$$< \Delta r^2(\mathrm{t}) >_D = \frac{2r}{a} D_{rr}(r,\tau) \tag{1.13}$$

In a homogeneous solution where the generalized Stokes-Einstein equation is valid, the distinct mean squared displacement is equal to the one-particle MSD. However, in inhomogeneous

solutions, $<\Delta r^2(\tau)>_D$ can be different from $<\Delta r^2(\tau)>$ because $<\Delta r^2(\tau)>$ is a superposition of a long wavelength motion described by $<\Delta r^2(\tau)>_D$ plus a local motion in a cavity.

In experiments, the average value of rD_{rr} is used to calculate $<\Delta r^2(\tau)>_D$ from Eq. (1.13). The shear modulus of the sample is obtained from the generalized Stokes-Einstein equation in place of $<\Delta r^2(\tau)>$. Two-particle microrheology is advantageous in probing an inhomogeneous medium and in tracking the particles with irregular size and shape. Also the measurement length scale is larger compared to the one-particle microrheology providing results more similar to those obtained from bulk rheology.

For measurements of both one- and two-particle microrheology, the complex fluid must be sufficiently soft in order for the thermal fluctuation of embedded particles to be detectable. The resolution of detecting particles depends on the detection scheme and typically ranges from 1Å to 10nm. The upper limit of elastic modulus we are able to probe is determined by the size of the particle and detection resolution of the particle's fluctuation. If a micro-sized particle is used, a sample with an elastic modulus ranging up to about 10 to 500 Pa can be measured. As no external stress is associated in these methods, the experimental results are within the linear viscoelastic regime.

In this thesis, we develop the active and passive microrheology techniques using optical tweezers and measure mechanical properties of F-actin networks cross-linked with various actin binding proteins. In the passive measurement, one- and two-particle microrheology methods are employed to estimate the shear moduli. In the active measurement, we calculate the shear moduli by obtaining the mechanical responses of F-actin networks to an external force.

1.5 References

1. Lodish, H., Berk, A., Matsudaira, P., Kaiser, C. A., Krieger, M., Scott, M. P., Zipursky, S. L. & Darnell, J. (1999) Molecular Cell Biology, W.H. Freeman and Company.
2. Kojima, H., Ishijima, A. & Yanagida, T. (1994) Direct measurement of stiffness of single actin filaments with an without tropomyosin by in vitro nanomanipulation *PNAS* 91, 12962-12966.
3. Oosawa, F. (2001) in *Molecular Interactions of Actin*, eds. dos Remedios, C. G. & Thomas, D. D. (Springer, Berlin), Vol. 32, pp. 9-21.
4. Schroeder, T. E. (1973) Actin in dividing cells: contractile ring filaments bind heavy meromyosin *Proc Natl Acad Sci U S A* 70, 1688-92.
5. Selve, N. & Wegner, A. (1986) Rate of treadmilling of actin filaments in vitro *J Mol Biol* 187, 627-31.
6. Meyer, R. K. & Aebi, U. (1990) Bundling of actin filaments by alpha-actinin depends on its molecular length *J Cell Biol* 110, 2013-2024.
7. Ashkin, A. (1970) Acceleration and trapping of particles by radiation pressure *Phys Rev Letter* 24, 154-159.
8. Ashkin, A. (1971) Optical levitation by radiation pressure *Appl Phys Lett* 19, 283-285.
9. Ashkin, A. & Dziedzic, J. M. (1989) Optical Trapping and Manipulation of Single Living Cells Using Infrared-Laser Beams *Berichte Der Bunsen-Gesellschaft-Physical Chemistry Chemical Physics* 93, 254-260.
10. Ashkin, A. & Dziedzic, J. M. (1987) Optical Trapping and Manipulation of Viruses and Bacteria *Science* 235, 1517-1520.
11. Ashkin, A., Dziedzic, J. M. & Yamane, T. (1987) Optical Trapping and Manipulation of Single Cells Using Infrared-Laser Beams *Nature* 330, 769-771.
12. Neuman, K. C. & Block, S. M. (2004) Optical trapping *Review of Scientific Instruments* 75, 2787-2809.
13. Ghislain, L. P., Switz, N. A. & Webb, W. W. (1994) Measurement of Small Forces Using an Optical Trap *Review of Scientific Instruments* 65, 2762-2768.
14. Litvinov, R. I., Shuman, H., Bennett, J. S. & Weisel, J. W. (2002) Binding strength and activation state of single fibrinogen-integrin pairs on living cells *Proceedings of the National Academy of Sciences of the United States of America* 99, 7426-7431.
15. Rohrbach, A. & Stelzer, E. H. K. (2002) Trapping forces, force constants, and potential depths for dielectric spheres in the presence of spherical aberrations *Applied Optics* 41, 2494-2507.
16. Svoboda, K., Schmidt, C. F., Branton, D. & Block, S. M. (1992) Conformation and Elasticity of the Isolated Red-Blood-Cell Membrane Skeleton *Biophysical Journal* 63, 784-793.
17. Baumann, C. G., Bloomfield, V. A., Smith, S. B., Bustamante, C., Wang, M. D. & Block, S. M. (2000) Stretching of single collapsed DNA molecules *Biophysical Journal* 78, 1965-1978.
18. Bustamante, C., Marko, J. F., Siggia, E. D. & Smith, S. (1994) Entropic Elasticity of Lambda-Phage DNA *Science* 265, 1599-1600.
19. Wang, M. D., Yin, H., Landick, R., Gelles, J. & Block, S. M. (1997) Stretching DNA with optical tweezers *Biophys J* 72, 1335-1346.

20. Bryant, Z., Stone, M. D., Gore, J., Smith, S. B., Cozzarelli, N. R. & Bustamante, C. (2003) Structural transitions and elasticity from torque measurements on DNA *Nature* 424, 338-41.
21. Bustamante, C., Bryant, Z. & Smith, S. B. (2003) Ten years of tension: single-molecule DNA mechanics *Nature* 421, 423-7.
22. Bustamante, C., Macosko, J. C. & Wuite, G. J. (2000) Grabbing the cat by the tail: manipulating molecules one by one *Nat Rev Mol Cell Biol* 1, 130-6.
23. Grier, D. G. (2003) A revolution in optical manipulation *Nature* 424, 810-816.
24. Perkins, T. T., Quake, S. R., Smith, D. E. & Chu, S. (1994) Relaxation of a single DNA molecule observed by optical microscopy *Science* 264, 822-826.
25. Block, S. M., Goldstein, L. S. & Schnapp, B. J. (1990) Bead movement by single kinesin molecules studied with optical tweezers *Nature* 348, 348-352.
26. Svoboda, K. & Block, S. M. (1994) Force and velocity measured for single kinesin molecules *Cell* 77, 773-84.
27. Svoboda, K., Schmidt, C. F., Schnapp, B. J. & Block, S. M. (1993) Direct observation of kinesin stepping by optical trapping interferometry *Nature* 365, 721-727.
28. Mallik, R., Carter, B. C., Lex, S. A., King, S. J. & Gross, S. P. (2004) Cytoplasmic dynein functions as a gear in response to load *Nature* 427, 649-52.
29. Mammen, M., Helmerson, K., Kishore, R., Choi, S. K., Phillips, W. D. & Whitesides, G. M. (1996) Optically controlled collisions of biological objects to evaluate potent polyvalent inhibitors of virus-cell adhesion *Chem Biol* 3, 757-63.
30. Molloy, J. E., Burns, J. E., Kendrick-Jones, J., Tregear, R. T. & White, D. C. (1995) Movement and force produced by a single myosin head *Nature* 378, 209-12.
31. Rief, M., Rock, R. S., Mehta, A. D., Mooseker, M. S., Cheney, R. E. & Spudich, J. A. (2000) Myosin-V stepping kinetics: a molecular model for processivity *Proc Natl Acad Sci U S A* 97, 9482-6.
32. Lang, M. J., Fordyce, P. M. & Block, S. M. (2003) Combined optical trapping and single-molecule fluorescence *J Biol* 2, 6.
33. Brau, R. R., Tarsa, P. B., Ferrer, J. M., Lee, P. & Lang, M. J. (2006) Interlaced Optical Force-Fluorescence Measurements for Single Molecule Biophysics *Biophys J* 91, 1069-1077.
34. Gittes, F. & Schmidt, C. F. (1998) Back-focal-plane detection of force and motion in optical traps *Biophysical Journal* 74, A183-A183.
35. Mason, T. G. & Weitz, D. A. (1995) Optical Measurements of Frequency-Dependent Linear Viscoelastic Moduli of Complex Fluids *Physical Review Letters* 74, 1250-1253.
36. Mason, T. G., Gisler, T., Kroy, K., Frey, E. & Weitz, D. A. (2000) Rheology of F-actin solutions determined from thermally driven tracer motion *Journal of Rheology* 44, 917-928.
37. Dasgupta, B. R., Tee, S. Y., Crocker, J. C., Frisken, B. J. & Weitz, D. A. (2002) Microrheology of polyethylene oxide using diffusing wave spectroscopy and single scattering *Phys Rev E Stat Nonlin Soft Matter Phys* 65, 051505.
38. Valentine, M. T., Perlman, Z. E., Gardel, M. L., Shin, J. H., Matsudaira, P., Mitchison, T. J. & Weitz, D. A. (2004) Colloid surface chemistry critically affects multiple particle tracking measurements of biomaterials *Biophysical Journal* 86, 4004-4014.

39. Crocker, J. C., Valentine, M. T., Weeks, E. R., Gisler, T., Kaplan, P. D., Yodh, A. G. & Weitz, D. A. (2000) Two-point microrheology of inhomogeneous soft materials *Phys Rev Lett* 85, 888-91.
40. Landau, L. D., Lifshitz, E. M., Kosevich, A. B. d. M. & Pitaevskii, L. P. (1986) Theory of elasticity, Pergamon Press.

2 Development of the Technique to Probe the Mechanical Properties of F-actin Network

2.1 Background

Cells are dynamic structures capable of generating and reacting to physical cues in their environment. For example, the morphology and orientation of endothelial cells are altered by shear stress created by blood flow (1). Myoblast differentiation is controlled by substrate compliance; when a substrate is too rigid or soft, the differentiation is delayed (2). Tensional force in embryo development is critical in regulating the morphogenic processes linked to cell migration, epithelial mesenchymal transition and functional differentiation (3, 4). Also, the stiffness of extracellular matrix which is frequently altered in injured tissue significantly influences cell growth, viability, differentiation and migration (5, 6). Therefore, to better understand the dynamics and functions of a cell, it is essential to study its mechanical properties.

A variety of experimental techniques have been developed to investigate the mechanical properties of cell *in vivo* (Fig. 2.1). Early studies using magnetic particle measured the viscoelastic properties and intracellular motions of cells (7). In magnetic cytometry, the beads are dispersed in culture medium and added to a prepared adherent cell. An external magnetic filed applies a torque to a phagocytized bead and the cell deformation is calculated by tracking the position of the bead. To a limited extent, the magnetic cytometry might aid in noninvasive assessment of cellular properties. However, the bead response is sensitive to a surface coating protein and motility of the organelle containing the bead. Also, precision controls of force and detection are limited because the applied force depends on the magnetic field and the bead position is calculated from optical images. The local viscoelastic properties of cell can be probed

by atomic force microscopy (AFM). Compared to magnetic cytometry, higher resolutions of applied force and detection can be obtained. However, a cantilever deforms a cell with contact and a detailed description of contact geometry is required in estimating mechanical properties. Cell properties can also be determined by deforming the whole cell. A single cell is held by two microplates and tension/compression is applied to the cell by increasing/decreasing the separation between the two plates. This method provides the mechanical properties of a cell in a wide range of strain. The mechanical properties at large deformations are particularly important for the study of vascular endothelial and smooth muscle cells which are subject to a large stretch in arterial walls (8). Another technique is micro-aspiration where a cell surface is extended into the pipette. A suspended cell is attached to the mouth of the pipette with the minimum value of the suction pressure. Another step change in pressure causes the cell to be aspirated into the pipette and the steady-state value of the extension is determined by the viscosity of the cell. However, measurement using micropipettes is limited for the study of suspended cells. Also, as relatively large deformations occur on both cell and cell membrane, mechanical model including internal structure and proper boundary conditions is required for interpretation of experimental results.

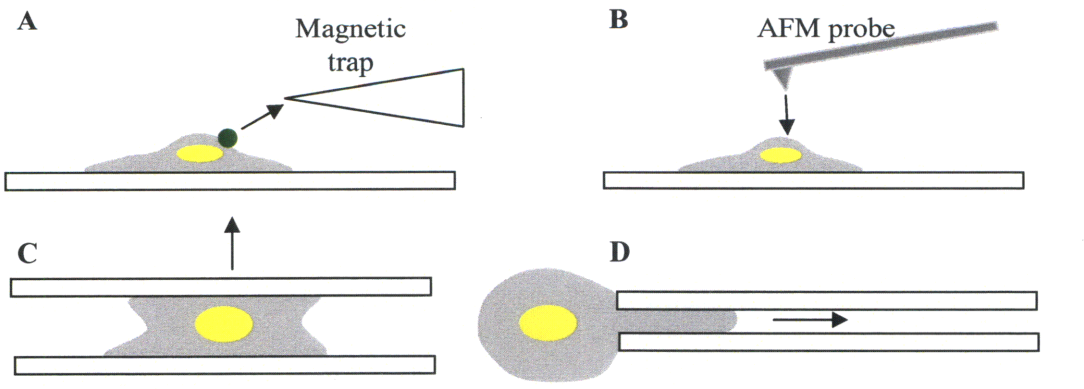

Figure 2.1 Methods to probe mechanical properties of cells. Arrow indicates the direction of applied force. (A) Magnetic cytometry. (B) Atomic force microscopy (C) Cell stretching (D) Micropipette aspiration.

Although many measurements of mechanical properties of cell have been performed, the complexity and heterogeneity of the cell structure make the further study of its mechanical properties difficult. Instead, *in vitro* study using reconstituted F-actin networks was proposed. In most of *in vitro* studies, mechanical properties of F-actin networks have been measured by bulk rheometry. Actin gel is prepared between the two plates and the external shear stress is applied by rotating one of the plates. The mechanical properties are then estimated by measuring the resulting strain response. Similarly to the mechanical properties of cell, F-actin networks also exhibit a plateau modulus at long time scale with a power law behavior at short time scales.

Although this method is useful when probing global properties of F-actin network, the measurement scale is much larger than the characteristic length scale of F-actin network which is determined by length of actin filament and mesh size. Comparison of experimental results has shown discrepancies between these large length scale measurements and microrheometry measurements using micro-scale beads (9). Another limitation of bulk rheology is that each measurement requires large sample volume, typically >200μL. One-particle and two-particle microrheology can overcome these limitations, because the mechanical properties of F-actin network are estimated by monitoring the thermal fluctuations of micro–sized colloidal spheres embedded in the network. However, thermal motion of the embedded tracer is difficult to detect when the elastic modulus of the material gets higher. Also, the probe particle that is much smaller than the pore in the network can lead to a misinterpretation (10). In addition, recent experiments have highlighted that mechanical force is a critical parameter in determining mechanical properties of reconstituted network. While the elasticity of the F-actin network is far lower than cellular elasticity (11, 12), F-actin networks subject to external prestress exhibits the mechanical properties comparable to those of cells (13). Several network models (14, 15) and

computational studies (16, 17) were proposed to explain such a nonlinear mechanical behavior. However, experiment at microscale is required to test the previous models and elucidate the microscopic origin of the nonlinear behavior

We develop passive and active microrheology techniques using optical tweezers that can manipulate a micron-sized colloidal particle with highly focused beams of light. The high resolution application of force and detection afforded by our method enable us to investigate how the mechanical response of the probe particle is altered by adding a different ABP. Also our active measurement is capable of applying local excitation to F-actin network at the comparable scale to the mesh size.

2.2 Methods and Materials

2.2.1 Passive Microrheology

Thermal fluctuations of an embedded bead are recorded at 50 kHz using the position detection system of the optical tweezers. The complex compliance of the matrix, $\alpha(f)$, is computed from the power spectral density of the thermal motion using the fluctuation-dissipation theorem and the Kramers-Kronig relation (18). The frequency-dependent complex shear modulus, $G(f)$, is determined by the generalized Stokes-Einstein relation $G(f) = (6\pi a\alpha(f))^{-1}$, where a is the radius of the bead. The storage shear modulus, $G'(f)$, and loss shear modulus, $G''(f)$, are obtained from the real and imaginary components of $G(f)$ respectively.

2.2.2 Active Microrheology

While passive microrheology monitors the passive movement of the bead embedded in an F-actin network, an external force is applied to the embedded bead in the active microrheology. The mechanical properties of the F-actin network are estimated by measuring the spatio-temporal responses of the bead.

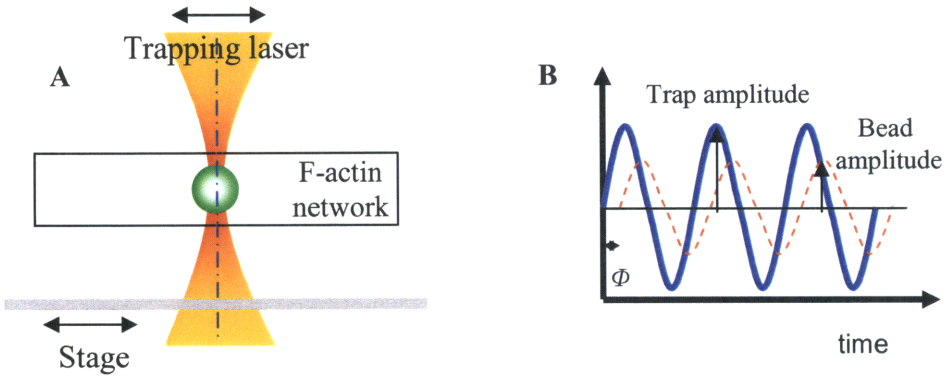

Figure 2.2 Active microrheology using sinusoidal input. (A) With the embedded bead captured using optical tweezers, sinusoidal force is applied by oscillating either the trapping laser or the stage. (B) The mechanical properties of F-actin network are estimated from bead responses including its amplitude and phase delay (Φ) to the oscillation.

Sinusoidal force is applied to the microsphere which is embedded in the F-actin matrix by oscillating the optical tweezers using AODs such that

$$x_t(t) = A_t \sin(\omega t), \tag{2.1}$$

where A_t is the amplitude of the trap displacement and ω_i is the input frequency of oscillation. Positions of both the optical tweezers and microsphere are detected by two separate PSDs simultaneously. The response of the bead, x_b, to this sinusoidal input is approximated by

$$x_b(t) = A_b \sin[\omega t - \theta_b(\omega)], \tag{2.2}$$

where A_b is the amplitude of the bead response and θ_b is the phase delay of the response relative to x_t. Finally, the force on the particle is computed using

$$f(t) = k[x_t(t) - x(t)] = F \sin[\omega t - \theta_f(\omega)], \tag{2.3}$$

where k is the stiffness of the optical trap, F is the magnitude of the force and θ_f is the resulting phase of the force relative to x_t. The phase angle difference, $\Delta\theta$ (= θ_b - θ_f), between the force and the bead response can be used to determine both storage and loss shear moduli by

$$G(f) = G'(f) + iG''(f) = \frac{\bar{F}(f)}{6\pi a \bar{x}_{bead}(f)}[\cos(\Delta\theta(f) + i\sin(\Delta\theta(f)], \tag{2.4}$$

where $\overline{F}$ is the force amplitude, $\overline{x}_{bead}$ is the amplitude of the bead response, and $\Delta\theta$ is the phase delay between the $F(t)$ and $x_{bead}(t)$. A perfectly elastic material will exhibit no phase delay, while a perfectly viscous material will exhibit a phase delay of 90°. For small deformation, the amplitude of the trapping laser is 200nm and the frequencies range from 0.2π to 20π rad/s.

Another active microrheology approach is to monitor the position of a trapped particle in response to a sudden increase in force. An embedded particle can be subjected to a sudden increase in external force by quickly displacing the trap away from the particle. In this case the forcing function is

$$f(t) = k[x_0 - x(t)], \tag{2.5}$$

where k is the stiffness of the optical trap and x_0 is the initial displacement of the trap relative to the bead. We fit the time dependent position of the bead to an exponential function:

$$x(t) = B\left[1 - \exp\left(\frac{-t}{\tau}\right)\right], \tag{2.6}$$

where B is the final equilibrium position of the bead and τ is the time constant of the system, both of which are dependent on the trap stiffness and mechanical properties of the medium. For complex solutions, this model might not account for structural reorganizations spanning on different time scales and may not capture the complete material response. However, it provides a simple description of the material response that can be compared and fit to classical linear viscoelastic systems such as the Voigt model (spring and dashpot in parallel) (19), providing intuition into the properties of the material.

2.3 Results

2.3.1 Test of the Methods for Water

Both passive and active methods were developed and tested to estimate the properties of water as a control experiment. As water is a purely viscous solution, thermal motion of the bead is confined using optical tweezers during the experiment. Assuming the optical tweezers behave as an elastic spring, the storage shear modulus is determined by $G' = k_{trap}/(6\pi a)$ where a is the radius of the bead and k_{trap} is the stiffness of the optical trap, and the loss shear modulus is determined by $G'' = 2\pi f \mu_{water}$ where μ_{water} is a viscosity of water. As shown in Fig. 2.3, experimental estimations of shear moduli of water are consistent with theoretical values. We note that the way to estimate the modulus cause disagreements at very high and low frequencies.

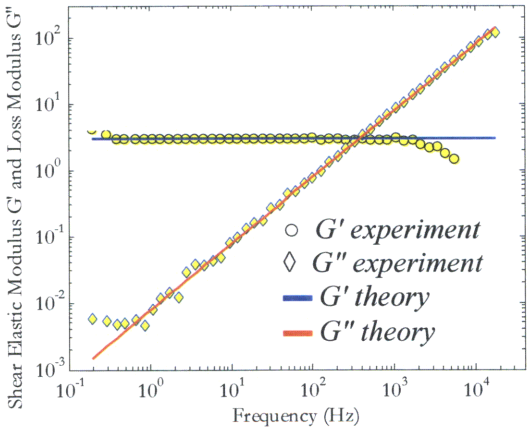

Figure 2.3 Test of the passive microrheology for water. By monitoring thermal fluctuation of the microsphere in water, our passive measurement estimates the properties of the water in the frequency ranging from 1 to 10^3Hz.

In the active measurement, the bead is captured by optical tweezers and oscillated at various frequencies. For the bead responses, the amplitude is relatively independent of the frequency while phase delay was linearly proportional to the frequency of oscillation. We also perform the same experiment at different trap stiffness. When the stiffness of the trapping laser is increased, the amplitude of the bead movement increases but the phase delay decreases.

Assuming water is a purely viscous solution, these behaviors agreed well to a theoretical expectation.

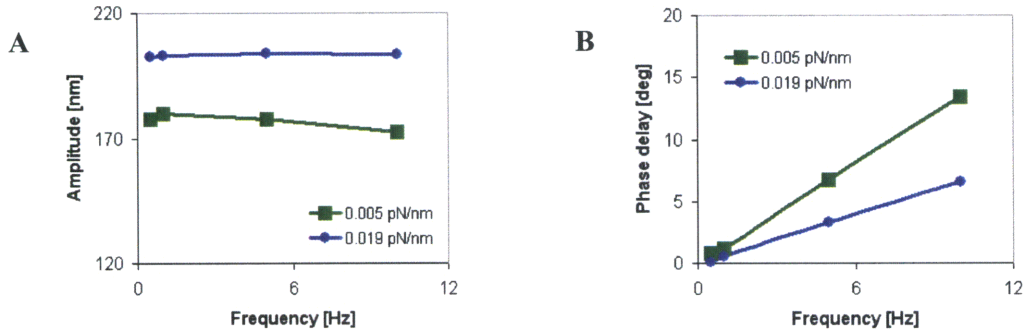

Figure 2.4 Test of the active microrheology for water. (A) The amplitude of the bead displacement increases as the stiffness of the trapping laser increases. (c) The phase delay of bead displacement increases as the oscillation frequency increased. The stiffer optical tweezers reduces the phase delay of the bead response.

Also, an instantaneous force is applied to water and actin networks by abruptly displacing the trapping laser 100 nm, which then pulls the bead to a new equilibrium position. For the solutions studied, the final displacement of the bead is independent of material, demonstrating that the stiffness of the trap dominates the elastic response over this length scale. However, time constants increased with actin concentration, indicating that the viscosity of the solution increased. For water, the measured time constant of ~ 35μs agrees with that predicted of 31.4μs for η = 1mPa·s and k = 0.3pN/nm.

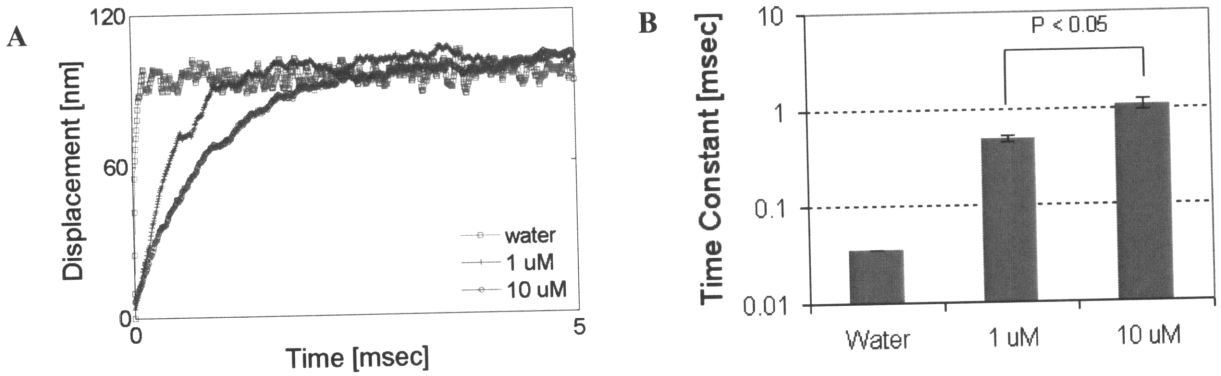

Figure 2.5 Response of a bead in water and F-actin solution to transient force. (A) Time-displacement response of a bead in water and F-actin solutions to transient force. A force is applied to the bead by quickly displacing the trap 100 nm away from the original position while the bead trajectory is monitored. Each curve is fitted to an exponential function to estimate the final equilibrium position of the bead and the time constant of the response. For all the samples the fit value, *B,* is ~ 100 nm. (B) The average time constants are 0.035, 0.49, and 1.08 ms for water (□), 1 μM actin (+), and 10 μM actin (o), respectively.

2.3.2 Test of the Methods for F-actin Gel

We also tested the methods for F-actin gels. To form a cross-linked F-actin network, 26 μL of ABP(either α-actinin or filamin) is mixed with 2 μL of 1μm-diameter bead solution and 6 μL of 10× Polymerization buffer (50 mM Tris-HCl, 500 mM KCl, 2 mM MgCl2, 2 mM CaCl2, 2 mM DTT, 5 mM ATP, 0.01% (w/v) NaN3, pH 7.5). Network formation is initiated by adding 26 μL of actin to the mixture. The experiment is run after 2hrs of polymerization of the final solution in custom-made flow channel. Details of the protocol including protein preparations are described in Chapter 3.

Thermal motion of the beads embedded in the F-actin network (c_A = 10μM, [filamin]/[actin] = 0.01) are recorded at 50-kHz for 30 seconds. The shear moduli of G' and G'' are estimated by two methods as explained in Chapter 1. One is derived from the evolution of the MSD trace and the other from the spectral density of the bead fluctuation. As shown in Fig. 2.6, both analyses estimate the similar values of shear moduli. However, the results by the former can be noisy at low frequency due to the time of the measurement.

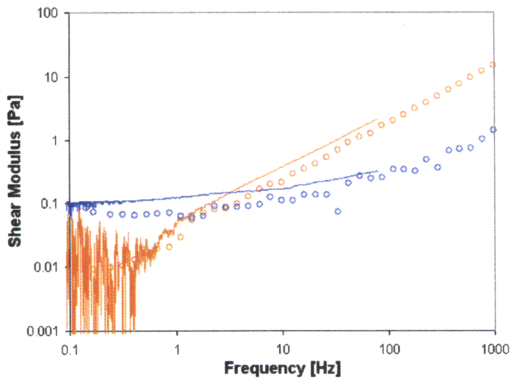

Figure 2.6 Shear moduli estimated by two methods in passive measurement. Both G' (blue) and G'' (orange) estimated from MSD traces (line) of bead show the same result to those from spectral density of the fluctuation (circle).

The active measurement using an instantaneous force is applied to α-actinin/F-actin networks, too. At low actin concentration (c_A = 1μM), F-actin networks polymerized with α-actinin ($c_{\alpha\text{-}actinin}$ = 0.1μM and 0.01μM) show the similar behavior to F-actin solutions without α-actinin. In contrast, at high actin concentration (c_A = 10μM), the embedded bead reaches the equilibrium position slowly as α-actinin concentration increases. Time constant for the F-actin network without α-actinin is 1.1ms. However, when the relative concentration of α-actinin (R_α) to the fixed concentration of actin (c_A = 10μM) increases to 0.01 and 0.1, the time constant of the bead response increase to 4.0ms and 19.4ms (Fig. 2.7C). To see the effect of filament length on viscosity of the F-actin network, α-actinin/F-actin network is polymerized in the presence of capping and severing protein of gelsolin. At the same concentrations of actin and α-actinin (c_A = 10μM, R_α = 0.1), the F-actin network polymerized with gelsolin exhibits the less time constant compared to the F-actin network without gelsolin, suggesting that the viscosity of F-actin network decreases as the average length of actin filament decreases.

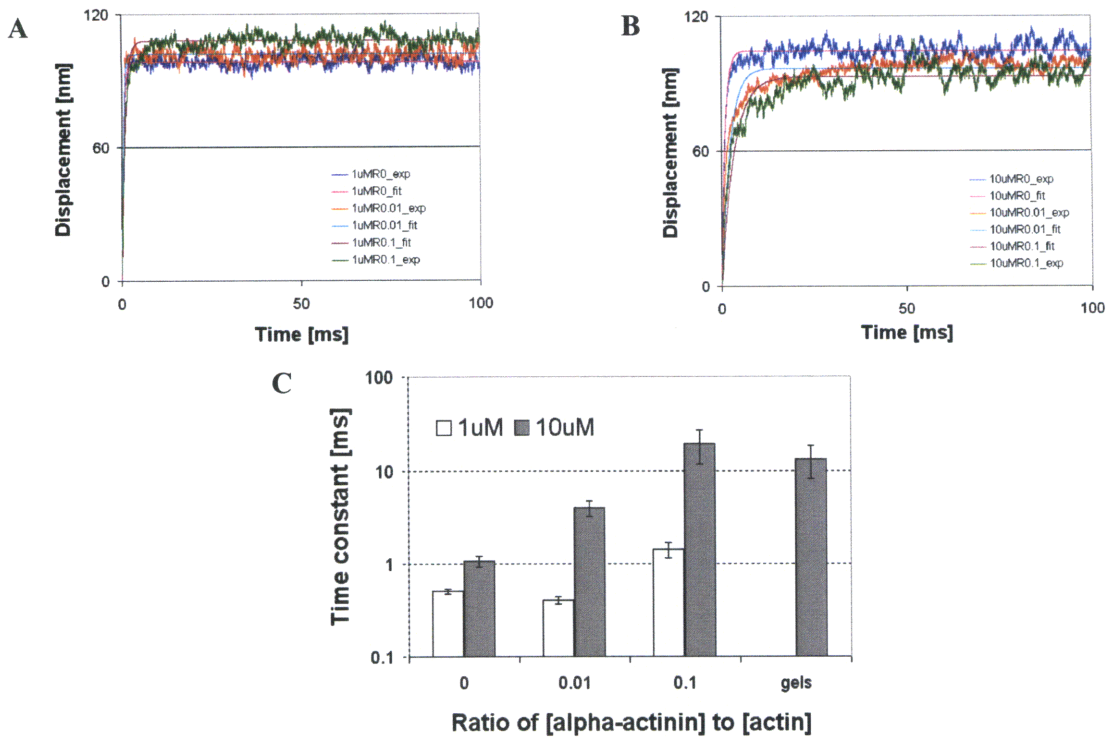

Figure 2.7 Responses of the beads embedded in α-actinin/F-actin networks. (A) For the F-actin network of 1μM, no significant difference is observed in the bead responses although ABP α-actinin is added. (B) Addition of α-actinin significantly delays the time for the bead to reach the final equilibrium position implying that the viscosity of the F-actin network increases. (C) Time constant increases as the concentration of α-actinin increases, which is more distinct at the actin concentration of 10μM. However, when gelsolin is added during the network organization, the time constant decreases. 'gels' refers to the F-actin network with α-actinin($R_{\alpha\text{-}actinin/actin} = 0.1$) and gelsolin($R_{actin/gelsolin} = 200$).

2.4 Discussion

Using optical tweezers, both passive and active microrheology techniques were developed and tested to estimate the mechanical properties of water and F-actin network. The passive method is used to measure the frequency-dependent mechanical properties by tracking the thermal motion of the microsphere which is embedded in the sample. Because chemical interactions between probe particle and protein network is crucial to obtain a viscoelasticity of biopolymer network such as F-actin (10), the microsphere is coated with PEG to prevent undesirable protein interactions.

The active method measures the mechanical properties by obtaining a response of a sample to an external force. Recent works showed that both cells and F-actin networks exhibit nonlinear behaviors to external forces (13, 20, 21). The active method can be applied to investigate the relationship between the elasticity of the F-actin network and the physical force by estimating the mechanical properties at various strains. The force in the optical tweezers ranges between 1pN and a couple hundreds pN, which are comparable to the forces developed in cellular processes including cell adhesion, migration, and molecular motor-cargo system. Therefore, our measurement of mechanical properties is performed in a more physiological condition, compared to the previous studies using magnetic cytometry or AFM. Moreover, the active microrheology can be used to probe the structural alterations of F-actin network. When the size of the probe particle is comparable to the mesh size of F-actin network, our method should be able to probe the mechanical interactions of actin binding proteins with actin filaments as well as to estimate the local properties by displacing the embedded microsphere (Fig. 2.8).

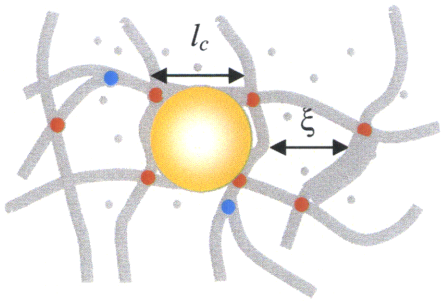

Figure 2.8 Schematic of microsphere embedded in F-actin network. The microsphere (yellow) is embedded in the F-actin network in which the actin binding proteins (red) cross-link single filaments (thin gray) or bundled filaments (thick gray). The mechanical response of the bead to the external force will depends on molecular interactions between constituents and mechanical properties of actin filaments. l_c and ξ represent cross-linking distance and mesh size, respectively.

Two types of force were used in the active methods; sinusoidal and step-like forces. When a sinusoidal force is applied, the shear moduli of F-actin network is estimated from the amplitude and phase delay of bead response. In the method using a step-like force, the center of

the trap is displaced instantaneously and the position of the bead is tracked. The latter is similar to a creep test where a sample is subject to a constant force. The previous creep experiments using magnetic tweezers found that the enforced displacement of the bead embedded in F-actin solution exhibits a subdiffusive dependence on time $x \sim t^{0.75}$ and a viscous fluid motion $x \sim t$ at short and long time scales, respectively (22, 23). The short time scale behavior corresponds to a frequency dependence of the shear modulus $G \sim \omega^{0.75}$ at high frequency (24). Although our method is not a true creep experiment because the applied force to the bead decreases as the bead approaches the center of the optical trap, we could assume that a constant force is applied to the bead for the limited range of the bead displacement. The time-dependent bead responses between 40% and 60% of the total displacements also obey the power law $x \sim t^{\alpha}$ with the goodness of 99%. The exponents α are 0.71 and 0.65 for 1μM and 10μM actin concentrations, respectively, which are close to 0.75 observed at the short time scales in the previous measurements. When the relative concentration of α-actinin to actin (R_α) increases to 0.01 and 0.1, the α decreases to 0.58 and 0.59 for 1μM, and 0.54 and 0.48 for 10μM, suggesting that the bead undergo more elastic resistance imposed by cross-linking of actin filaments.

2.5 References

1. Dewey, C. F., Jr., Bussolari, S. R., Gimbrone, M. A., Jr. & Davies, P. F. (1981) The dynamic response of vascular endothelial cells to fluid shear stress *J Biomech Eng* 103, 177-85.
2. Engler, A. J., Griffin, M. A., Sen, S., Bonnemann, C. G., Sweeney, H. L. & Discher, D. E. (2004) Myotubes differentiate optimally on substrates with tissue-like stiffness: pathological implications for soft or stiff microenvironments *J Cell Biol* 166, 877-87.
3. Beloussov, L. V., Lakirev, A. V., Naumidi, II & Novoselov, V. V. (1990) Effects of relaxation of mechanical tensions upon the early morphogenesis of Xenopus laevis embryos *Int J Dev Biol* 34, 409-19.
4. Czirok, A., Rongish, B. J. & Little, C. D. (2004) Extracellular matrix dynamics during vertebrate axis formation *Dev Biol* 268, 111-22.
5. Chen, C. S., Tan, J. & Tien, J. (2004) Mechanotransduction at cell-matrix and cell-cell contacts *Annu Rev Biomed Eng* 6, 275-302.
6. Ebihara, T., Venkatesan, N., Tanaka, R. & Ludwig, M. S. (2000) Changes in extracellular matrix and tissue viscoelasticity in bleomycin-induced lung fibrosis. Temporal aspects *Am J Respir Crit Care Med* 162, 1569-76.
7. Valberg, P. A. & Feldman, H. A. (1987) Magnetic particle motions within living cells. Measurement of cytoplasmic viscosity and motile activity *Biophys J* 52, 551-61.
8. Matsumoto, T. & Hayashi, K. (1996) Stress and strain distribution in hypertensive and normotensive rat aorta considering residual strain *J Biomech Eng* 118, 62-73.
9. Schmidt, F. G., Hinner, B. & Sackmann, E. (2000) Microrheometry underestimates the values of the viscoelastic moduli in measurements on F-actin solutions compared to macrorheometry *Physical Review E* 61, 5646-5653.
10. Valentine, M. T., Perlman, Z. E., Gardel, M. L., Shin, J. H., Matsudaira, P., Mitchison, T. J. & Weitz, D. A. (2004) Colloid surface chemistry critically affects multiple particle tracking measurements of biomaterials *Biophysical Journal* 86, 4004-4014.
11. Hinner, B., Tempel, M., Sackmann, E., Kroy, K. & Frey, E. (1998) Entanglement, elasticity, and viscous relaxation of actin solutions *Physical Review Letters* 81, 2614-2617.
12. Xu, J. Y., Wirtz, D. & Pollard, T. D. (1998) Dynamic cross-linking by alpha-actinin determines the mechanical properties of actin filament networks *Journal of Biological Chemistry* 273, 9570-9576.
13. Gardel, M. L., Nakamura, F., Hartwig, J. H., Crocker, J. C., Stossel, T. P. & Weitz, D. A. (2006) Prestressed F-actin networks cross-linked by hinged filamins replicate mechanical properties of cells *Proceedings of the National Academy of Sciences of the United States of America* 103, 1762-1767.
14. Chaudhuri, O., Parekh, S. H. & Fletcher, D. A. (2007) Reversible stress softening of actin networks *Nature* 445, 295-298.
15. Xu, J. Y., Schwarz, W. H., Kas, J. A., Stossel, T. P., Janmey, P. A. & Pollard, T. D. (1998) Mechanical properties of actin filament networks depend on preparation, polymerization conditions, and storage of actin monomers *Biophysical Journal* 74, 2731-2740.
16. Head, D. A., Levine, A. J. & MacKintosh, E. C. (2003) Deformation of cross-linked semiflexible polymer networks *Physical Review Letters* 91, 108102.

17. Onck, P. R., Koeman, T., van Dillen, T. & van der Giessen, E. (2005) Alternative explanation of stiffening in cross-linked semiflexible networks *Physical Review Letters* 95, 178102.
18. Chaikin, P. M. & Lubensky, T. C. (1995) Principles of Condensed Matter Physics, Cambridge University Press.
19. Ward, I. M. & Sweeney, J. (2004) An introduction to the mechanical properties of solid polymers, Wiley.
20. Bursac, P., Lenormand, G., Fabry, B., Oliver, M., Weitz, D. A., Viasnoff, V., Butler, J. P. & Fredberg, J. J. (2005) Cytoskeletal remodelling and slow dynamics in the living cell *Nat Mater* 4, 557-61.
21. Matthews, B. D., Overby, D. R., Mannix, R. & Ingber, D. E. (2006) Cellular adaptation to mechanical stress: role of integrins, Rho, cytoskeletal tension and mechanosensitive ion channels *J Cell Sci* 119, 508-18.
22. Amblard, F., Maggs, A. C., Yurke, B., Pargellis, A. & Leibler, S. (1996) Subdiffusion and Anomalous Local Viscoelasticity in Actin Networks *Phys Rev Lett* 77, 4470-4473.
23. Uhde, J., Feneberg, W., Ter-Oganessian, N., Sackmann, E. & Boulbitch, A. (2005) Osmotic force-controlled microrheometry of entangled actin networks *Phys Rev Lett* 94, 198102.
24. Gittes, F., Schnurr, B., Olmsted, P. D., MacKintosh, F. C. & Schmidt, C. F. (1997) Microscopic viscoelasticity: Shear moduli of soft materials determined from thermal fluctuations *Physical Review Letters* 79, 3286-3289.

3 Investigating the Effect of Actin Binding Proteins on Microstructure and Mechanical Properties of F-actin Network

Actin filaments (F-actin) are the dominant structural constituents in the cytoskeleton. Orchestrated by various actin binding proteins (ABPs), F-actin are assembled into higher-order structures such as networks and bundles that provide mechanical support for the cell and play important roles in numerous cellular processes Although mechanical properties of F-actin networks have been extensively studied, underlying mechanism of the network's elasticity is still unclear because the measurement depends on the scale and method. Here, we developed both *passive* and *active* microrheology techniques using optical tweezers to estimate the mechanical properties of F-actin networks at the comparable length scale to cells. For the *passive* approach we tracked the motion of a thermally fluctuating colloidal sphere to estimate the frequency-dependent complex shear modulus of the network. In the *active* approach, we used an optical trap to apply a driving force to an embedded microsphere and monitored the response to obtain the viscoelasticity of the network. While both *active* and *passive* measurements exhibit similar results at low strain, the F-actin network subject to a high strain exhibits a non-linear behavior which is analogous to strain-hardening observed in the macroscale measurements. Using confocal and TIRF microscopy, we also characterize the microstructure of reconstituted F-actin networks in terms of filament length, mesh size, and degree of bundling. We propose a model of network connectivity by investigating the effect of filament length on the mechanical properties and structure.

3.1 Background

Cells sense, generate and respond to forces in their surroundings through cytoskeletal dynamics, and mechanical force plays important roles in fundamental cellular processes such as migration, cytokinesis and apoptosis (1-3). Actin, one of the principal constituents of the cytoskeleton, contributes to the mechanical integrity of the cell and is involved in numerous cellular functions organizing various microstructures according to functional demands (4, 5). Structural assembly of F-actin, critical in these processes, is regulated by over 100 actin binding proteins (ABPs) (6, 7). Two major structures of F-actin organized by ABPs are the cross-linked network and filament bundle. For example, the ABP filamin assembles filaments into three-dimensional orthogonal networks serving as a scaffold for cell motility and signaling (8, 9); in contrast, the ABP α-actinin forms thick bundles at high concentration contributing to structural stability of the cell providing added mechanical strength (10, 11). Therefore, an understanding of cytoskeletal mechanical properties governed by dynamic interactions between actin and ABPs is essential for understanding cell mechanics and the associated biological phenomena.

Cell experiments revealed that the cytoskeleton exhibits both elastic and viscous characteristics under applied stress (12, 13). Since it is difficult to accurately characterize the mechanical properties of the cytoskeleton *in vivo* due to active remodeling as well as the presence of numerous other, uncontrolled factors, *in vitro* experiments on re-constituted gels of F-actin have proven useful (14-19). *In vitro* studies have characterized the viscoelastic properties of F-actin polymerized from purified actin in combination with various ABPs. Many of these measurements of mechanical properties have been performed using a bulk rheometer, which yields global properties of the F-actin matrix. Discrepancies have been observed, however, between these large length scale measurements and microrheometry using micron-scale beads

(20). These have been attributed to a variety of factors including the non-uniform local stress field, different deformation modes (21), the formation of a depletion zone around the microbead (22, 23), and other effects present when the bead is comparable in size to the characteristic dimensions of the actin mesh, both of which tend to be on the scale one to several microns (24). While this similarity of length scales complicates interpretation of the results of microrheometry, it also provides an opportunity to probe the local mechanical response and provide insight into the specific roles of ABP in mediating rheological behavior. Other experiments have demonstrated the novel feature that actin gels stiffen with increasing strain up to a point, then rapidly soften as strain is further increased (15, 25-29). Actin network under shear deformation exhibits an irreversible non-linear behavior suggesting either network remodeling or rupture of network bonds (26). However, compressive force imposed on a dendritic actin network results in reversible stress softening suggesting it might be caused by a filament buckling (27). The mechanisms for both the increase and sudden fall in modulus remain a subject of debate. Although models to explain these findings of actin cytoskeleton have been proposed (19, 27, 30), observation of network's response at the microscale will undoubtedly help elucidate the origin of this non-linear behavior.

Here, we employ both passive and active microrheology to measure mechanical properties at the microscale using optical tweezers. Optical tweezers-based microrheology provides the advantage of high-precision force control in the rage of 0.1 ~ 100pN while simultaneously monitoring the motion of the bead with nanometer resolution (31). Although this technique has been used to measure viscoelastic properties of fd viruses and micellar solutions (32, 33), its application to study F-actin networks has been limited (34). In our passive approach, we track the motion of a thermally fluctuating microbead to estimate the frequency dependent

complex shear modulus of the F-actin network over a wide frequency range of $10^{-1} \sim 10^{4}$ Hz. For the active approach, we apply a sinusoidal driving force to an embedded microbead and monitor its response to obtain the viscoelastic properties of the network. In particular, microscale non-linear behavior of F-actin network is demonstrated by performing the active measurement at large deformation.

We investigate the effect of ABPs on mechanical properties of F-actin networks using the *passive* and *active* techniques. To correlate mechanical properties with structural geometry, both material properties and microstructure of cross-linked F-actin network are probed as a function of ABP concentration. We use confocal microscopy and total internal reflection fluorescent (TIRF) microscopy to visualize the F-actin networks organized with filamin, α-actinin, and gelsolin. Unique features of F-actin networks polymerized with each ABP are visualized and quantified in terms of mesh size and degree of bundling. We vary average length of actin filaments using gelsolin and investigate how the length of individual filaments alters network formation and its mechanical properties. While previous rheological measurements on entangled F-actin solutions have demonstrated that the thermal motion of particle is more constrained as the length of filament increases and mesh size decreases (16, 35), to our knowledge, no comparable measurements have been reported in cross-linked F-actin networks. Based on our measurements, we propose a model to explain how the length of individual actin filaments influences a connectivity of the cross-linked network and further its elasticity.

3.2 Methods and Materials

3.2.1 Reconstituted In Vitro F-actin Networks

Lyophilized actin monomers and lyophilized α-actinin both from rabbit skeletal muscle are purchased from Cytoskeleton, Inc (Denver, CO). Activity and purity of actin are tested with sodium dodecyl sulfate-polyacrylamide gel electrophoresis (SDS-PAGE). Polymerized actin filaments are separated from the non-polymerized G-actin by centrifugation at 100,000g for 40min (36) and both supernatants and pellets are loaded on a 4-12% Bis-Tris gel (NP0321BOX; Invitrogen, Carlsbad, CA). The protein bands stained with Commassie blue shows that most of G-actin is polymerized into F-actin (Fig. 3.1A). Protein activity is confirmed by examining the geometry of polymerized actin filaments in the micrographs (Fig. 3.1B and C). Recombinant filamin-A is purified from Sf9 cell lysates (37) and recombinant human gelsolin is produced in *Escherichia coli* (38).

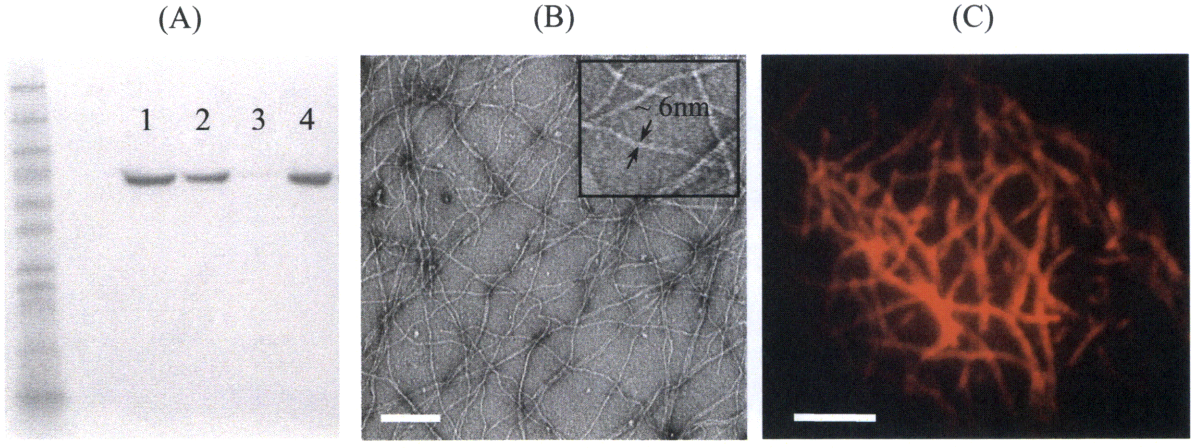

Figure 3.1 Characterization of actin. (A) Scanned image of the polyacrylamide gel. Lane #1, G-actin kept overnight on ice, #2 , G-actin after centrifuge without polymerization, #3 , supernatant after centrifugation of polymerized actin, and #4, pellet after centrifugation of polymerized actin. Bands observed in the gel confirmed that actin is in monomeric form in G-buffer and most of G-actin is polymerized into F-actin during polymerization. (B) Electron microscope image of F-actin which are negatively stained with 2% uranyl acetate (scale bar, 200nm). *Inset*: The radius of actin filament is measured to be approximately 6nm. (C) TIRF microscopy shows that the length of polymerized actin filaments is varying over 20 μm (scale bar, 5μm).

Actin monomers are diluted in fresh G-buffer (5 mM Tris-HCl, 0.2 mM $CaCl_2$, 0.5mM DTT, 0.2 mM ATP, pH 8.0) and incubated on ice for at least two hours. Gelsolin, filamin or α-actinin are gently mixed with the actin monomer, followed by the addition of PEG-coated beads diluted in G-buffer. Actin polymerization is initiated by adding a tenth of the final volume of F-buffer (50 mM Tris-HCl, 500 mM KCl, 2 mM $MgCl_2$, 2 mM $CaCl_2$, 2 mM DTT, 5 mM ATP, 0.01% (w/v) NaN_3, pH 7.5). The sample is gently mixed by pipetting and immediately loaded into a custom-made flow chamber, with dimensions 25.8 mm x 8 mm x 0.1 mm (~ 20μL). Microspheres are firmly embedded in the F-actin network after several hours of polymerization. Concentrations of actin, filamin, α-actinin, and gelsolin are varied depending on the experiment.

3.2.2 PEG-coated Microspheres

0.5-μm and 1-μm radius, amino functionalized beads (2.73% solids, Polybead Amino Microspheres; Polysciences, Warrington, PA) are coated with mPEG-NHS (5 kDa; Nektar, San Carlos, CA) to prevent protein absorption as described previously (39) with the following modifications. 40 μL of stock beads are diluted with 200 μL of de-ionized water. This solution is spun down for 10 minutes at 14000 rpm in a benchtop centrifuge, supernatant is removed and the bead pellet is resuspended with 200 μL of methanol. Next, the bead solution is again centrifuged as described above, the supernatant is removed and the bead pellet is resuspended with 200 μL of 10 mg/mL PEG-NHS diluted in one part of DMSO and four parts of methanol. After gently mixing the bead solution for two hours at room temperature, the beads are stored at 4°C with continuous rotation to prevent aggregation by sedimentation. Beads are used within 6 months of preparation.

3.2.3 Characterizing F-actin Microstructure

Reconstituted F-actin structure polymerized with various ABPs are visualized and characterized in terms of mesh size and degree of filament bundling. For visualization, fluorescently labeled actin (A-12373; Invitrogen, Carlsbad, CA) and rhodamine phalloidin (R415; Invitrogen, Carlsbad, CA) are used to stain actin filaments in confocal microscopy (Axiovert 200M; Carl Zeiss, Inc., Thornwood, NY) and TIRF microscopy (40), respectively. In confocal microscopy, actin filaments are labeled by polymerizing regular actin monomers in the presence of labeled monomers at a molar ratio of 5:1. The sample is fixed by paraformaldehyde to minimize thermal fluctuations during image acquisition. A stack of 71 images is obtained with 100nm separation to obtain the 3-dimensional (3D) structure. Images are then deconvolved with HUYGENS ESSENTIAL software (Scientific Volume Imaging, Hilversum, The Netherlands) and assembled to construct the 3D image by IMARIS software (Bitplane, Zurich, Switzerland). Mesh size of the structure is determined by two methods. Each area surrounded by actin filaments is calculated and mesh diameter (ξ) is given by $\xi = (4\times\text{Area}/\pi)^{1/2}$. It is also estimated by measuring the peak-to-peak distance in the intensity profiles of the images. Corrections to these 2D measurements for three-dimensionality of the network are made according to Overby et al (41). The degree of bundling is estimated by normalizing the intensity of the actin filaments by the intensity of single actin filaments in background.

3.2.4 Estimating Mechanical Properties

Mechanical properties of F-actin networks cross-linked with various actin binding proteins are estimated by using the passive and active microrheology developed in chapter 2.

3.3 Results

3.3.1 Effect of Filamin on F-actin Network

Filamin/F-actin gels are prepared by polymerizing actin with filamin and gelsolin ([actin]/[gelsolin] = 250). They are visualized by confocal microscopy to investigate effects of cross-linking on F-actin network microstructure. For F-actin networks cross-linked with filamin, homogeneous networks are obtained only over a limited range of the ratio of filamin to actin concentration (R_f) such as between 0.001 and 0.01 at a fixed actin concentration of 10μM (Fig. 3.2). When the concentration of filamin is less than R_f = 0.0001, F-actin networks form an inhomogeneous structure with a large local variation, which is similar to the heterogeneity observed in F-actin networks cross-linked with low concentration of heavy meromyosin (42). In the magnified image (Fig. 3.2B) of the F-actin network at R_f = 0. 01 in Fig. 3.2A, cross-linking points of actin filaments appear to be at high-angle branchings.

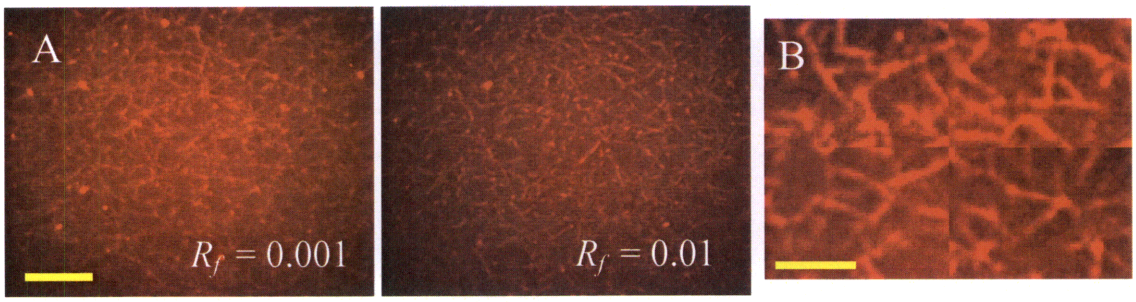

Figure 3.2 Confocal microscopy of F-actin organized by filamin. Images are projections of 71 layers each separated by 100nm. (A) Images of F-actin cross-linked with two different concentrations of filamin (scale bar, 10μm). In a limited range of R_f between 0.001 and 0.01, the cross-linked F-actin networks exhibit uniform and fine microstructures. (B) Higher magnification images of F-actin cross-linked by filamin with R_f = 0.01 (scale bar, 2μm). The images show filamin forming F-actin cross-links at high angle.

F-actin/filamin networks are characterized in terms of their mesh size which is one of important parameters in determining network mechanical properties. Mesh sizes for the homogeneous F-actin/filamin networks at both R_f = 0.001 and R_f = 0.01 are ~ 1μm (Fig. 3.3A

and B), which is similar in value to the mesh size in F-actin/scruin network (43). It suggests that the mesh size of a cross-linked network is not determined by the concentration of ABP, but rather, that of actin.

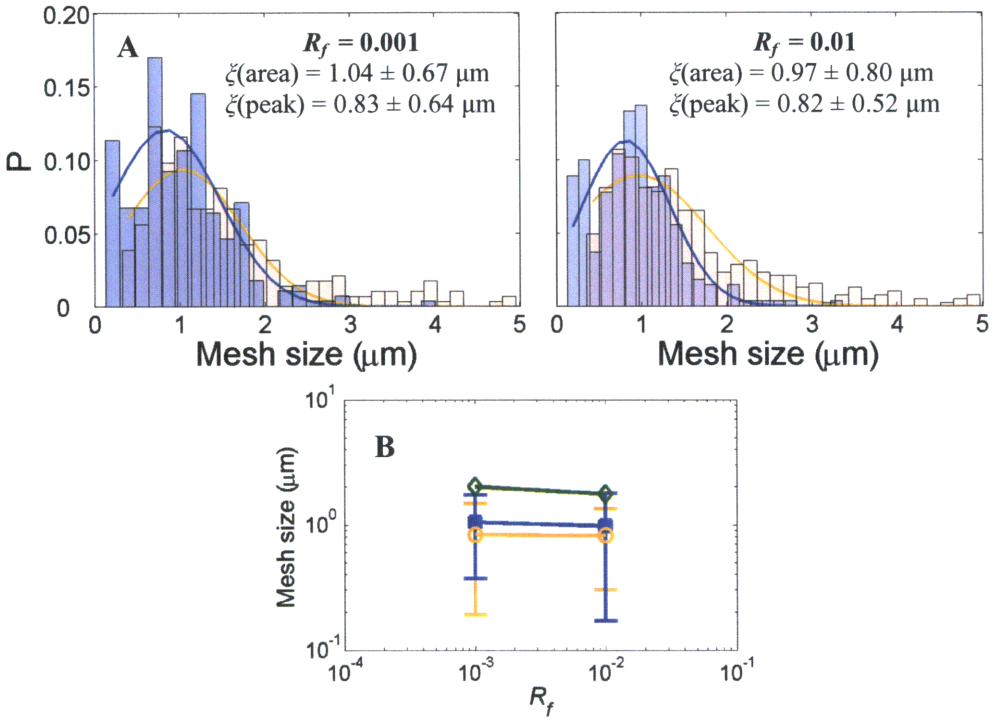

Figure 3.3 Microstructural characterization for filamin/F-actin networks. Mesh sizes computed from the mesh area (orange) and the peak-to-peak distance (blue) in the images. 3D mesh size (green) is estimated using the properties of 2D meshes. (A) Distributions of mesh size, ξ, in the F-actin networks cross-linked with filamin at various R_f. (B) Mean and standard deviation of mesh size plotted against R_f.

Mechanical properties of the F-actin networks are estimated by passive and active methods. For C_A = 10μM and R_f = 0.01, the frequency dependent shear modulus is estimated by the passive measurement using compliance function (Fig. 3.4A). At low frequency, G' dominates over G'' and approaches a constant value. At high frequency, $G'' > G'$ and G' scales as $f^{0.75}$ (Fig. 3.4A).

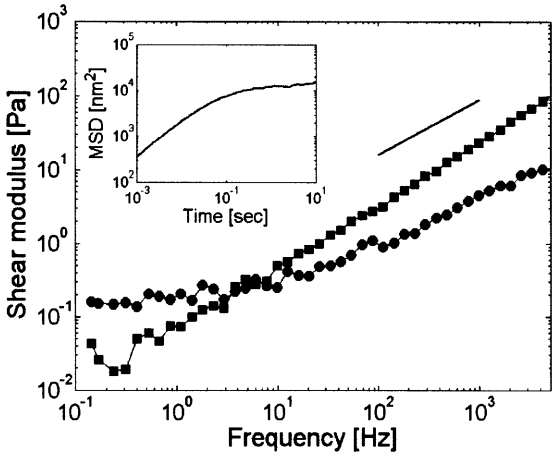

Figure 3.4 Frequency-dependent mechanical properties in passive microrheology for F-actin networks with C_A = 10μM at R_f = 0.01. The complex shear moduli G' (circles) and G'' (squares) of F-actin networks are estimated over 4 decades of frequency by tracking the thermal fluctuations of an embedded microsphere. Solid line has a slope of 0.75. *Inset*: MSD of the microsphere.

Active measurements were performed at low amplitude, ±200nm, for the same F-actin/filamin network. The mechanical responses of the microsphere to sinusoidal excitation have different phase delays and amplitudes depending on excitation frequency (*Top inset* in Fig. 3.5A). As frequency increases, viscous dissipation increases as indicated by large hysteresis in the curves (Fig. 3.5A). Shear modulus of the F-actin network is estimated at each frequency (Fig. 3.5B) using Eq. 2 and the values are in good agreement with the result by passive measurement in Fig. 3.4. To investigate the effect of large strain, the active measurement was performed at the large oscillatory movement of the stage. As the applied strain increases, the response becomes non-linear as indicated by distortion of the force response (Fig. 3.5C). The Lissajous curve for the corresponding response exhibits a more distinct evidence of non-linear behavior, too (Fig. 3.5D). However, this microscale non-linear behavior is weak, compared to the significant increase of modulus by strain hardening observed in the bulk measurements (15, 19). In all other measurements of the mechanical properties, we set the excitation amplitude at a low level of ±200nm to minimize the effect of strain.

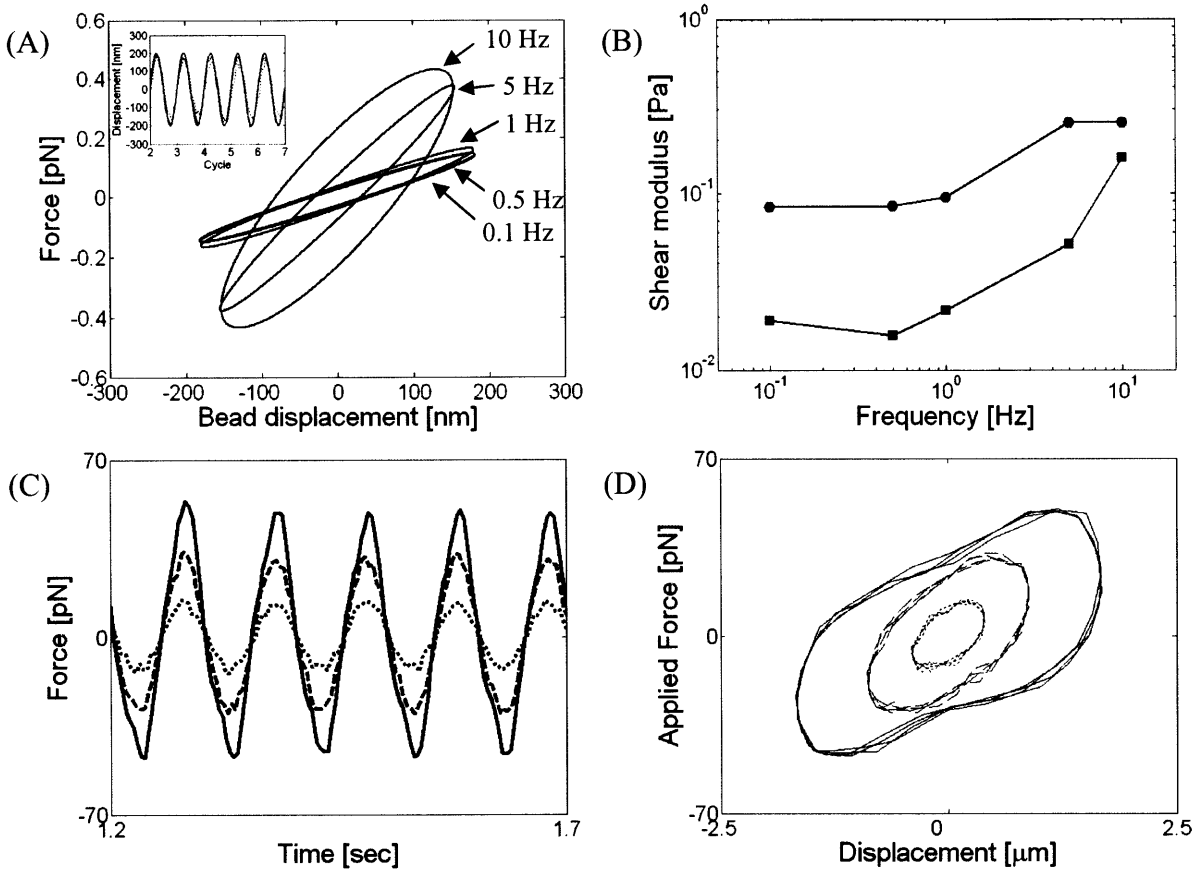

Figure 3.5 Active microrheology for F-actin networks cross-linked with filamin. (A) In the active measurement a sinusoidal force is applied to an embedded microsphere using optical tweezers. As the frequency increases, viscous dissipation increases as seen by a wider hysteresis in the force vs. bead displacement plot. *Inset*: sample traces of the position of the trapping laser (thick solid line) and the responses of a microsphere for 0.5Hz (thin solid line) and 5Hz (dotted line) excitation frequencies. (B) Storage (circle) and loss (square) moduli of F-actin network obtained using the active approach. (C) Mechanical response of cross-linked F-actin network subject to large oscillatory deformation. Symbols in the figures correspond to the applied deformation: 400nm (dotted line), 800nm (dashed line), and 1600 nm (solid line). The force amplitude increases as the applied deformation increases. As indicated by the distortions in the force curves, the network exhibits a non-linear response at large deformation. (D) Corresponding Lissajous figure. The ellipse-shape Lissajous curve is deformed by the non-linear behavior at large deformation.

The effect on mechanical properties of cross-linking with filamin was studied using both active and passive techniques at C_A = 10μM. As filamin concentration is increased from R_f = 0.01 to 0.04, both G' and G'' increase over the entire frequency range (Fig. 3.6A). Relaxation frequency of the network (f_r), defined as the frequency when $G'(f_r) = G''(f_r)$, increases 23 fold as

R_f increases 4 times. Complex shear moduli obtained by active measurement at low strain exhibits a similar value to the passive result (Fig. 3.6B). Plateau storage shear modulus, G_0, estimated as that at the minimum value in G'' over the range of frequencies tested, also increases 14 fold as R_f increases.

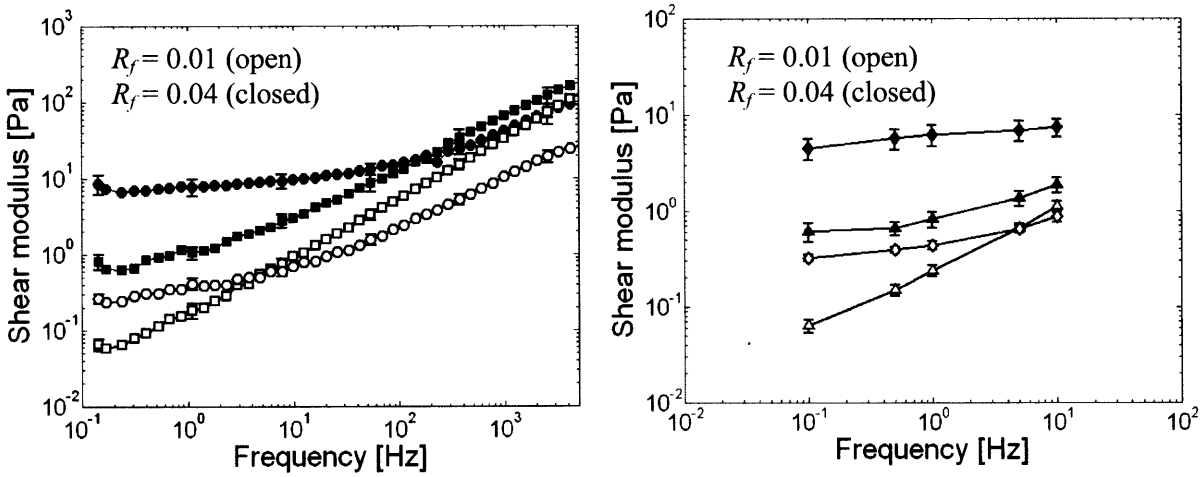

Figure 3.6 Effect of cross-linker fractional concentration, R_f, on complex shear modulus. Storage and loss shear moduli are estimated for C_A = 10μM at R_f = 0.01 (open) and R_f = 0.04 (closed). G' (circle) and G'' (square) by passive method, G' (diamond) and G'' (triangle) by active method. In both passive (A) and active (B) measurements, shear moduli increase as R_f increases.

3.3.2 Effect of α-actinin on F-actin Network

α-actinin/F-actin gels are prepared by polymerizing actin with α-actinin and gelsolin ([actin]/[gelsolin] = 250). They are visualized by confocal microscopy to investigate effects of bundling on F-actin network microstructure. For F-actin organized by α-actinin, as the relative concentration of α-actinin (R_α) to the fixed concentration of actin (C_A = 10μM) increases, the degree of bundling increases as noticed by relative intensity of the filaments in the confocal images (Fig. 3.7A). While a relatively homogeneous network is observed at low concentrations (R_α < 0.2), actin filaments form thick bundles at higher concentrations making the F-actin/α-actinin structure inhomogeneous. In the magnified image (Fig. 3.7B) of R_α = 0.2 in Fig. 3.7A, embedded bundles of actin filament stand out compared to surrounding actin filaments.

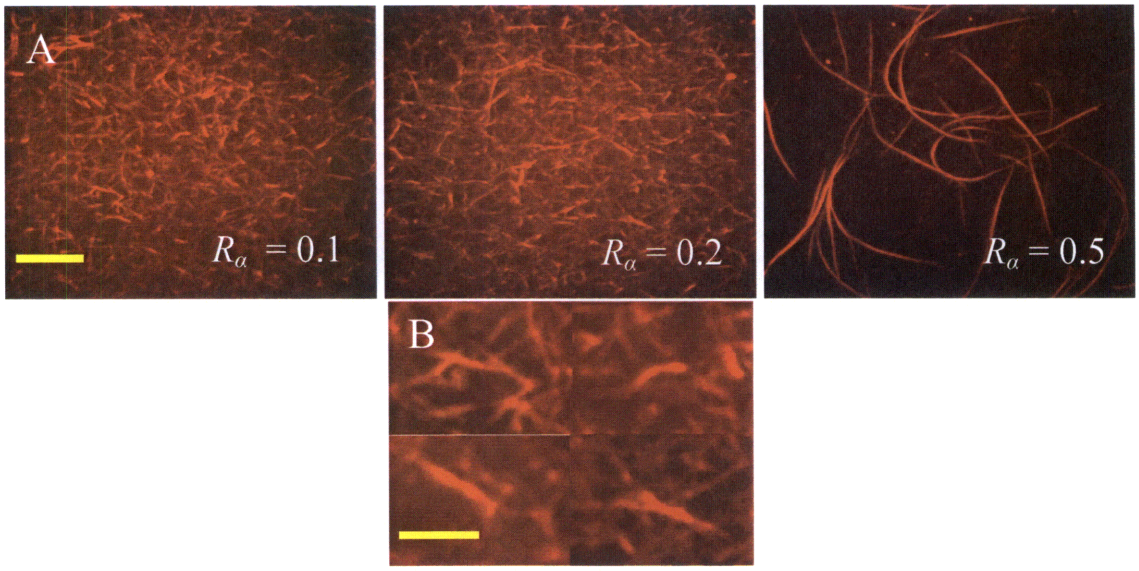

Figure 3.7 Confocal microscopy of F-actin organized by α-actinin. (A) Images of F-actin organized with various concentrations of α-actinin (scale bar, 10μm). Degree of bundling increases as the concentration of α-actinin increases relative to the concentration of actin. (D) Higher magnification images of filaments with R_α = 0.02 showing the evolution toward more highly bundled filaments (scale bar, 2μm).

In contrast to filamin/F-actin network, mesh size of F-actin/α-actinin networks increases with the concentration of α-actinin (Fig. 3.8). As more filament bundles are formed with increasing R_α, bundling by α-actinin increases the mesh size of the F-actin network. The degree of filament bundling is represented as the normalized intensity value of the filaments (Fig. 3.8C). The bundled structures observed at high concentration of α-actinin increases the degree of heterogeneity of the network.

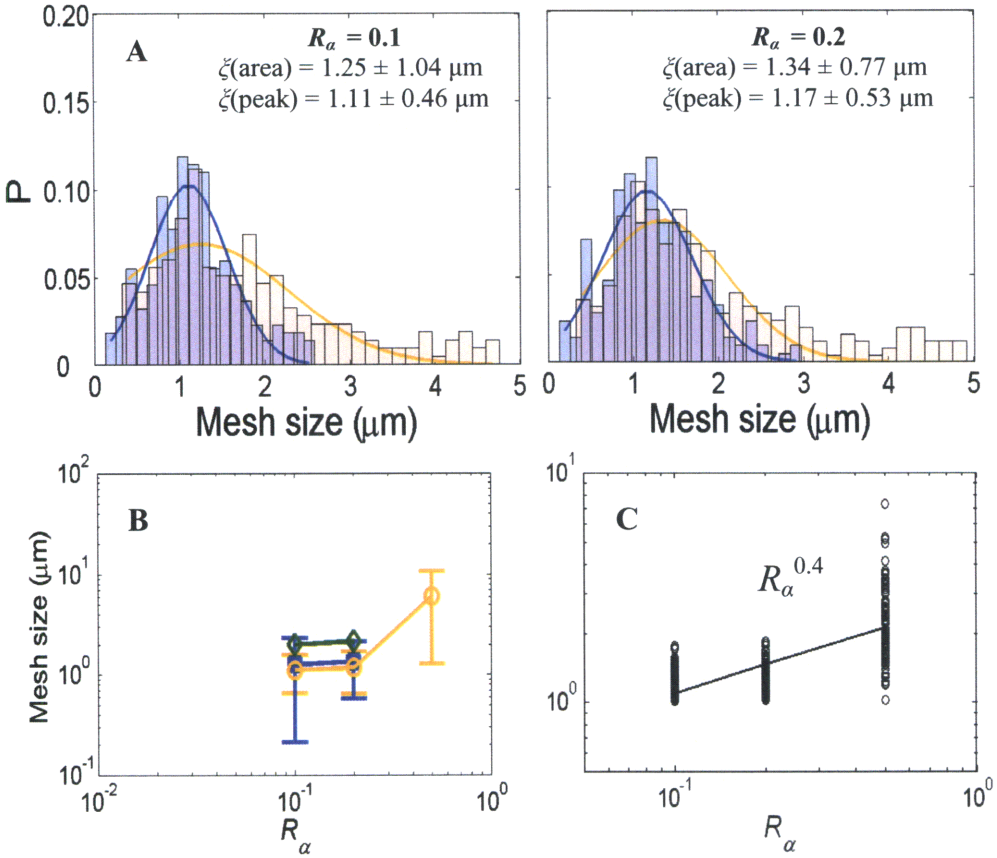

Figure 3.8 Microstructural characterization for α-actinin/F-actin networks. (A) Distributions of mesh size, ξ, in the F-actin networks organized by α-actinin at various R_α. (B) Mean and standard deviation of the mesh size plotted against R_α. As R_α increases, more filament bundles are formed and the mesh size of the networks increases. (C) Distributions of normalized filament intensity of the filaments in the F-actin networks at various R_α.

3.3.3 Effect of Gelsolin on F-actin Network

We investigate the effect of mean filament length on mechanical properties and microstructure of cross-linked F-actin networks by using a capping and severing ABP gelsolin. First, we characterize the length of actin filaments by using TIRF microscopy. Biotinylated actin ([nonlabeled actin]:[biotin-actin] = 5:1) is polymerized in the absence and presence of gelsolin, and labeled with Alexa-Fluor 555 phalloidin (A34055; Invitrogen, Carlsbad, CA). In the addition of gelsolin, the molar ratio of gelsolin to actin is 1:1000. For visualization, they are immobilized

on a streptavidin-coated glass surface. As shown in Fig. 3.9, most of actin filaments polymerized in the absence of gelsolin are much longer than those polymerized in the presence of gelsolin.

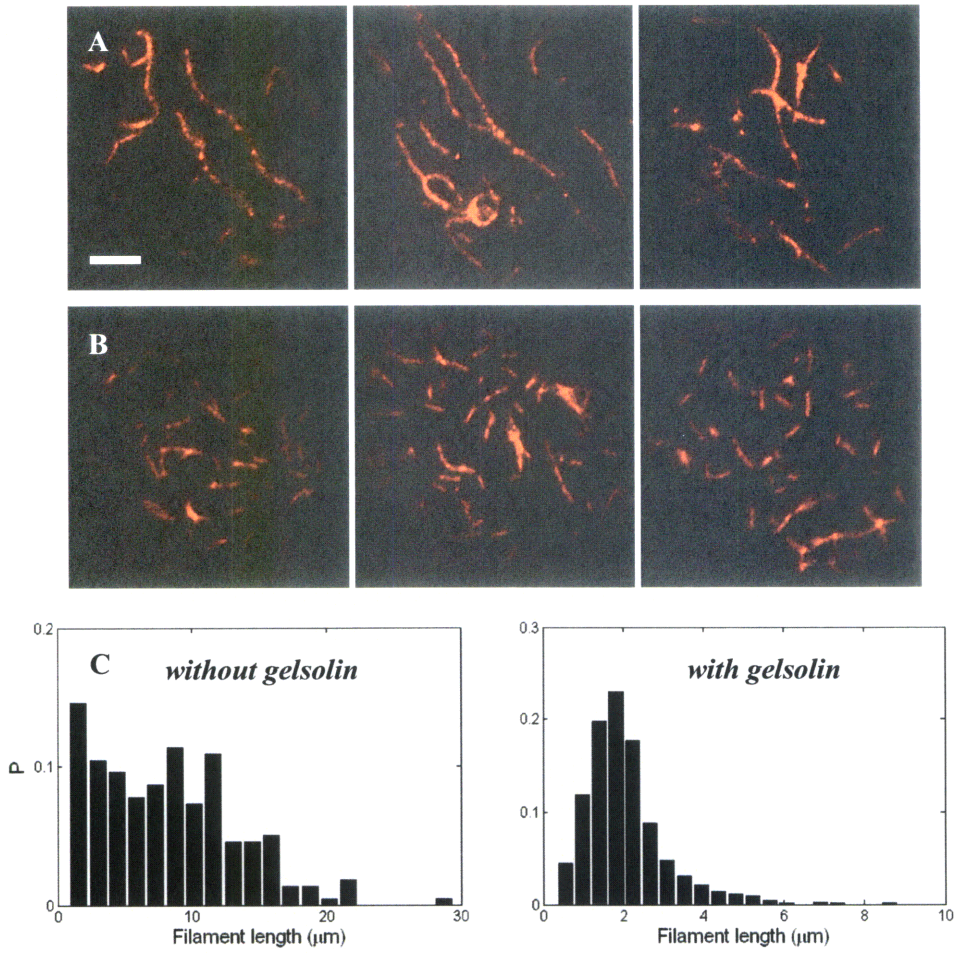

Figure 3.9 Effect of gelsolin on filament length. Micrographs of surface bound single actin filaments labeled with Alexa-Fluor 555 phalloidin (scale bar, 5 μm). Actin filaments polymerized in the absence (A) and presence (B) of gelsolin exhibited clear differences in filament length. (C) Length distributions of actin filament measured from micrographs.

From the length distributions of actin filaments measured from micrographs, number-average length (L_n) and weighted-average length (L_w) are calculated by

$$L_n = (\sum N_i L_i)/(\sum N_i) \tag{3.1}$$

$$L_w = (\sum N_i L_i^2)/(\sum N_i L_i) \tag{3.2}$$

where L_i is the filament length and N_i is the number of filament of L_i (44). The addition of gelsolin decreased L_n from 8.2 ± 5.2μm to 2.2 ± 1.4μm. However, the ratios of L_w to L_n for actin

filaments in the presence and absence of gelsolin were 1.3 and 1.4, respectively, indicating the shapes of the distributions were similar. Taking the gelsolin concentration added to the actin into account, the decrease of the filament length was very close to the measurement by Janmey et al. (44). We also visualize cross-linked F-actin networks (c_A = 10μM, R_f = 0.01) organized by actin filaments with different average lengths, too. TIRF images show that actin filaments in networks polymerized without gelsolin (Fig. 3.10A) are much longer than those in networks polymerized with gelsolin (Fig. 3.10B). In the confocal images, some of long filaments are found only in the network without gelsolin, too (Fig. 3.10C). Mesh sizes in the network appear to be independent of gelsolin, and therefore, independent of the length of the actin filaments forming the network (Fig. 3.10E and F).

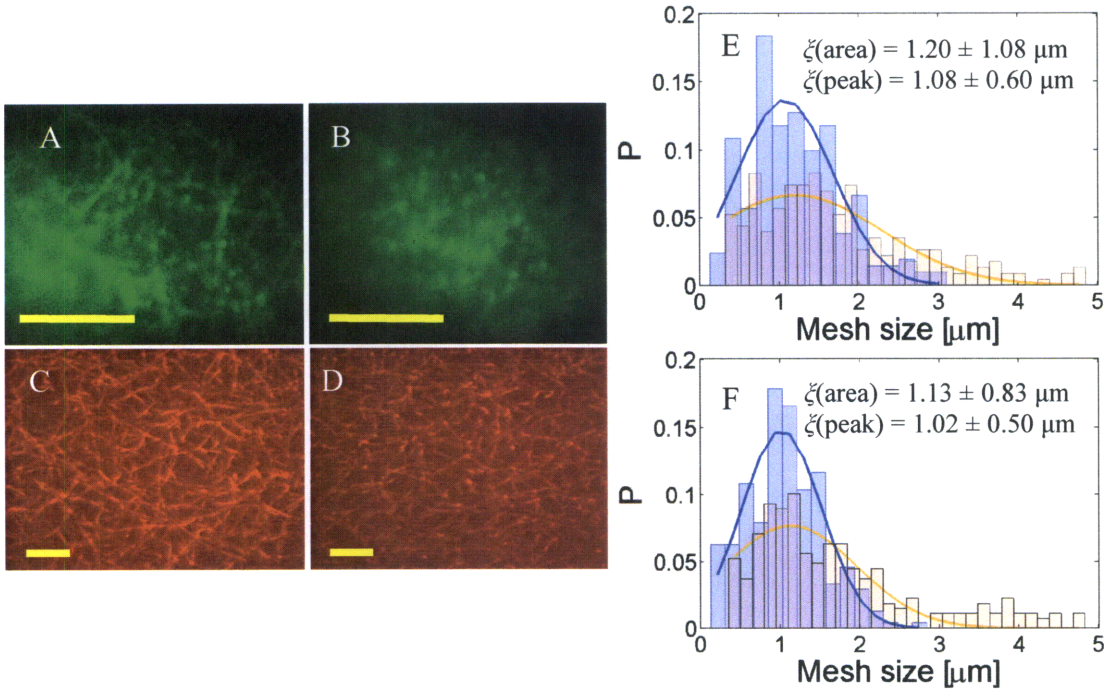

Figure 3.10 Effect of gelsolin on microstructure and microrheology of F-actin network. TIRF (A,B) and confocal microscopy (C,D) images of F-actin/filamin network polymerized in the absence (A,C) and presence (B,D) of gelsolin (scale bar, 10μm). Although longer actin filaments are observed in the F-actin network polymerized in the absence of gelsolin, the mesh size distributions obtained by two different methods (see text for details) are similar for the network without gelsolin (E) and the network with gelsolin (F).

Mechanical properties of the F-actin networks organized in the presence and absence of gelsolin were estimated using the microrheology techniques developed in Chapter 2. In both passive and active measurements, the F-actin network polymerized in the absence of gelsolin exhibited the smaller G' and G''. It suggests that the network elasticity decreases as the length of actin filaments decreases by adding gelsolin. Plateau values seen in the MSD curves also showed that greater steric and elastic constraints are imposed in networks polymerized with longer actin filaments (*inset* in Fig. 3.11A). The relaxation times ($= f_r^{-1}$) are approximately 0.2 sec for both short- and long-filament networks.

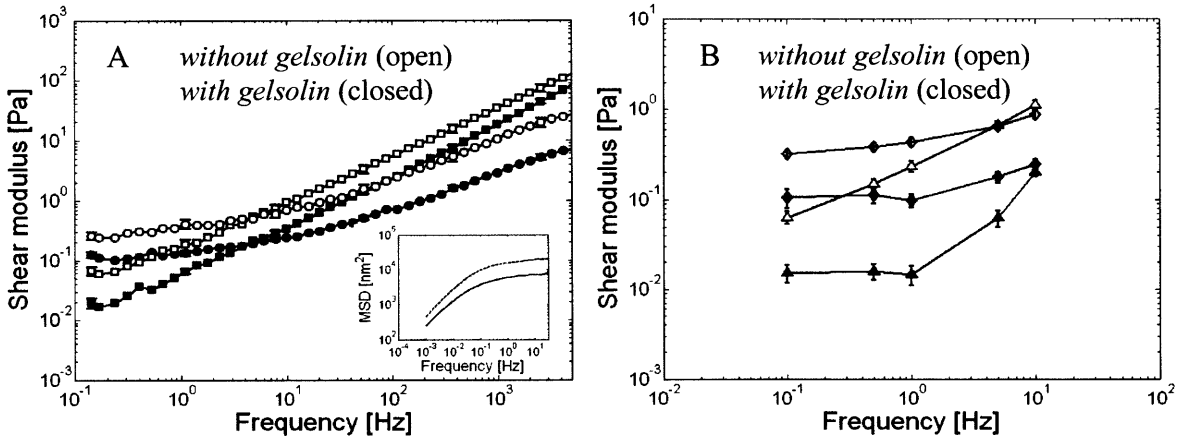

Figure 3.11 Frequency dependent shear moduli of F-actin networks without gelsolin (open symbols) and with gelsolin (closed symbols) are measured using passive (A) and active (B) methods. G' (circle) and G'' (square) by passive method, G' (diamond) and G'' (triangle) by active method. The moduli obtained from the two methods exhibit similar results. Both G' and G'' are higher for the F-actin network polymerized in the absence of gelsolin (longer filaments) over the entire frequency range. *Inset* in (A): MSD curves for the F-actin networks in the presence (dotted) and absence (solid) of gelsolin.

To probe the mechanical response of F-actin networks to different sized particles, networks are also probed using microspheres with a = 1 μm. With the large microspheres as well, both G' and G'' measured by the active method agrees well with corresponding values obtained with passive rheology. Agreement between the two methods does not depend on the average length of filaments as compared in Figs. 3.12A (no gelsolin) and Fig. 3.12B (with

gelsolin). Relaxation times for both networks are similar, ~1 sec, but larger than the 0.2 sec relaxation time found in measurements with the smaller microsphere, a = 0.5μm. G_0 decreases as the average length of actin filament decrease (Fig. 3.12C). Although there is a discrepancy in G_0 between a = 0.5 μm and a = 1 μm measurements, the G_0 of the network without gelsolin is higher than that with gelsolin indicating that, when the network is formed by long filaments, fluctuations of the embedded microsphere are more confined.

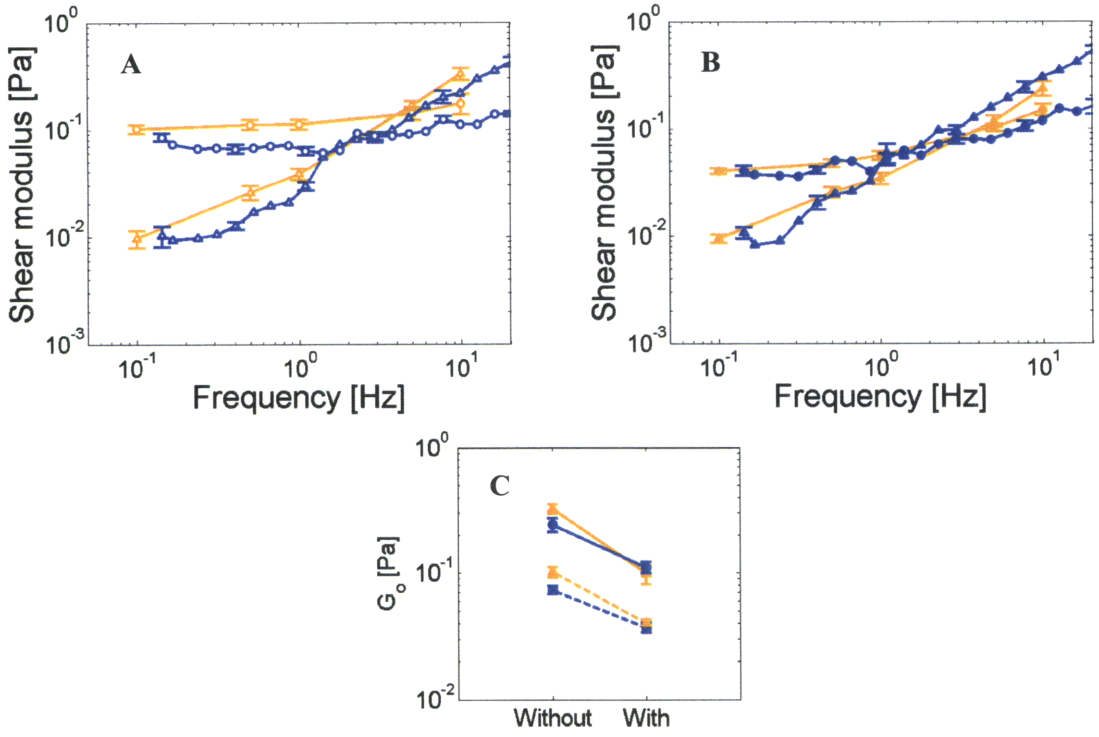

Figure 3.12 Effects of probe size, filament length and measurement method on microrheology of cross-linked F-actin networks. Using a larger microsphere with radius a = 1μm, the complex shear moduli are estimated for the F-actin networks polymerized in the absence (A) and presence (B) of gelsolin. G' (circle) and G'' (triangle) by passive (blue) and active (orange) methods. Both passive and active measurements exhibit similar results independent of filament length. (C) Comparison of G_0 obtained by passive (blue circles) and active (orange triangles) measurements for the F-actin network with and without gelsolin. F-actin networks formed with short filaments are less stiff than those formed with long filaments. The decrements in G_0 are similar, independent of the microsphere's dimension (solid: a = 0.5μm; dotted: a = 1μm).

3.4 Discussion

In these experiments, we sought to study the effects of actin filament length, method of measurement (active vs. passive and small vs. large probe), degree of cross-linking, and strain amplitude on the frequency-dependent shear moduli of reconstituted actin gels using a carefully characterized system. Other studies have typically reported the effects of these parameters individually, and not many have studied the effect of filament length and strain-dependent rheology at the microscale. In addition, because minor differences in experimental protocol can lead to significant effects on measured moduli, we felt that it would be useful to have one complete set of measurements examining these multiple effects in a single system under tight experimental control.

Passive and active microrheology produce similar results for F-actin networks, provided the strains are small and in the linear regime. We employed two complementary methods to measure gel microrheology using optical tweezers. In the passive approach, frequency–dependent complex modulus was obtained over 4 decades in frequency by tracking thermal fluctuations of microspheres embedded in F-actin networks. The F-actin networks exhibit a plateau modulus (G_0) and a low G'' indicative of solid-like behavior at low frequencies. However, at high frequencies, G' exhibits a significantly greater frequency-dependence compared to the weak power law observed in cells (13, 45). In active measurements, the complex shear modulus is estimated by monitoring the mechanical response to the external force using optical tweezers. Previous studies showed that actin and myosin networks exhibit different viscoelastic responses when measured by the active method compared to the passive method, which was attributed to tension in the filaments induced by myosin (34). Since our system lacks motor proteins and applied strains are comparable to the plateau values of MSD at long time, the active and passive

results show good agreement for our cross-linked F-actin networks. However, the mechanical moduli (G' and G'') of the *in vitro* F-actin networks are three to five orders of magnitude smaller than those of living cells (12, 13, 46). This large discrepancy can be attributed to the internal stresses in living cells arising from acto-myosin contraction, external adhesion, and potentially to the complexity of the cytoskeletal structure with the wide variety of ABPs found in a cell (34, 46). It is also important to note that our approaches are limited in that they probe local mechanical properties by monitoring the motion of a single particle. Single particle microrheology can be sensitive to the local environment of the embedded particle and the degree to which the particle is coupled to the matrix. Two-point microrheology overcomes these limitations by measuring the correlated motion of two particles (47). As the length scale in the correlated motion is much larger than the size of the particle, two-point microrheology better reflects the bulk mechanical properties.

Employing the active measurement, we obtain the microscale non-linear behavior of cross-linked F-actin network. When the loading is increased, in the present experiment by increasing the amplitude of stage oscillation, a force response for the F-actin network become non-linear resulting in a distortion of the Lissajous curve. This strain-dependent non-linear behavior at the microscale is qualitatively analogous to the mechanical properties of reconstituted actin gels under prestress probed at the macroscale (15, 26, 27) in that G' is observed to increase as the bead amplitude increases. However, the non-linearity observed in the present measurements is considerably smaller. The difference can be attributed to several reasons. It should be noted that the strain and stress estimated here are not the differential values which has been measured in the macroscopic measurement with prestress using a rheometer (15) , but rather, the total amounts in the response to progressively larger sinusoidal oscillations of the

bead. Also, in the macroscopic measurements, applied shear stress produces a non-affine deformation of the cross-linked F-actin network (48, 49) inducing extension in some actin filaments and compression in others. As the thermal undulation in the stretched filaments is reduced, network elasticity increases. By contrast, in our microscale measurements, local excitation using a probe particle deforms the nearby filaments within a characteristic distance comparable to the size of the probe particle. While the macroscale method estimates global properties by measuring the response of the entire network, the active microrheology probes local mechanical properties by obtaining the network response to a force which is in a physiological range. Therefore, our techniques can be applied to obtain a network response when cross-linking ABP undergoes unbinding or unfolding as observed in the single molecule assay (50). Further study of strain-dependent microrheology for F-actin networks cross-linked with other ABPs will provide a better understanding of the microscopic origin of non-linear behavior in the F-actin networks.

The effects of ABP concentration are similar at the microscale to previous macroscale measurements. As filamin concentration increases for a given concentration of actin, G_0 increases 14 times as R increases 4 times. This is approximately consistent with previous macroscale studies showing a scaling of $G_0 \sim R^{\beta}$, with typical exponent, β from 0.4 to 2 depending on the ABP used (17, 18, 43). For example, a short and rigid ABP, scruin, has a scaling exponent of 2 and a heavy meromyosin (HMM) network follows the scaling $G_0 \sim R^{1.2}$. As the dependence of G_0 on R reflects the molecular characteristics of the ABP (e.g., molecular structure, binding affinity and degree of dimerization (18)), filamin would appear to behave in a manner more similar to scruin than to HMM. It should be noted, however, that the scaling of the modulus as a function of actin binding protein varies different depending on the magnitude of R

(26, 42). For the pre-stressed and highly cross-linked actin networks, the moduli are remarkably insensitive to concentrations of actin and actin binding protein (15).

Elasticity of the F-actin network is influenced by the length of actin filaments constituting the network. Gelsolin, a severing and capping protein, was used to regulate the contour length of actin filaments (44) and mechanical properties of the network polymerized in the absence and presence of gelsolin were compared (Fig. 3.11). *In vitro*, F-actin polymerizes to contour lengths, L, of about 2 to 70μm with a mean length of 20μm (51) and the average length of actin filaments can be adjusted by the concentration of gelsolin (44). The gelsolin concentration used in these experiments regulates L to be 2μm, consistent with Janmey et al (44). G_o of cross-linked F-actin networks formed in the absence of gelsolin is higher than that in the presence of gelsolin, similar to the behavior seen with entangled F-actin solutions (16, 20). However, the effect on G_0 of gelsolin is smaller for cross-linked F-actin networks than for entangled F-actin solutions. While the elastic response of F-actin solutions is dominated by the entanglement length, L_e, the elasticity of a F-actin network is determined by the distance between cross-link points, L_c. Assuming affine deformations , the plateau storage shear modulus G_0 of a cross-linked F-actin network can be described by (52)

$$G_0 \sim \frac{\kappa^2}{kT}\xi^{-2}L_c^{-3}, \tag{3.3}$$

where ξ is the mesh size, κ is the bending modulus of actin filament, k is the Boltzmann constant, and T is the absolute temperature. If the networks with filamin are mostly cross-linked with negligible bundling, κ and ξ should not change with filament length as confirmed by our confocal images (Fig. 3.2) and their characterizations (Fig. 3.3). L_c in Eq. 3 is determined by the concentration of cross-linking protein (17). We note, however, that Eq. 3 fails to account for changes in filament length. When the length of actin filaments is much larger than the mesh size,

most ABPs cross-link filaments at the intersection points forming a well-defined highly interconnected network. In contrast, if the length of actin filaments is comparable to or only slightly greater than the mesh size, many loose ends exist, which contribute little to the overall stiffness of the network. (Imagine the filaments of Fig. 3.13A being cut at random locations.). Reducing the length of individual filaments leads to more loose ends in the network configuration thereby altering network connectivity. The resulting effect is a network that is less capable of withstanding stress, and therefore exhibits a smaller modulus. Our findings therefore suggest that the mechanical response of cross-linked actin networks to the external force is affected by filament length, which affects network connectivity, as well as L_c.

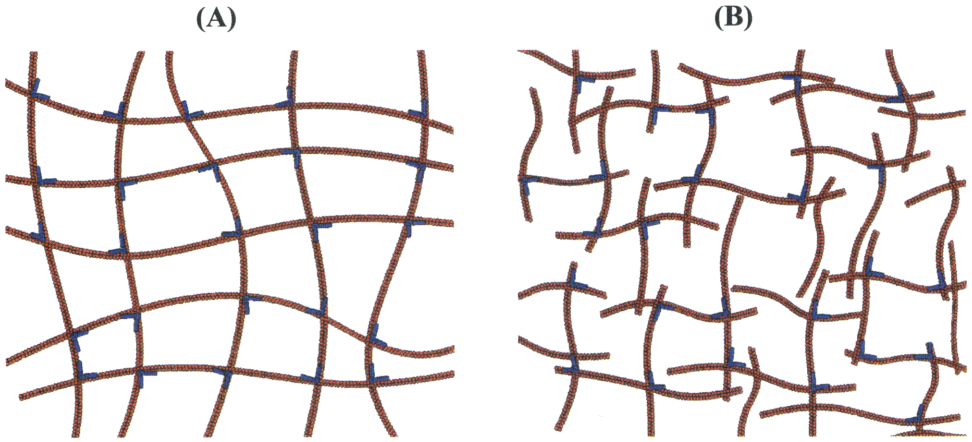

Figure 3.13 Schematic illustrations of F-actin network organized by long (A) and short (B) actin filaments at identical concentrations of actin filaments and cross-linkers. In the network with long filaments (A), most filaments are attached at each crossing point by ABPs that are arranged regularly along the filaments. In contrast, the network with short filaments (B) forms incomplete loops with many loose ends, and their arrangement is random compared to the network in (A). This difference in structure would cause the network with short filaments to be less stiff than the one with long filaments.

Size of the probe particle also has an effect on measured network viscoelasticity. To further investigate the effects of characteristic length scales in F-actin network microrheology, mechanical properties of F-actin network were probed using a larger microsphere (a = 1 μm) and the results compared to those obtained with the smaller one (a = 0.5 μm). G_0 of the network with

L = 20 μm is consistently higher than that with L = 2 μm, however, values of G_0 are approximately 2~3 fold lower when measured using the larger microsphere as compared to the smaller one (Fig. 3.12C). That is, the elastic modulus of the F-actin network probed by the tracer whose diameter is comparable to the length of actin filaments is smaller than that measured by the probe tracer which is much smaller than the filament length. Interestingly, a significant transition in G_0 has been observed in entangled F-actin solutions when the average length of actin filaments is close to the diameter of the microsphere used in the measurements (16, 20), which could, in both cases, be attributable to a local depletion zone created in the vicinity of a probe tracer. In network formation, long actin filaments are depleted from the immediate vicinity of the microsphere through a combination of their high bending stiffness and steric exclusion. Therefore, the microsphere resides in an environment that is more viscous than elastic leading to a reduced G' but having little impact on G''. This is reflected in the observation that the larger microsphere exhibits a smaller relaxation frequency (f_r) at which G' = G''. Also the larger microsphere exhibits a scaling $G'' \sim f^{0.85}$ at high frequency indicating that the local environment behaves in a manner more reminiscent of a Newtonian fluid as compared to the scaling $G'' \sim f^{0.75}$ observed with a = 0.5 μm and L = 20 μm.

In summary, we developed the methods of passive and active microrheology using optical tweezers and observed the mechanical properties of homogeneous F-actin networks. The effects of length scale on both network elasticity and microstructure were investigated by controlling actin filament length and probe size. The microscale non-linear behavior of cross-linked F-actin network is obtained using the active measurement at high strain. The results presented here and future studies with different actin binding proteins will provide insight into the microscopic origin of mechanical properties in cross-linked F-actin network.

3.5 References

1. Janmey, P. A. & McCulloch, C. A. (2007) Cell mechanics: integrating cell responses to mechanical stimuli *Annu Rev Biomed Eng* 9, 1-34.
2. Khan, S. & Sheetz, M. P. (1997) Force effects on biochemical kinetics *Annu Rev Biochem* 66, 785-805.
3. Vogel, V. & Sheetz, M. (2006) Local force and geometry sensing regulate cell functions *Nat Rev Mol Cell Biol* 7, 265-75.
4. Bartles, J. R. (2000) Parallel actin bundles and their multiple actin-bundling proteins *Current Opinion in Cell Biology* 12, 72-78.
5. Stossel, T. P., Fenteany, G. & Hartwig, J. H. (2006) Cell surface actin remodeling *J Cell Sci* 119, 3261-4.
6. dos Remedios, C. G., Chhabra, D., Kekic, M., Dedova, I. V., Tsubakihara, M., Berry, D. A. & Nosworthy, N. J. (2003) Actin binding proteins: regulation of cytoskeletal microfilaments *Physiol Rev* 83, 433-73.
7. Pollard, T. D. & Cooper, J. A. (1986) Actin and actin-binding proteins. A critical evaluation of mechanisms and functions *Annu Rev Biochem* 55, 987-1035.
8. Stossel, T. P., Condeelis, J., Cooley, L., Hartwig, J. H., Noegel, A., Schleicher, M. & Shapiro, S. S. (2001) Filamins as integrators of cell mechanics and signalling *Nat Rev Mol Cell Biol* 2, 138-45.
9. Feng, Y. & Walsh, C. A. (2004) The many faces of filamin: a versatile molecular scaffold for cell motility and signalling *Nat Cell Biol* 6, 1034-8.
10. Meyer, R. K. & Aebi, U. (1990) Bundling of actin filaments by alpha-actinin depends on its molecular length *J Cell Biol* 110, 2013-2024.
11. Wachsstock, D. H., Schwartz, W. H. & Pollard, T. D. (1993) Affinity of alpha-actinin for actin determines the structure and mechanical properties of actin filament gels *Biophys J* 65, 205-14.
12. Bausch, A. R., Moller, W. & Sackmann, E. (1999) Measurement of local viscoelasticity and forces in living cells by magnetic tweezers *Biophys J* 76, 573-9.
13. Fabry, B., Maksym, G. N., Butler, J. P., Glogauer, M., Navajas, D. & Fredberg, J. J. (2001) Scaling the microrheology of living cells *Physical Review Letters* 87, 148102.
14. Claessens, M. M. A. E., Tharmann, R., Kroy, K. & Bausch, A. R. (2006) Microstructure and viscoelasticity of confined semiflexible polymer networks *Nature Physics* 2, 186-189.
15. Gardel, M. L., Nakamura, F., Hartwig, J. H., Crocker, J. C., Stossel, T. P. & Weitz, D. A. (2006) Prestressed F-actin networks cross-linked by hinged filamins replicate mechanical properties of cells *Proceedings of the National Academy of Sciences of the United States of America* 103, 1762-1767.
16. Liu, J., Gardel, M. L., Kroy, K., Frey, E., Hoffman, B. D., Crocker, J. C., Bausch, A. R. & Weitz, D. A. (2006) Microrheology probes length scale dependent rheology *Physical Review Letters* 96, 118104.
17. Tharmann, R., Claessens, M. M. A. E. & Bausch, A. R. (2007) Viscoelasticity of isotropically cross-linked actin networks *Physical Review Letters* 98, 088103.
18. Wagner, B., Tharmann, R., Haase, I., Fischer, M. & Bausch, A. R. (2006) Cytoskeletal polymer networks: the molecular structure of cross-linkers determines macroscopic properties *Proc Natl Acad Sci U S A* 103, 13974-8.

19. Xu, J. Y., Tseng, Y. & Wirtz, D. (2000) Strain hardening of actin filament networks - Regulation by the dynamic cross-linking protein alpha-actinin *Journal of Biological Chemistry* 275, 35886-35892.
20. Schmidt, F. G., Hinner, B. & Sackmann, E. (2000) Microrheometry underestimates the values of the viscoelastic moduli in measurements on F-actin solutions compared to macrorheometry *Physical Review E* 61, 5646-5653.
21. Maggs, A. C. (1998) Micro-bead mechanics with actin filaments *Physical Review E* 57, 2091-2094.
22. Levine, A. J. & Lubensky, T. C. (2002) Two-point microrheology and the electrostatic analogy *Phys Rev E Stat Nonlin Soft Matter Phys* 65, 011501.
23. Morse, D. C. (1998) Viscoelasticity of concentrated isotropic solutions of semiflexible polymers. 2. Linear response *Macromolecules* 31, 7044-7067.
24. Schmidt, C. F., Barmann, M., Isenberg, G. & Sackmann, E. (1989) Chain Dynamics, Mesh Size, and Diffusive Transport in Networks of Polymerized Actin - a Quasielastic Light-Scattering and Microfluorescence Study *Macromolecules* 22, 3638-3649.
25. Gardel, M. L., Nakamura, F., Hartwig, J., Crocker, J. C., Stossel, T. P. & Weitz, D. A. (2006) Stress-dependent elasticity of composite actin networks as a model for cell behavior *Physical Review Letters* 96, 088102.
26. Gardel, M. L., Shin, J. H., MacKintosh, F. C., Mahadevan, L., Matsudaira, P. & Weitz, D. A. (2004) Elastic behavior of cross-linked and bundled actin networks *Science* 304, 1301-1305.
27. Chaudhuri, O., Parekh, S. H. & Fletcher, D. A. (2007) Reversible stress softening of actin networks *Nature* 445, 295-298.
28. Storm, C., Pastore, J. J., MacKintosh, F. C., Lubensky, T. C. & Janmey, P. A. (2005) Nonlinear elasticity in biological gels *Nature* 435, 191-4.
29. Janmey, P. A., Hvidt, S., Lamb, J. & Stossel, T. P. (1990) Resemblance of Actin-Binding Protein Actin Gels to Covalently Cross-Linked Networks *Nature* 345, 89-92.
30. Janmey, P. A., McCormick, M. E., Rammensee, S., Leight, J. L., Georges, P. C. & MacKintosh, F. C. (2007) Negative normal stress in semiflexible biopolymer gels *Nat Mater* 6, 48-51.
31. Brau, R. R., *et al.* (2007) Passive and active microrheology with optical tweezers *Journal of Optics a-Pure and Applied Optics* 9, S103-S112.
32. Addas, K. M., Schmidt, C. F. & Tang, J. X. (2004) Microrheology of solutions of semiflexible biopolymer filaments using laser tweezers interferometry *Physical Review E* 70, 021503.
33. Atakhorrami, M. & Schmidt, C. F. (2006) High-bandwidth one- and two-particle microrheology in solutions of wormlike micelles *Rheologica Acta* 45, 449-456.
34. Mizuno, D., Tardin, C., Schmidt, C. F. & MacKintosh, F. C. (2007) Nonequilibrium mechanics of active cytoskeletal networks *Science* 315, 370-373.
35. Wong, I. Y., Gardel, M. L., Reichman, D. R., Weeks, E. R., Valentine, M. T., Bausch, A. R. & Weitz, D. A. (2004) Anomalous diffusion probes microstructure dynamics of entangled F-actin networks *Physical Review Letters* 92, -.
36. Zuchero, J. B. (2007) In vitro actin assembly assays and purification from acanthamoeba *Methods Mol Biol* 370, 213-26.

37. Nakamura, F., Osborn, E., Janmey, P. A. & Stossel, T. P. (2002) Comparison of filamin A-induced cross-linking and Arp2/3 complex-mediated branching on the mechanics of actin filaments *Journal of Biological Chemistry* 277, 9148-9154.
38. Kwiatkowski, D. J., Janmey, P. A. & Yin, H. L. (1989) Identification of Critical Functional and Regulatory Domains in Gelsolin *Journal of Cell Biology* 108, 1717-1726.
39. Valentine, M. T., Perlman, Z. E., Gardel, M. L., Shin, J. H., Matsudaira, P., Mitchison, T. J. & Weitz, D. A. (2004) Colloid surface chemistry critically affects multiple particle tracking measurements of biomaterials *Biophysical Journal* 86, 4004-4014.
40. Brau, R. R., Tarsa, P. B., Ferrer, J. M., Lee, P. & Lang, M. J. (2006) Interlaced Optical Force-Fluorescence Measurements for Single Molecule Biophysics *Biophys J* 91, 1069-1077.
41. Overby, D., Ruberti, J., Gong, H. Y., Freddo, T. F. & Johnson, M. (2001) Specific hydraulic conductivity of corneal stroma as seen by quick-freeze/deep-etch *Journal of Biomechanical Engineering-Transactions of the Asme* 123, 154-161.
42. Luan, Y., Lieleg, O., Wagner, B. & Bausch, A. R. (2008) Micro- and macrorheological properties of isotropically cross-linked actin networks *Biophys J* 94, 688-93.
43. Shin, J. H., Gardel, M. L., Mahadevan, L., Matsudaira, P. & Weitz, D. A. (2004) Relating microstructure to rheology of a bundled and cross-linked F-actin network in vitro *Proc Natl Acad Sci U S A* 101, 9636-9641.
44. Janmey, P. A., Peetermans, J., Zaner, K. S., Stossel, T. P. & Tanaka, T. (1986) Structure and Mobility of Actin-Filaments as Measured by Quasi-Elastic Light-Scattering, Viscometry, and Electron-Microscopy *Journal of Biological Chemistry* 261, 8357-8362.
45. Hoffman, B. D., Massiera, G., Van Citters, K. M. & Crocker, J. C. (2006) The consensus mechanics of cultured mammalian cells *Proceedings of the National Academy of Sciences of the United States of America* 103, 10259-10264.
46. Wang, N., Tolic-Norrelykke, I. M., Chen, J., Mijailovich, S. M., Butler, J. P., Fredberg, J. J. & Stamenovic, D. (2002) Cell prestress. I. Stiffness and prestress are closely associated in adherent contractile cells *Am J Physiol Cell Physiol* 282, C606-16.
47. Crocker, J. C., Valentine, M. T., Weeks, E. R., Gisler, T., Kaplan, P. D., Yodh, A. G. & Weitz, D. A. (2000) Two-point microrheology of inhomogeneous soft materials *Phys Rev Lett* 85, 888-91.
48. Head, D. A., Levine, A. J. & MacKintosh, E. C. (2003) Deformation of cross-linked semiflexible polymer networks *Physical Review Letters* 91, 108102.
49. Onck, P. R., Koeman, T., van Dillen, T. & van der Giessen, E. (2005) Alternative explanation of stiffening in cross-linked semiflexible networks *Physical Review Letters* 95, 178102.
50. Ferrer, J. M., Lee, H., Chen, J., Pelz, B., Nakamura, F., Kamm, R. D. & Lang, M. J. (2008) Measuring molecular rupture forces between single actin filaments and actin-binding proteins *Proc Natl Acad Sci U S A* 105, 9221-6.
51. Kaufmann, S., Kas, J., Goldmann, W. H., Sackmann, E. & Isenberg, G. (1992) Talin anchors and nucleates actin filaments at lipid membranes. A direct demonstration *FEBS Lett* 314, 203-205.
52. Mackintosh, F. C., Kas, J. & Janmey, P. A. (1995) Elasticity of Semiflexible Biopolymer Networks *Physical Review Letters* 75, 4425-4428.

4 Correlating Mechanical Response of F-actin Network with Single Molecule Interaction

The actin cytoskeleton has long been a focus of attention due to its biological significance and unique rheological properties. Although F-actin networks have been extensively studied experimentally and several theoretical models have been proposed, the detailed molecular interactions between actin binding proteins (ABPs) and actin filaments that regulate network behavior remains unclear. In this Chapter, we correlate the mechanical behavior of the F-actin network with the molecular interactions between actin and ABP. In studies at the network level, we obtain mechanical properties of cross-linked F-actin networks as a function of strain and response of the network to a local excitation. At the critical force at which the network elasticity decreases, the network response also exhibits abrupt transitions indicative of the rupture or unfolding of cross-links. In studies at single molecule level, using an *in vitro* assay that allows direct measurements on the bond between one actin cross-linking protein and two actin filaments, we demonstrate the force-induced unbinding and unfolding of filamin. The critical forces prove to be similar, 70 ± 23 pN for unbinding and 57 ± 19 pN for unfolding, suggesting that both are important mechanisms governing cytoskeletal rheology. The forces at the transitions in the network responses show the similar loading rate dependence to the molecular unbinding force, suggesting that they are originated from rupture at cross-links. Also, we test the reversibility of the mechanical properties of F-actin networks cross-linked with filamin and streptavidin, and provide additional proof that the strain-softening of F-actin network is caused by the force-induced rupture at cross-link. These measurements are interpreted with the aid of a computational simulation of the experiment to provide greater insight into physical mechanisms.

4.1 Background

Actin is the most abundant protein found in eukaryotic cells. Actin binding proteins (ABPs) regulate the assembly of actin filaments (F-actin) into various structures that provide physical support for the cell and play important roles in numerous cellular processes. Cytoskeletal rheology has captured the interest of many researchers because of its importance in telegraphing numerous biological processes, but also due to the rich variety of observed behavior. The network is highly nonlinear; under large deformation, the elastic modulus increases with applied stress, while under small deformation, the network response is linear. At small amplitudes, the complex shear modulus *in vivo* typically exhibits a weak power law, undergoing a transition from primarily elastic behavior at low frequencies to one dominated by viscous effects at high frequencies (1, 2). Attempts to reproduce these characteristics in the linear regime using *in vitro* systems (3-5), typically a reconstituted actin gel with one or more cross-linking proteins present, have met with limited success. Early experiments found a much higher frequency dependence with values of shear modulus that were orders of magnitude lower than those observed in cells. More recently, it has been shown that network prestrain plays a critical role, stiffening the matrix to the point that moduli become comparable to the in vivo values (6, 7). Even then, however, the modulus exhibits a different frequency dependence, ranging from nearly constant value for the storage modulus (G') at low frequencies, with a gradual transition to a weak power law at higher frequencies. To complicate the situation further, different cross-linking proteins apparently affect the linear rheological behavior in different ways, depending in part on whether the network forms large-diameter bundles (stress fibers) (8), or organizes the actin filaments into a more orthogonal network (9). Also, the mechanical properties of ABP seem to be more important in determining the nonlinear behavior of F-actin network. Deletion of the hinge

domain in filamin significantly alters the nonlinear behavior of the cross-linked F-actin network (7). The experiments using various cross-linking constructs show that the detailed molecular structure determines a critical stress at which the network modulus decreases (10). Many of these fascinating characteristics remain unexplained, but have been a source of much recent debate.

A similar range of views also exist in the modeling community. Various models have been proposed and each has its own proponents. These can be classified into several broad categories, which can be characterized as the cellular solids model, the tensegrity model, and the biopolymer model. In the tensegrity model (11), an interaction is proposed between certain elements that are in tension and others that are under a compressive state. These latter could either be internal structures such as the microtubules or external tethering to a substrate or extracellular matrix. Theoretical descriptions of tensegrity show that the storage modulus depends primarily upon the level of prestrain in the network and is relatively independent of the properties of the matrix elements themselves. In contrast, the cellular solids model is based on earlier description of macroscopic fibrous materials (12, 13), in which the elastic behavior is entirely determined by the bending stiffness of the elastic fibers and the fiber concentration. Neither of these models has been extended to include viscoelastic behavior, so they provide no information on the unique frequency dependence described above. One can also view the actin network as a semi-dilute solution of polymers, the biopolymer model, with or without cross-links, that are thermally-active. Because of the long persistence length of actin, the individual filaments of an actin gel exhibit slight deviations from straight segments between cross-link points, but these slight fluctuations provide for the network elasticity at low strains. Some recent models have incorporated the effects of prestrain, and produce predictions that capture much of the linear behavior (14).

Based on these previous experimental studies and models, despite many fundamental differences, the prevailing view is that prestrain is a critical factor. In living cells, this can result from a combination of external tethering via an assortment of adhesion receptors and internal contraction due to the activity of myosin motors and other forces that associate with the actin filaments. In this highly prestrained condition, the cross-links are subjected to relatively high loads, likely sufficient to cause them to either unfold or unbind, giving rise to entirely new phenomena such as matrix irreversibility and network remodeling under stress. While unfolding and unbinding can both give rise to a certain degree of hysteresis, the underlying mechanisms and relevant time scales will differ. For example, if a strained cross-link unbinds, the filaments will locally rearrange, and the "dangling" cross-linking protein might form a new bond at a different location in the network, potentially (but not necessarily) resulting in a new equilibrium state of a remodeled network. If this same cross-linker unfolds, when the stress is released, the protein may refold given sufficient time, and return to the original state. Both the times scales for reaching equilibrium and the potential for remodeling differ in these two scenarios, and it therefore becomes an important question as to whether unbinding or unfolding is the dominant behavior in high stress states, especially given the perceived importance of high prestrain or prestress in living cells. Previously, the unfolding characteristic of filamin was well described by the measurements using AFM (15, 16). The single molecule assay measured both unbinding and unfolding forces of a filamin cross-linking two actin filaments (17). However, understanding the dominant mechanism of actin-ABP complex in a stressed F-actin network still remains challenging.

In this Chapter, we explore the question of whether unfolding or unbinding is more likely to occur in F-actin network subject to external deformation. In order to address this question, we

investigate the mechanical behavior of both cross-linked F-actin network and actin-ABP complex. Using the active microrheology, we estimate the mechanical properties of cross-linked F-actin network at various strains and obtain the microscale nonlinear behavior. The network elasticity increases up to a critical level of strain and then decreases suggestive of local collapse of the network as higher strains are applied. We also develop other two methods employing an optical trap that provide insight into single molecule events. One is a single molecule pulling assay in which a single actin filament forms a tether with another actin filament via one specific cross-linker, and an optical trap is used to precisely control the applied force. Another method is introduced, in which the mechanical response of a reconstituted actin gel to a local force is monitored, providing insights into single molecule events in a 3D network. In the isolated single molecule measurement, unfolding is distinguished from unbinding by the sawtooth pattern with intervals ~30nm observed in the force-extension curves. Both unfolding and unbinding occur at similar levels of force, but unbinding is more frequent than unfolding. Further analysis of measurements at different pulling angles suggests that torsion or shear induce rupture at smaller force. Compared with the results from single molecule assays, the responses of an F-actin network also show similar transitions in the force-extension curves indicating that similar events, both bond rupture and unfolding, can be identified. The responses of the network to a large deformation are characterized in terms of critical force, transition displacement, and loading rate. By comparing the loading rate dependence of the transitions observed in the network responses with the single molecule unbinding events, we suggest that the network relaxation is originated from unbinding of cross-linker. The reversibility tests for the mechanical properties of cross-linked F-actin network support that network behavior is dominantly regulated by the cross-link rupture.

4.2 Methods and Materials

4.2.1 Active Microrheology at High Strain

The active microrheology developed in Chapter 2 is used to estimate the mechanical properties of F-actin network at various strains. A microsphere embedded in the F-actin network is trapped by the tweezers and a sinusoidal force is applied to the network by displacing the sample relative to the trap. The stage is moved with amplitudes of ±0.2 – 2.0μm at a constant frequency of 10Hz to apply various strains to the F-actin network. The increment of the stage is either ±100 or ±200nm. Positions of both microsphere and stage are recorded simultaneously. The applied force is calculated from the displacement of the microsphere multiplied by the stiffness of the tweezers. Sample deformation is estimated by subtracting the displacement of the microsphere from the stage movement. We fit both the force and deformation to sinusoidal functions and the shear modulus G are estimated from the equation,

$$G = G' + iG'' = \frac{\bar{F}}{6\pi a \bar{x}}\left[\cos(\Delta\theta) + i\sin(\Delta\theta)\right] \tag{4.1}$$

where $\bar{F}$ is the amplitude of the applied force, $\bar{x}$ is the amplitude of the bead response, and $\Delta\theta$ is the phase delay between the $F(t)$ and $x(t)$. Shear moduli estimated at various strains yield strain-dependent mechanical properties for the F-actin network. Shear modulus and deformation of F-actin network are normalized by its initial value and size of the microsphere, respectively.

4.2.2 Protein Preparation

G-actin is prepared by dissolving lyophilized G-actin from rabbit skeletal muscle (Cytoskeleton Inc., Denver, CO) in fresh G-buffer [5 mM Tris-HCl, 0.2 mM $CaCl_2$, 0.5mM DTT, 0.2 mM ATP, pH 8.0] and incubated on ice for ~2 hours. For biotinylated actin filaments, 20 μl of 20μM nonlabeled actin monomer is mixed with 5 μl of 20 μM biotinylated actin (Cytoskeleton Inc.,

Denver, CO). Actin polymerization is initiated by adding a tenth of the final volume of 10× F-buffer [50 mM Tris-HCl, 500 mM KCl, 2 mM $MgCl_2$, 2 mM $CaCl_2$, 2 mM DTT, 5 mM ATP, 0.01% (w/v) NaN_3, pH 7.5]. Recombinant filamin A is purified from Sf9 cell lysates (18) and recombinant human gelsolin is produced in *Escherichia coli* (19). Both were stored at -80°C before use.

4.2.3 Attachment of Single Actin Filament to Microsphere

1-μm diameter, carboxylated polystyrene beads (Polysciences Inc., Warrington, PA) are coated with gelsolin as described in Suzuki et al. (20) with the 400 μg proteins: 5μl of 10mg/ml actin, 10μl of 5mg/ml gelsolin, 26μl of 10mg/ml bovine serum albumin (BSA), and 40ul of 1mg/ml rhodamine-BSA (See the details in Appendix). The gelsolin-coated beads are stored in a rotator at 4°C in the dark. 25μl bead solution is diluted with 25 μl of the buffer solution [25 mM imidazole-HCl (pH 7.4), 25 mM KCl, 4mM $MgCl_2$, 0.1 mM $CaCl_2$, 0.1 mM ATP, 1 mM DTT, and 0.04% NaN_3] and sonicated for 30 seconds. The bead solution is washed four times with 50μl of the same buffer by centrifugation at 6000rpm for 4 min. After the last centrifugation, the beads are resuspended with 10ul buffer solution and are mixed with 2.5ul of 5μM F-actin labeled with rhodamine-phalloidin. The mixture is incubated overnight in a rotator at 4°C in the dark. Under these concentrations of bead and F-actin, a microsphere bound to a single actin filament is obtained.

4.2.4 Single Molecule Assay

As described previously (17), single molecule (SM) assay was employed to probe molecular interaction between actin filament and ABP. Briefly, a custom-made flow chamber (25.8mm × 6 mm × 0.1mm) is prepared by attaching a KOH-etched coverslip to a microscope slide with double-sided tape. The sample is loaded from one end and the flow of sample solution is

facilitated by using a pipette tip connected to a vacuum pump. The experimental sample is prepared by the following procedure: (1) incubation of 2mg/ml biotinylated BSA in PBT [100 mM phosphate buffer (pH 7.5), 0.1% (vol/vol) Tween, pH 7.5]; (2) washing with PBT; (3) incubation of 0.1mg/ml streptavidin in PBT; (4) washing with 1× F-buffer containing with 3mg/ml BSA; (5) incubation of 50mM biotinylated actin filament in 1× F-buffer containing 3mg/ml BSA; (6) washing with 1× F-buffer containing 3mg/ml BSA; (7) incubation of 20nM filamin in 1× F-buffer with 3mg/ml BSA; (8) incubation of F-actin bound to gelsolin bead in a 1:100 dilution. 20uL of sample solution is loaded in each incubation step and 100μL of buffer is used in washing. Incubation steps are performed for 20 min in a dark, humidity-preserving chamber at room temperature. However, another washing with 40μL 1× F-buffer is added 20 seconds after flowing in actin filaments at step (5). As a result, the actin filaments bound on the streptavidin substrate are aligned along the flow direction, which would be a pulling direction. The flow chamber is sealed with nail polish to prevent evaporation of the sample during experiment.

Beads tethered to the actin filament are readily distinguished from other beads by a confined movement. Approximately 20 to 30 tethered beads are observed per field of view. Optical tweezers force spectroscopy (OTFS) is used to probe interaction between the actin filament and filamin. Tethered beads are located and centered in the detection zone using an automated centering routine and are captured by the stationary trapping laser with the stiffness ranging from 0.5 to 0.75pN/nm. Force is applied to a complex comprised of one filamin protein cross-linking two actin filaments by translating the sample relative to the trap at a constant speed of 5μm/s. At the same time, the displacement of the bead is monitored with the detection laser.

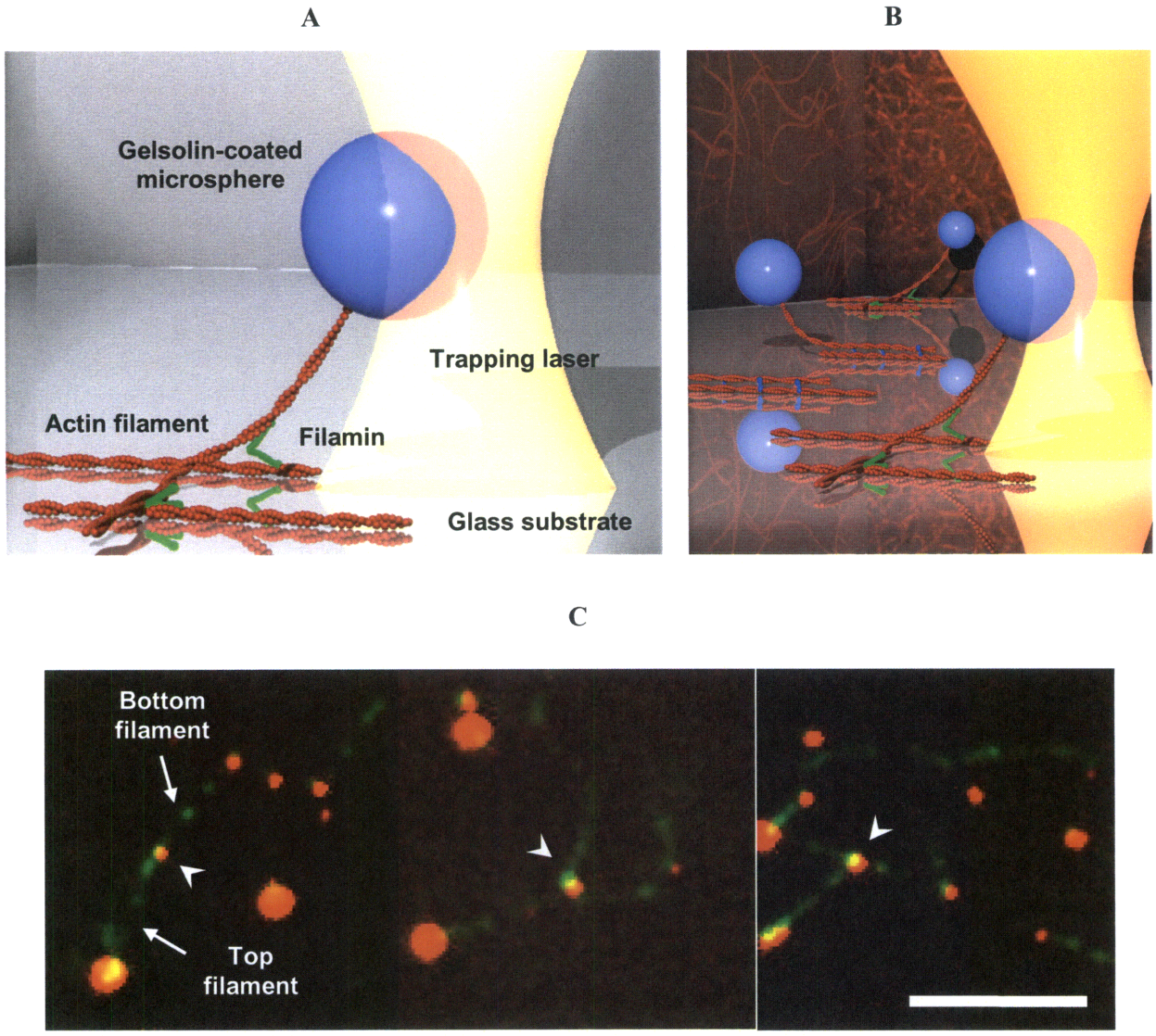

Figure 4.1 Single molecular assay. (A) The bottom actin filament is biotinylated and immobilized by bonding to a streptavidin-coated glass substrate. The top actin filament is tethered to a gelsolin coated microbead. Two actin filaments are cross-linked with ABP filamin and the stage is translated while the microsphere is constrained by the optical trap. Displacement of the microsphere is monitored to determine the force of interaction between the ABP and the actin filaments. (B) 3D drawings of single molecular assay. Filamin in green which forms networks of actin filaments shown as a confocal image on the right wall and alpha-actinin in blue which bundles actin filaments, shown as an image on the left wall, are probed using this assay configuration. (C) Confocal micrograph showing a complex formed by an ABP filamin (small red spots) cross-linking two actin filaments (shown in green). Actin filament and filamin were conjugated with Alexa Fluor 488 and ds-Red, respectively. The gelsolin beads (large red circles) were labeled with BSA conjugated with Alexa Fluor 555. Arrowhead indicates the cross-linking point where the top and bottom actin filaments are cross-linked. (Scale bar: 5μm)

Actual bead position and trap stiffness are calibrated after each measurement as described previously (21).

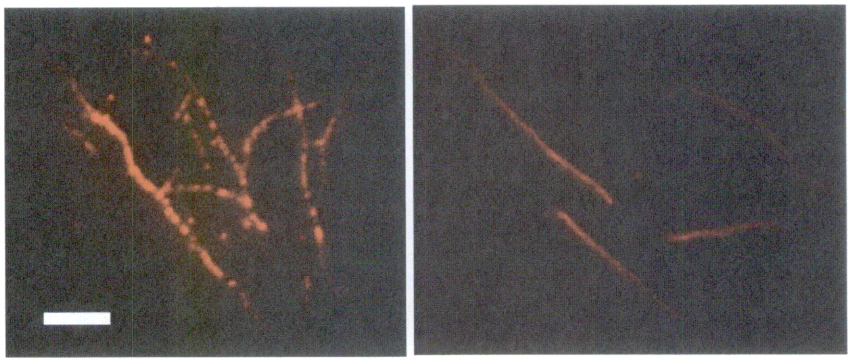

Figure 4.2 Micrographs showing surface-bound actin filaments are parallel to the pulling direction which is the same direction of the flow cell. In the images, the flow cell direction is along the diagonal from the lower right to upper left. (scale bar, 5μm)

4.2.5 Network Pulling Assay

To investigate the mechanical response of F-actin gel to a local force, we prepare two actin networks as described in Chapter 3. One is F-actin network cross-linked with filamin and the other is entangled F-actin solution without ABP. Briefly, solutions of gelsolin, filamin, microspheres, and 10× F-buffer are gently mixed. After addition of G-actin, the final solution is loaded into the custom-made flow chamber within 10 sec. The sample is polymerized for 2 hr at room temperature and the chamber is sealed with nail polish. Final concentration of actin is 10μM, and the molar ratio of filamin to actin is 0.01. The gelsolin concentration used in these experiments regulates the average length of actin filament to be approximately 5μm.

Optical tweezers are used to apply a local force to a cross-linked F-actin network and observe the response. In a similar manner to the Single Molecule Assay, an embedded bead is captured and the stage is displaced to apply a local force to the network. The stage speed is a constant 5μm/s. The force applied to the network can be estimated by multiplying the distance of the microsphere from the center of the trap by the stiffness of the trap.

4.3 Results for Molecular Interaction

4.3.1 Force-induced Unbinding of Cross-linking Protein

In single molecule experiment, a typical force-extension curve for unbinding (Fig. 4.3A) exhibits an initial gradual increase in force, that rapidly accelerates as extension increases. When the force reaches a critical level, between 50 and 170pN, it relaxes abruptly to a value near zero. At the loading rates of 400-2000 pN/s, multiple force peaks, ranging from two to six per pull, were generally observed indicating either reattachment of the unbound filament or multiple binding locations along a single filament. Note that the bead snaps back to its baseline location after each final break as well as for intermediate drops in traces containing multiple drops. The overall extension before rupture ranges from 500nm to 2500nm, considerably in excess of the contour length of filamin even when accounting for unfolding. Our assay consists of several linking components, thus this large extension is ascribed to additional compliance such as bending of actin filaments at the surface attachment point, rotation of the molecular linkages, and bending of actin filament at the bead attachment location. Also, the length of the bound actin filament and the distance between bead and cross-linking point will significantly influence the overall extension before rupture.

For each pulling measurement, we estimate the pulling rotational angle of the trapped bead by monitoring its x- and y-axis displacements. Due to the arrangement of stage and PSD with angle in our microscope, the stage movement for loading is along the x-axis in Fig. 4.3B. The surface bound actin filaments are generally aligned parallel to the pulling direction by washing steps shortly after flowing actin filaments. As a result, deviation from the x-axis indicates that the vector connecting the position of the trapped bead and the cross-linking point is not oriented along the pulling axis, causing the bead displacement relative to the trap center to

deviate from the x-axis, and leading to a situation in which a torque may be applied to the bond in addition to the pulling force. While this arrangement complicates the nature of the applied force, it also provides the advantage of helping to distinguish unbinding of filamin from unfolding when multiple transitions occur in a pull. Approximately 86% of rupture-like traces in which the force goes back to baseline after transition exhibit a different angle upon continued pulling confirming that a different bond is being stressed after rupture of the previous one.

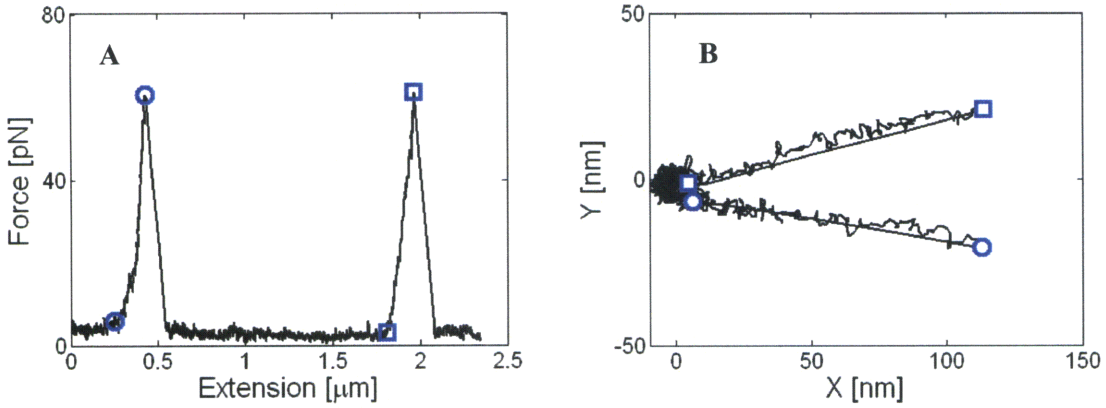

Figure 4.3 Molecular response of actin-ABP upon unbinding. (A) In the force vs. extension curve, the force increases until the first bond ruptures and it increases again as another bond is formed. The forces relax back to baseline, zero force, after ruptures. (B) The corresponding x-y plot shows two different slopes confirming that two molecule interactions are probed at the pull.

From the x-y plots of bead displacement, we calculate the angle for all pulling trajectories and can therefore identify how the rupture force varies as a function of angle. No noticeable change in rupture force is observed for angles smaller than 45° (Fig. 4.4A). However, when the bead trajectory deviates from the pulling direction by more than 45°, rupture force decreases significantly. Similar angle dependency of rupture force is observed at both high and low loading rates. Considering a possible configuration of the proteins in our assay, filamin would be subjected to the more shear/torsional forces in addition to the extensional force as the angle increases. Therefore, this result suggests that filamin/F-actin binding ruptures at lower levels of force when shear/torsional force is applied.

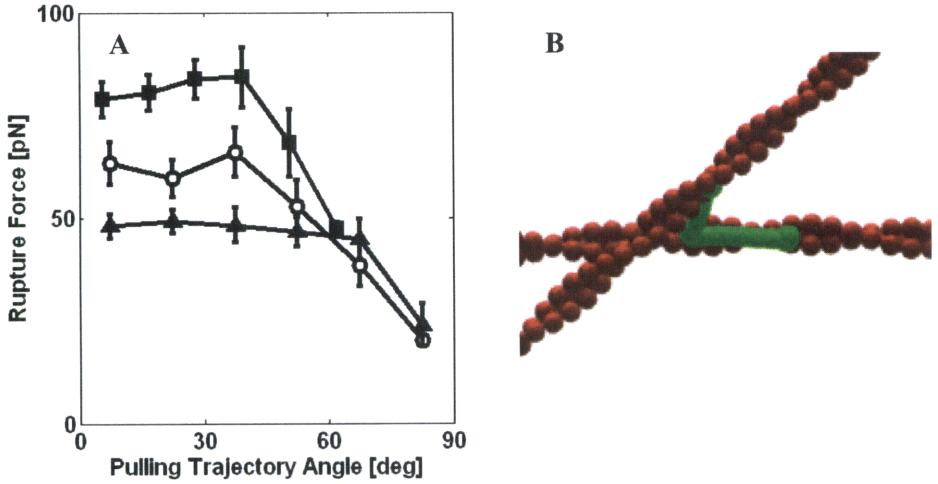

Figure 4.4 Dependence of rupture on pulling angle. (A) The pulling trajectory angle is the angle formed between the pulling direction and the direction of force acting on the bead (see text). Rupture force for filamin starts to decrease at an angle of ~ 45° at both low (5-50pN/s, ○) and high (400-2000pN/s, ■) loading rates, while the rupture force for α-actinin (▲) exhibits a constant value up to ~70°. (B) Top view of the assay where two actin filaments (red) cross-linked with ABP (green) form an angle of 45°. Results for filamin at low loading rate (○) and α-actinin (▲) are adapted from reference (17)

We also investigated the effect of loading rate on force-induced unbinding. The loading rate is defined as the slope of a linear fit to the force vs. time trace just prior to rupture. Rupture force is observed to increase with loading rate in both low and high speed pulling regimes (Fig. 4.5). A linear increase in force with the logarithm of loading rate was also observed in other molecular interactions (22) and agrees with theoretical predictions (23-25). The rupture force data exhibit two regimes with different slopes, implying either the presence of two barriers in the energy landscape of the filamin/F-actin binding or the occurrence of rebinding at the low loading rate. The change in the slope of force is attributed to the suppression of an outer energy barrier by external force (24). A similar behavior has been shown in other molecular complexes such as actomyosin, avidin-biotin, and selectin-ligand bonds (26-29). Previous measurements for α-actinin/F-actin rupture also found two lifetime regimes (30). Since filamin and α-actinin have

calponin homology actin binding domain which is a conserved sequence in other ABPs (31-33), the presence of multiple energy barriers might be a general characteristic of ABP/F-actin binding.

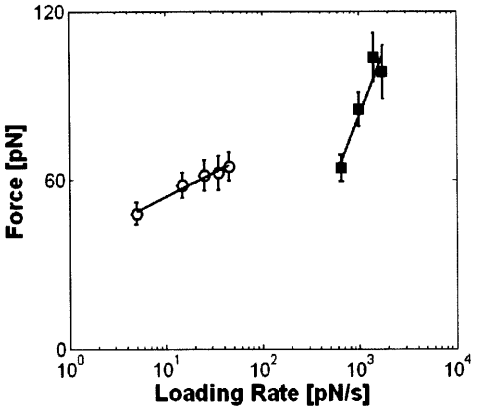

Figure 4.5 Dependence of rupture force on loading rate. The general tendency is for the rupture force to increase with loading rate. However, the slope of force at the high loading rate (■) is much higher than that at the low loading rate (○) in the single molecule measurements. Results for low loading rate are adapted from reference (17)

4.3.2 Force-induced Unfolding of Cross-linking Protein

Approximately 20% of our measurements probe unfolding of Ig domains in filamin exhibiting different force-extension traces from those of unbinding events. At a critical force ranging from 29 pN to 94 pN, the typical trace exhibits multiple drops of 4-10pN (6-15nm in bead displacement) with decrease of force slope. The number of drops in the unfolding region range from 8 to 17. Fast Fourier Transform (FFT) analysis of the potential unfolding trace confirms that the trace exhibits a repeating pattern with periods of ~ 25nm, which is comparable to the change of contour length by unfolding of an Ig domain measured in the AFM measurement (15). Compared to the unbinding trace in Fig. 4.3, the force does not relax back to baseline and the transitions follow along the same x-y trajectory, even during multiple force drops.

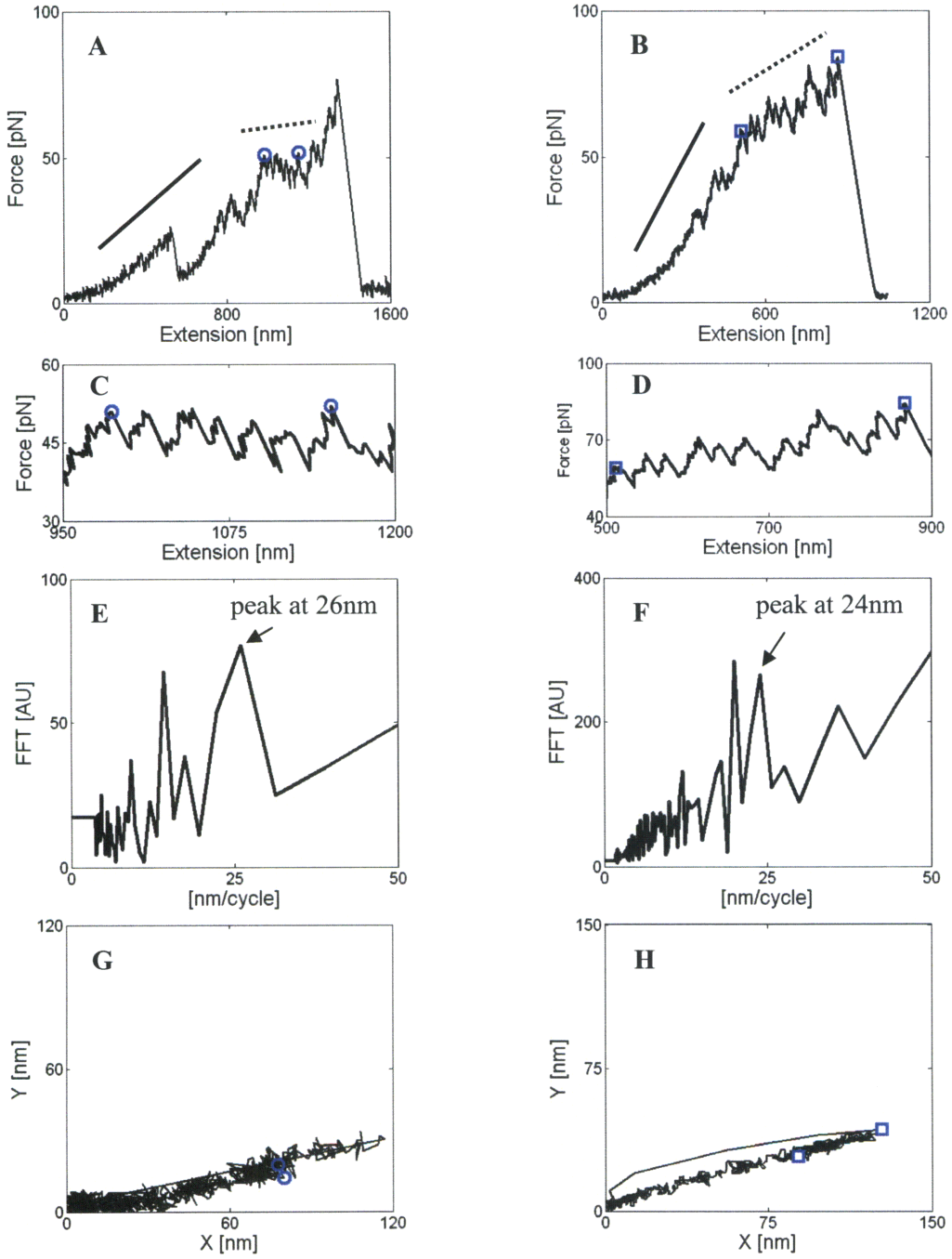

Figure 4.6 Molecular response of actin-ABP upon unfolding. (A,B) In typical force vs. extension curves for unfolding, a sawtooth like pattern is observed in the trace indicating unfolding of individual filamin Ig domains. Force slope during unfolding (dotted line) is less than that before the unfolding initiates (solid line). (C,D) The change in contour length by unfolding can be estimated by measuring the distance between peaks (x-axis in nm) of the repeating pattern in the enlargements of the dotted region. (E,F) Fast Fourier Transform of the unfolding traces estimate the period of the trace is approximately 25nm. (G,H) Repeating transitions exhibited in the unfolding trace are along the same pulling trajectory.

To further characterize the period of the peaks observed in the unfolding trace, we calculate the distance between force peaks in the force-extension curves and, using a Gaussian fit, find the period between the transitions to be 28 ± 5 nm.

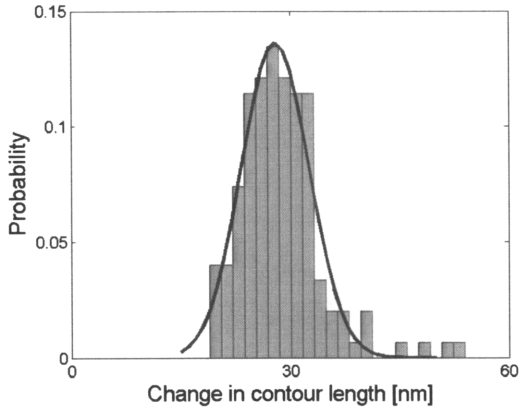

Figure 4.7 Histogram of the change in contour length measured from the peak distances from the data (n=154). The Gaussian fit estimates the average value to be 28 ± 5 nm.

4.3.3 Force Distributions for Unbinding and Unfolding

We obtain the force distributions for both unbinding and unfolding by measuring the peak forces in the force-extension curves. As indicated by the overlap of two histograms in Fig. 4.8, force level distributions for unbinding and unfolding are remarkably similar. The force at which the unfolding and unbinding occurs is 57 ± 19 pN and 70 ± 23 pN, respectively. This similarity in critical force level is consistent with our observations that both unbinding and unfolding occur at the same pulling speed although unfolding is less frequent.

To estimate the kinetic parameters in the actin/filamin molecular interaction, we implement the theoretical model developed by Hummer and Szabo (25) referred to here as the HS model. Three parameters can thus be computed from the experimental results of rupture force and loading rate; the intrinsic rate constant (k_{off}) in the absence of external force, the position of the transition state ($x^{\ddagger}$), and the molecular spring constant (κ_m).

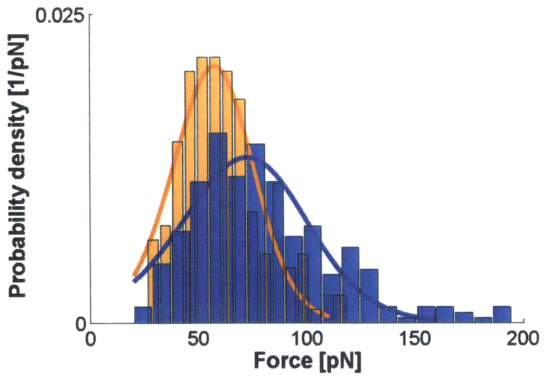

Figure 4.8 Unbinding and unfolding force distributions. Probability density functions for unbinding (blue) and unfolding (orange) are obtained by measuring the critical force at which the respective events occur. Average forces for unfolding and unbinding are 57 ± 19pN and 70 ± 23pN, respectively. HS model (solid line) provides a good fit for both force distributions and estimates the kinetic parameters, results of which are summarized in Table 4.1.

Unbinding and unfolding force distributions can be fit to the model (Fig. 4.8), both yielding $R^2 = 0.88$. Assuming a single subunit rupture, values for apparent k_{off} are computed to be 1.70 s^{-1} for unbinding and 0.52 s^{-1} for unfolding. In the bulk scale experiment using the stopped flow method (34), k_{off} for filamin/actin binding was determined to be 0.6 s^{-1}, 2-3 times lower than our estimation. This difference may be due to the difference in measurement techniques and the dependence of unbinding force on the experimental parameters such as loading angle and speed. The transition distances for unbinding and unfolding are 0.27 nm and 0.14 nm, and the spring constants are 646 pN/nm and 266 pN/nm, respectively. Given κ_m and $x^{\ddagger}$, the height of the free energy barrier, $\Delta G^{\ddagger}$, can be computed as $1/2\ \kappa_m\ x^{\ddagger 2}$. For unfolding $\Delta G^{\ddagger}$ is 6.8 k_BT, higher than the value of 5.6 k_BT for unbinding, indicating that more energy is required for unfolding. This helps to explain why unfolding occurs less frequently than unbinding in our measurements even though the critical force levels are similar.

Loading rate (400 pN/s – 2000 pN/s)				
	k_{off} [s^{-1}]	$x^{\ddagger}$ [nm]	κ_m [pN/nm]	ΔG [k_BT]
Unbinding	1.70	0.27	646	5.6
Unfolding	0.52	0.46	266	6.8
Loading rate (5 pN/s – 50 pN/s)				
Unbinding	0.087	0.19	820	3.6

Table 4.1 HS model parameters. The results for the loading rate of 5-50 pN/s (17) were listed for comparison.

4.4 Results for F-actin Network

4.4.1 Strain-dependent Mechanical Properties of F-actin Networks

Using the active microrheology described in Chapter 2, we obtain strain-dependent mechanical properties of F-actin networks. The amplitude of the stage oscillation increases from ±0.2μm up to ±2μm with an increment of ±0.1μm. The network deformation is calculated by subtracting bead displacement from stage oscillation. The network viscoelasticity is estimated using the equation 4.1. Each measurement of shear storage modulus is normalized by the value at lowest strain and network deformation is normalized by the radius of probe particle.

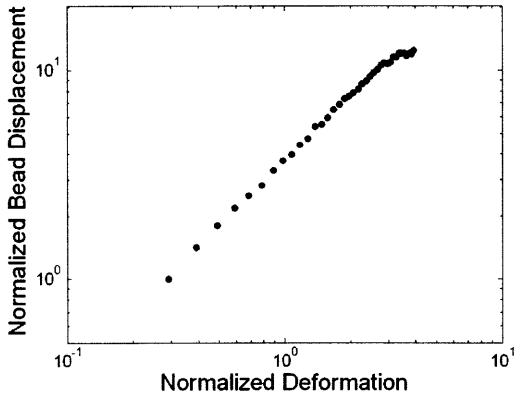

Figure 4.9 Bead displacement as a function of network deformation. Bead displacement and network deformation are normalized by its initial value and bead radius, respectively. As the network deformation increases, the bead displacement increases. However, at the deformation above the critical value, increase of the bead displacement is reduced indicating a rupture of the network.

For the entangled F-actin solution to which no ABP is added (c_A = 30μM), the elasticity of the network monotonically decreases with increasing strain [Fig. 4.10A]. As there is no physical connection between actin filaments, they can be displaced by the microsphere's oscillation leaving the fewer filaments in the region. In contrast, the elasticity of the F-actin network cross-linked with filamin (c_A = 30μM, R_f = 0.01) increases up to a critical level of strain and then decreases suggestive of local collapse of the network as large strain is applied [Fig. 4.10B]. In the relation between applied force and deformation in the F-actin network, force at which the network collapse occurs is approximately 20pN [Fig. 4.10B, inset]. Same experiment is performed for the F-actin network cross-linked with α-actinin (c_A = 20μM, R_α = 0.01). Because α-actinin tends to form filament bundles at high concentrations (35), we visualized the α-actinin/F-actin network and confirmed that our experimental condition minimized bundling of actin filaments resulting in a homogeneous network. The α-actinin/F-actin network exhibits the similar behavior in the strain-dependent mechanical properties [Fig. 4.10C], compared with the filamin/F-actin network. It might be because both filamin and α-actinin have a conserved actin-binding domain exhibiting the similar binding interaction with actin filament (33, 36).

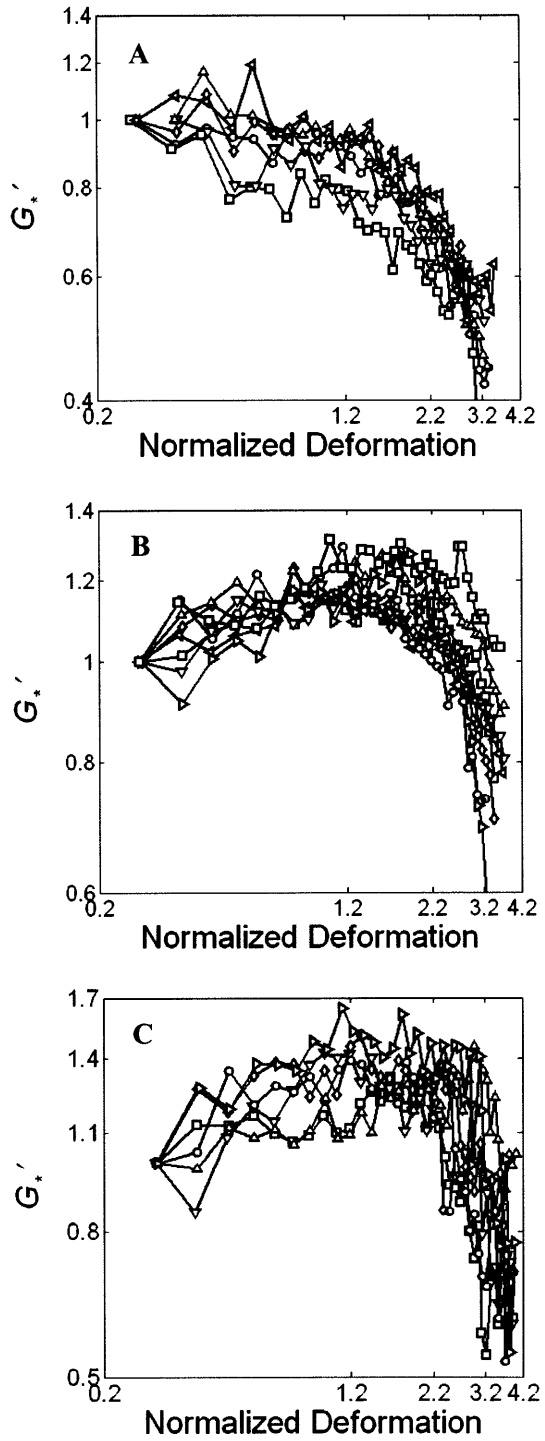

Figure 4.10 Normalized elastic modulus G_*' as a function of the network deformation normalized by the size of the probe particle. (A) For the entangled F-actin solution, G_*' decreases as the applied strain increases. (B) For the F-actin network cross-linked with filamin, G_*' increases with applied force up to a critical value and decreases for higher. (C) The F-actin network cross-linked with α-actinin also exhibits the similar behavior in the strain-dependent mechanical properties to the filamin/F-actin network.

4.4.2 Mechanical Response of F-actin Network to Local Excitation

In measurements of strain-dependent microrheology, we have observed nonlinear mechanical properties of the cross-linked F-actin networks. To elucidate the origin of the strain-hardening and strain-softening, we also investigate the mechanical response of F-actin network to the local excitation. An embedded microsphere is captured with the optical tweezers and local force is imposed by moving the sample relative to the trap at a constant velocity of 5μm/s using a piezoelectric stage. Applied force is estimated from the bead position relative to the center of the optical trap and the network displacement is calculated by subtracting bead position from the stage position. Typical curves of force vs. displacement for the cross-linked F-actin network and entangled F-actin solution are shown in Fig. 4.11. For the F-actin network cross-linked with filamin (c_A = 10μM, R_f= 0.01), the traces exhibit a single (61%) or multiple (39%) transitions at which the force does not drop to zero [Fig. 4.11A], suggestive of abrupt alterations in the network structure surrounding the microsphere. The force at these transitions ranges from 10pN to 65pN. Further deformation of the network causes the microsphere to move out of detection region resulting in the truncations of the curves. The same measurement is performed on the entangled F-actin solution (c_A = 10μM) and an abrupt transition is also observed in the force-displacement curves [Fig. 4.11B]. However, in contrast to the cross-linked F-actin network, those transitions occur at larger displacement and the force relaxes to zero level after the transitions.

The displacement of the bead which is embedded in a cross-linked F-actin network should cause deformations of both actin filament and ABP. Depending on the initial configuration, the actin filaments surrounding the bead undergo deformation such as bending, stretching, and twisting. When ABP is close to the bead and is in front of the bead path,

mechanical deformation is imposed on the ABP directly. Also, if the ABP is cross-linking the actin filaments undergoing large deformation, the ABP is subject to an indirect deformation. Therefore, mechanical properties of both actin filament and ABP play an important role in determining the response of the network to a bead displacement. The latter might have the similar configuration of the components to the single molecule assay. Compared with the single molecule measurements, similar transitions observed in the network's responses suggest that these originate from unbinding and unfolding of the stressed cross-linkers by deformation of actin filaments [Fig. 4.11C].

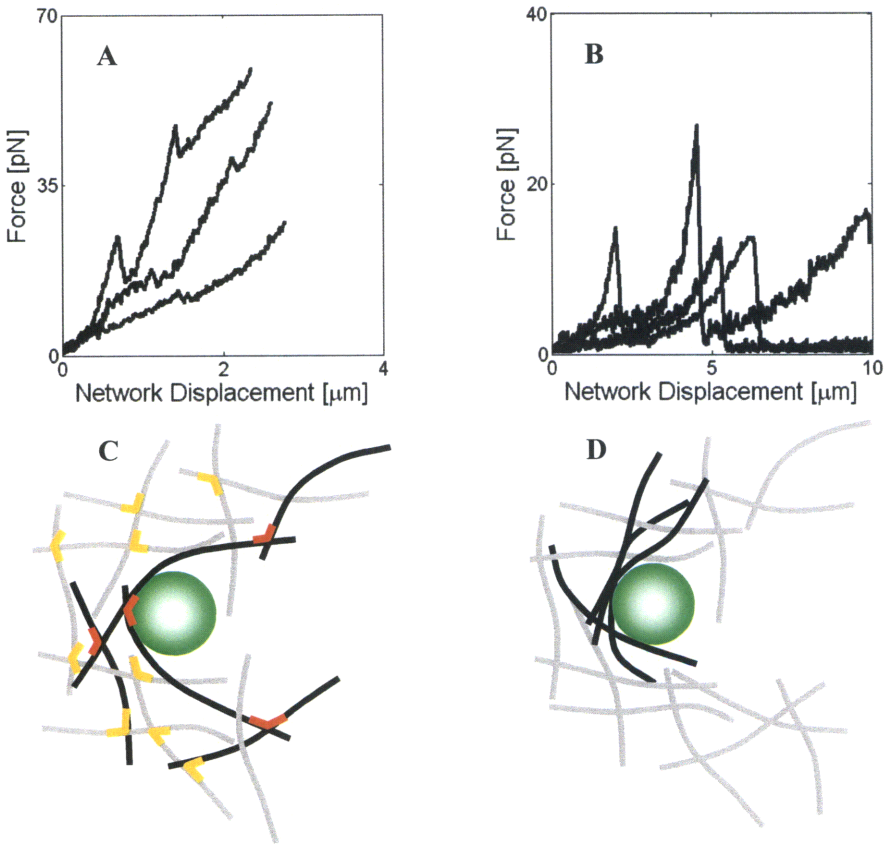

Figure 4.11 Force-displacement curves for the cross-linked F-actin network and entangled F-actin solution. (A) For the cross-linked F-actin network, the force responses exhibit a single or multiple transitions where the force does not relax to zero level. (B) For the entangled F-action solution, the force relaxes to baseline after transition. Schematic view of the bead embedded in a cross-linked F-actin network (C) and entangled F-actin solution (D). Bead displacement deforms both F-actin (gray) and ABP (yellow) in F-actin network. The most stressed actin filaments (black) may cause a rupture of the deformed ABPs (red) leading to an abrupt transition in bead response.

The mechanical response of the entangled F-actin solution should depend on both configuration and entanglement of actin filaments in the vicinity of the microsphere. If the filaments are tightly entangled surrounding the microsphere, they will be bent and piled up in front of the microsphere during its displacement. Depending on the strength of entanglement, the actin filaments can be buckled with the further deformation. Otherwise, the deformed actin filaments can slip out of the microsphere resulting in a transient dislocation of the microsphere to a neighboring mesh. This behavior can be shown as another increase in force following the transition in the response [Fig. 4.11B].

To further identify the cause of the transition observed in the mechanical response of the cross-linked F-actin network, we characterize the critical force and bead displacement at transition. The force at transition is defined as a maximum force before the drop in the force-displacement plots shown in Fig. 4.11A and B. Transition displacement measures a corresponding movement of the microsphere at the force drop. As shown in Fig. 4.12, displacement at transition is 29±17nm for the cross-linked F-actin network, while it varies from 45 to 190nm for the entangled F-actin solution. The transitions occur at 38±18pN and 21±6.1pN for the cross-linked F-actin network and entangled F-actin solution, respectively. Compared to the entangled F-actin solution, the multiple transitions with smaller displacements exhibited in the cross-linked F-actin network imply that abrupt decreases in force might result from the forced-induced ruptures at cross-linkers or unfolding of cross-linkers. Unfolding of individual subdomain increases a contour length of filamin by ≈30nm (15), which is similar to the average value of transition displacement in our measurements. Multiple transitions exhibited in Fig. 4.11A are also similar to the typical unbinding and unfolding traces exhibited in the direct pulling of protein using AFM (15, 37) or optical tweezers (17, 38).

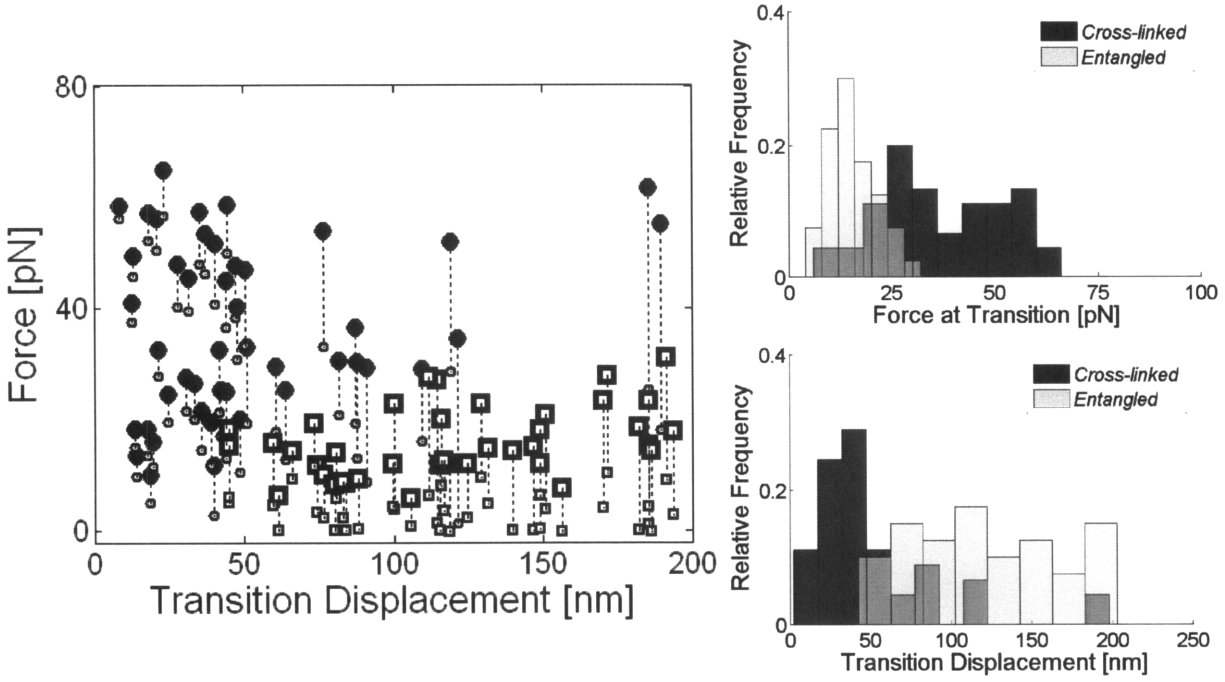

Figure 4.12 Relation of force and displacement at the transitions exhibited in the responses of the F-actin gels to a local excitation. For the F-actin network cross-linked with filamin (•), the transitions occur at the force of 37±17pN with the displacement of 29±17nm. In contrast, for the entangle F-actin solution (□), they are observed at the lower force of 21±6.1pN with the larger displacement of 117 ± 49nm. Small symbols connected with dotted lines indicate the forces after transitions.

We also calculated the loading rate from the slope of a linear-fit to the force versus time plot for each event. Critical forces for the transitions observed in both cross-linked network and entangled solution increases linearly in proportional to the logarithmic loading rate. However, the dependence of force on loading rate for cross-linked F-actin network is higher than that for entangled F-actin solution (Fig. 4.13A). Compared with the results for single molecule interaction, the loading rate dependence exhibited in the cross-linked F-actin network is considerably similar to that of the unbinding force between filamin and actin filament (Fig. 4.13B), suggesting that force drops in the transitions might be originated from the rupture at ABPs cross-linking actin filaments in F-actin network.

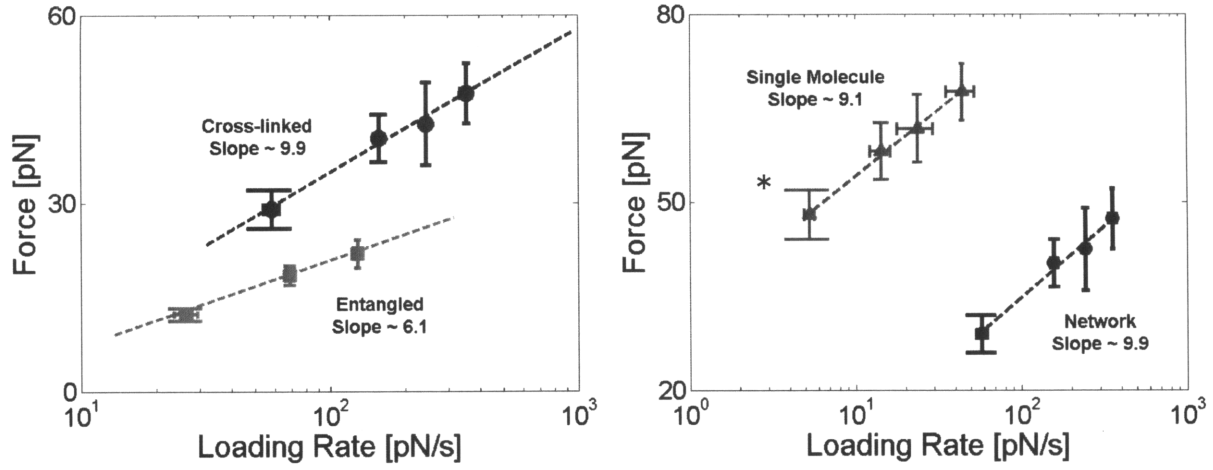

Figure 4.13 Loading rate dependence of force at transition. (A) Transition force for both F-actin network and entangled network increases as loading rate increase. However, higher dependence of force on loading rate is observed in cross-linked F-actin network. (B) The forces at the transitions observed in the network's responses (●) exhibit the similar loading rate dependence to the unbinding force (▲) between filamin and single actin filament. *Results are adapted from reference (17).

4.4.3 Reversibility of Network Elasticity

Compared with the molecular response of actin-filamin complex (17), the response of F-actin network to a local excitation have shown the similarities in terms of trace pattern, critical force for transition, and loading rate dependence. As a result, binding interaction rather than unfolding of ABP seems to be a dominant mechanism in causing the strain-softening of F-actin network. However, to better understand the origin of nonlinear behavior of F-actin network, we study a reversibility of mechanical behavior by estimating the properties for increasing and decreasing strain. Force-induced unbinding of filamin will be irreversible unless rebinding occurs at the same binding sites between actin filament and filamin, compared to the reversible process of unfolding as demonstrated in the AFM measurement (15). In the measurement for the F-actin network cross-linked with filamin (c_A = 30μM, R_f = 0.01), the mechanical properties are not reversible as indicated by the inconsistency between the elastic moduli measured for increasing and decreasing stress [Fig. 4.14A]. However, when the maximum applied force is less than the

critical value at which the strain-softening occurs, reversible mechanical properties is obtained. These suggest that strain-softening behavior in filamin/F-actin network is originated from an irreversible process of unbinding.

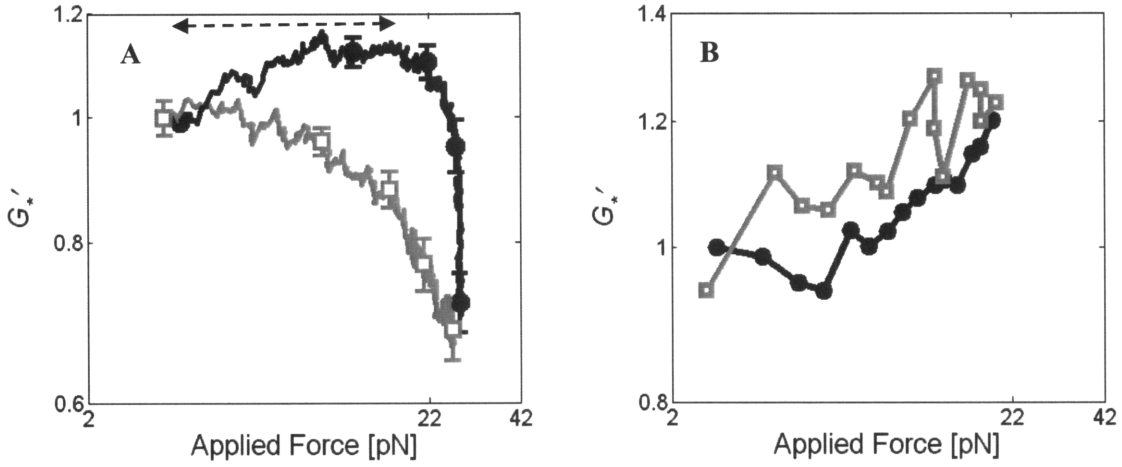

Figure 4.14 Irreversibility of strain-dependent mechanical properties of the cross-linked F-actin networks. (A) The storage shear moduli measured for increasing (●) and decreasing (□) strain amplitudes is not reversible as indicated by the hysteresis of the curves. (B) However, the reversibility is observed when the measurement is performed at the small force region (indicated by the arrow in (A)) in which strain-softening does not occur.

The role of ABP unbinding in the regulation of the mechanical properties is confirmed by performing an experiment for a F-actin network cross-linked with rigid ABP. Biotinylated actin is mixed with unlabeled actin at a 1:4 molar ratio, and the mixture is polymerized with streptavidin to form a rigidly cross-linked F-actin network (c_A = 20μM, R_s = 0.01). The mechanical properties are estimated with increasing and decreasing strain amplitude. Compared with the filamin/F-actin network, the network cross-linked with streptavidin also exhibits slight strain-stiffening. However, strain-softening is not observed even at the higher applied force and the mechanical properties are measured to be reversible. Because streptavidin-biotin binding is very strong with a dissociation constant of 10^{-15}M (39), rescue of the reversibility by replacing a cross-linker suggests that the strain-softening is attributed to the rupture at the cross-linker.

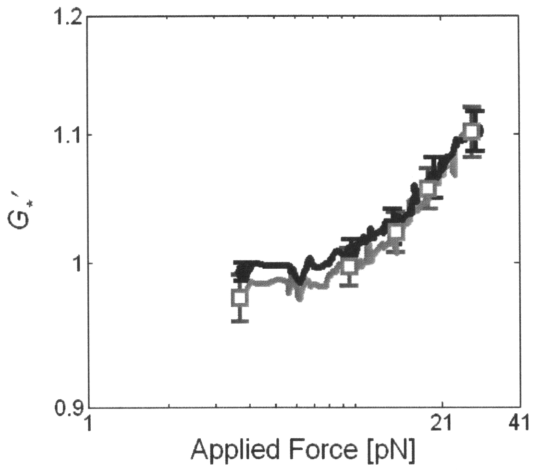

Figure 4.15 Reversibility of strain-dependent mechanical properties of the rigidly cross-linked F-actin networks. F-actin network cross-linked with streptavidin exhibits the similar value of mechanical properties not depending on the measurements.

In summary, we have obtained the microscale strain/stress-dependent mechanical properties of F-actin gels using the active rheology measurements, and we have demonstrated the mechanical responses of F-actin gels to the local excitation in the pulling experiments. By relating the decrease of the network elasticity at high strain with multiple decreases of force in the network responses, it was suggested that the molecular interaction of actin with an actin binding protein regulates the mechanical properties of F-actin gels. Compared with single molecule measurements, similar loading rate dependence of transition force is observed in the network measurements suggesting that the force drop at high strain is originated from bond rupture. In the test of reversibility of the network elasticity, we have shown that strain softening is irreversible process implying again it is due to rupture at cross-linker. Understanding how molecular interactions are manifested at the network elasticity is essential to building an actin cytoskeleton with a desirable mechanical behavior.

Our results present how the mechanical properties of the F-actin network are influenced by the rupture of ABP. Although the force-induced unbinding of filamin is the dominant

mechanism in the irreversible strain-softening, we do not exclude another possible cause of unfolding. For <20% of all events, mechanical properties measured for increasing and decreasing stress exhibited the similar values [Fig. 4.16], suggesting the network maintains its structure by ABP unfolding in response to a large deformation. The small probability of the reversible behavior is surprisingly consistent with the observation that unfolding is less frequent than unbinding when a cross-linking filamin is loaded by pulling one of actin filaments in single molecule measurements (17). From the results for both molecular interaction and network response, occurrence of forced-induced unfolding of filamin cross-linking actin filaments seems to be more sensitive to dynamic conditions such as force and loading rate (Lee et al. 2009). Even in the network responses, we note that some force-displacement curves exhibit undulation and a plateau region, which are similar to the sawtooth pattern (15, 37, 40) and abrupt change (38, 41) of the force slope observed during protein unfolding. However, the average displacement in the region where the potential unfolding occur is $\approx$ 137nm, which are less than the total stretching of a single filamin observed in the AFM measurement (15). While an extensional force by AFM is directly applied to a single filamin to induce unfolding its subdomains, the external force imposed by bead displacement causes multiple ABPs to either unfold or unbind at the same time. In addition, when F-actin network is under external force, filamin cross-linking actin filaments is deformed by shear and torsional forces, too. Complexity in the force application can cause an unbinding of cross-linker before its complete stretching by unfolding (42). Recent experiment to measure a rupture force of the filamin cross-linking two actin filaments also demonstrated that both unbinding and unfolding occurred at the similar force (17).

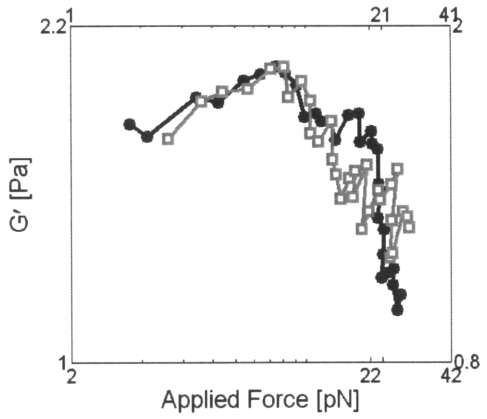

Figure 4.16 Reversible strain-dependent mechanical properties for potential unfolding. Mechanical properties for increasing (●, bottom and left axes) and decreasing (□, top and right axes) forces are reversible suggesting that the network maintain its structure through unfoldings of cross-linkers. Note that the axes have different scales but the same length.

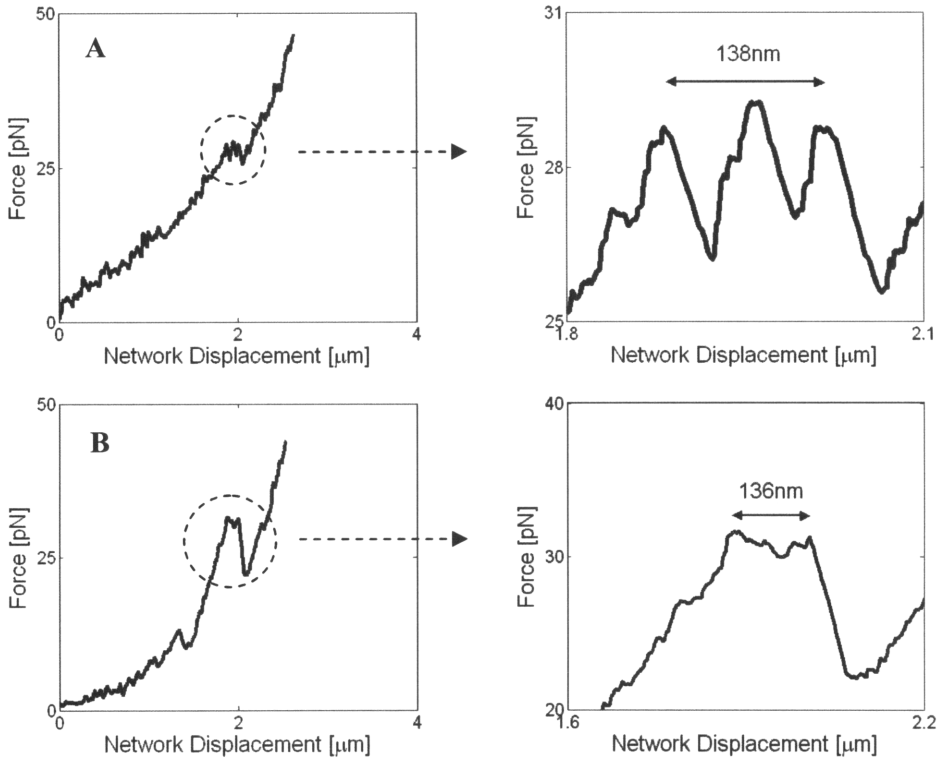

Figure 4.17 Network response for potential unfolding. Consecutive undulations (A) or a plateau (B) exhibited in the network response might be attributed to unfolding of filamin rather than unbinding. Enlargements of the dotted circles are shown on the right.

4.4.4 Computational Analysis of Network Response

(with the help by Taeyoon Kim)

A 3-dimensional actin network is generated via the polymerization and crosslinking of an initial structure with uniformly distributed actin monomers and randomly dispersed actin crosslinking proteins which form an orthogonal network like filamin using methods previously described (43). Actin concentration of the network used in this study is 12μM, the average length of the actin filaments is ~1.5μm, and the molar ratio of ABP to actin is 0.017. The width of a cubical computation domain is 5μm. Motions of actin filaments and ABPs are governed by Brownian dynamics, and they are also characterized by appropriate bending and extensional stiffness. After polymerization, all actin filaments are severed and clamped at the upper and lower boundaries (z-surfaces), and periodic boundary conditions are imposed on all other boundaries (x- and y-surfaces). A microbead with the diameter of 1.2 μm is then inserted into the actin network by replacing all filaments within a central spherical region with a rigid sphere. To simulate the network experiments, the microbead is forced to move in +x direction with the constant rate of 20 μm/s. During the simulation, unbinding of ABP follows Bell's equation with $k_{off} = 0.115\ s^{-1}$ and $x^{\ddagger} = 0.416$ nm; only extensional forces acting on the ABPs are considered. Both the sum of forces acting on the microbead in x direction and the state of each ABP (bound or free) are recorded as functions of bead displacement.

To substantiate the importance of unbinding of individual ABPs in the mechanical response of actin networks, we also employ our computational model. As can be seen in Fig. 4.18, the response measured in the simulation is qualitatively similar to those in Fig. 4.11A: an increase in the force and the existence of multiple transitions when the force drops abruptly. During bead displacement, a number of ABP unbinding events occur (red circles on the curve),

but most appear to be insignificant in that they are not reflected by any noticeable change in the force curve. However, there are two exceptions. In order to isolate the critical unbinding events, we apply two criteria: 1) the distance between the ABP and the surface of the microbead at the moment of unbinding must be < 500 nm, and 2) the ABP must lie within a cone centered on the +x-axis with an included angle of $2\pi/3$. Only three rupture events meet these criteria (blue circles). Two of these correspond to the sudden transitions of the mechanical response though one occurs early in the simulations and seems irrelevant. This implies that the multiple transitions observed in the experiment can be attributable to the unbinding of ABPs in close proximity to the microbead.

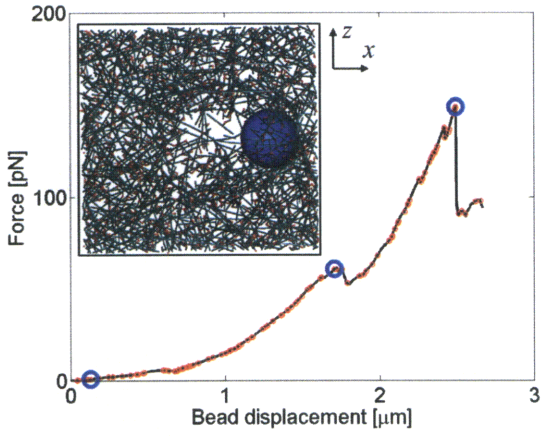

Figure 4.18 Mechanical response of an actin network simulated by a computational model. Red circles show all ABP rupture events, and blue circles show only those satisfying the two criteria described in the text. As in Fig. 4.11A, the force acting on the microbead rises with increased bead displacement, and two abrupt drops (arrow heads) in the applied force are evident. (Inset) The network consisting of actin filaments (cyan) and ABPs (red) with a microbead (blue) at a bead displacement of 2μm.

4.5 Discussion

Strain-dependent mechanical properties of actin gels are also observed at the microscale but are not reversible. When the applied strain increases, a non-linear response of the network is observed, characterized by local stress hardening followed by softening of the cross-linked F-

actin network. Although the observed microscale behavior is similar to the mechanical properties of an F-actin network under prestress probed at macroscale (7, 44), the increase in viscoelastic moduli is considerably smaller. The discrepancy can be caused by the differences in measurement method, scale and force application. While previous measurements apply a force shear or compression to F-actin network using bulk rheometry (6) or AFM (44), respectively, we apply a force in the order of pN using optical tweezers. As the measurement scale is in the order of μm, comparable to the size of cell, our method gives an opportunity to investigate the mechanical response of F-actin network to an excitation which is in a physiological range. Also, it should be noted that the shear modulus estimated here is not the differential modulus which has been obtained in the macroscopic measurement with prestress using a rheometer (7) , but rather, the response to progressively larger sinusoidal oscillations of the bead. We show that the critical bead force (F_b) at network softening is approximately 25pN (Fig. 4.14A). Assuming this force acts over an area equal to the cross-sectional area of the bead, it corresponds to an applied stress of ~32Pa which is similar in magnitude to σ_{max} found in bulk measurements (6, 7). Also, the maximum force (F_{cl}) a cross-link can hold is given by cF_b and c varies between 0 and 1 depending on configuration of a bead and surrounding filaments. If we assume a regular mesh with the stress distributed among four cross-links (45), comparing F_{cl} at c = 0.5 to the maximum stress from the bulk measurements by Gardel et al. (6, 7) we estimate the L_c to be ~ 2 μm which is larger than the mesh size (45). Compared to the unbinding force at the molecular level, the rupture forces at which the F-actin networks start to soften are less because the weakest bond should rupture first when network is stressed. In contrast to cross-linked F-actin network, the elasticity of entangled F-actin solution shows monotonic decrease as the applied stress increases.

This also suggests that unbinding between F-actin and filamin play a role in determining maximum regulate maximum sustainable forces by the actin network

Reversibility of the non-linear behavior was tested by measuring mechanical properties for increasing and decreasing applied strain. When the strain on the network increases, elasticity increases up to a critical strain, then decreases as more deformation occurs. In contrast to previous measurements of macroscale networks (44), microscale non-linear behavior is not reversible; network elasticity measured for decreasing strain exhibits a different trace from the measurement for increasing strain. Irreversibility in strain-dependent mechanical properties can be explained by network collapse and reorganization. In the region where elasticity decreases with increasing strain, the network configuration can be altered by rupture of individual actin filaments and/or unbinding of ABPs as the result of local stress (14, 46). Also, the flexibility of filamin can facilitate unbinding and rebinding leading to local reorganization of the network and changes in mesh size in the vicinity of the probe particle (7). In the previous study using AFM, reversible stress softening behavior was reported in dendritic actin networks (44). However, the network elasticity even at low strains was 985 Pa which is significantly higher than that of the reconstituted F-actin network with filamin, suggesting a denser actin network with extensive branching due to the presence of Arp2/3. Also, it should be noted that the whole actin network was deformed by compression in the AFM experiment, while a relatively small number actin filaments immediately surrounding the probe particle are deformed in microrheology.

Two assays, one with a single molecule and another with a 3D network have been utilized to probe unbinding and unfolding of filamin cross-linking actin filaments. For direct comparison between single molecule and network preparations, both assays have been prepared with similar components and performed on the same instrument platform. In the single-molecule

assay, one actin filament is immobilized on a rigid surface while the other filament is bound to a gelsolin-coated microsphere. By pulling the bead using OTFS, the force is applied to a single filamin/F-actin complex and results in either unbinding of actin filaments from filamin or unfolding of filamin subdomains. In the second, 3D assay, a microsphere is translated through a cross-linked actin gel while monitoring the resistive force. Because the microsphere is comparable in size to the gel microstructure, discrete events (drops in force) are observed, that can be related to individual rupture or unfolding events. Comparison of these two types of measurement provides new insights into the detailed nature of actin crosslinking by filamin.

In the single molecule assays, unbinding is characterized by a clear snapback of the bead to the baseline after rupture, analogous to the abrupt force drops seen in AFM measurements. But unlike AFM, the optical trap allows us to continue pulling on the bead after the rupture event and to simultaneously observe its trajectory in the x-y plane. This additional information allows us to observe and identify both unfolding and unbinding events. Unbinding is characterized by an abrupt drop in force, followed by a different pulling trajectory when (and if) the force rises again (see, e.g., Fig. 4.3), signifying that the point of attachment between the two actin filaments has moved. This could result either from the same filamin rebinding at another binding site along the same filament or a different actin filament, or from a second filamin bound at a different site coming into play and supporting the load. Transitions that do not relax back to baseline suggest unfolding, conformational changes, or rapid rebinding to the same site or to a different one very near to the first. Evidence supporting the conclusion that the site of binding remains the same comes from the pulling trajectories; if, as the force rises again, the subsequent trajectory follows the first, the site of attachment must be at, or very near, the initial one. Our results show that >86% of the transitions where the force relaxes back to baseline exhibit a

different pulling trajectory indicating multiple unbinding events. As just discussed, this can be explained by reattachment of the tethered actin filament or multiple bindings formed on the substrate-bound filaments.

Unfolding of ABP filamin is generally characterized by a regular sawtooth pattern exhibited in the force-extension curve. In these repeating transitions, the force does not relax back to zero and the pulling trajectories all lie along the same curve. The number of apparent force drops in the unfolding regime varies from 8 to 17, fewer than the 24 potential unfolding Ig domains of filamin. In cases for which the distance between force drops is irregular and larger, unfolding of several Ig domains may occur simultaneously. Also, the actin filament can unbind from filamin before all 24 subdomains of the filamin unfold. When the unbinding and unfolding events are grouped and analyzed separately, the levels of force required are found to be quite similar (70 ± 23pN for unbinding and 57 ± 19pN for unfolding) supporting this hypothesis. In our previous measurement at the low loading rate of 5-50pN/s (17), unbinding of filamin dominated and only a couple force drops were observed in the potential unfolding traces. Therefore, the distinct multiple transitions observed in this study suggest that loading rate is a critical factor in determining the likelihood of consecutive unfolding events. To further identify the unfolding of filamin, the distances between force peaks were calculated and the average period of the repeating pattern was found to be 28 nm. Each Ig domain of filamin consists of 96 amino acids. Assuming the distance between amino acids is 3.5Å (47), the theoretical change of contour length is expected to be ~ 34nm. Previously, Furuike et al. used an AFM to extend filamin directly using AFM and showed that the unfolding occurs in the force range between 50 to 220pN, leading to ~ 30nm change in the contour length (15). We have also observed a decrease in slope of the force-extension curves during unfolding, which is similar to the abrupt

change of force slope in both AFM and OTFS measurements of unfolding (15, 37, 38, 41). However, compared to the flattening of the slope observed in AFM measurements (15, 37), the peak force we observe continues to increase during consecutive unfolding. One important difference between our measurements with the optical trap and measurements by AFM is that the latter applies a tensional load directed from the point of surface tethering to the point of attachment to the AFM probe. In contrast, the load is applied indirectly by pulling an actin filament, and filamin in our assay experiences shear and torsional deformation as well as tension during pulling. In addition, the increase in length of filamin due to unfolding also causes a change in assay geometry resulting in a change in force application. These differences might help to explain why, in AFM extension, more Ig domains of filamin tend to unfold prior to rupture. The complex but more physiologically-relevant geometry of our assay may increase the possibility of unbinding after unfolding of several domains. As a result, relatively irregular and fewer repeats of undulation are exhibited compared to the regular sawtooth-like behavior observed in the AFM measurement (15).

One particularly interesting finding is that the critical forces for unbinding and unfolding are quite similar, suggesting that both are likely to be important mechanisms in regulating cytoskeletal mechanics and thereby influencing a wide range of dynamic behaviors. Two events occurring at the same force can confer a higher degree of modulation of cell responses to stress. Unfolding can allow for added compliance with the ability for the cytoskeleton to recover to its initial configuration when loads are relaxed. Unbinding, on the other hand, allows for shape remodeling of the cell. What factors regulate the tendency for one mechanism over the other remains unclear, although we have observed both at the similar force level.

A unique feature of our measurement method was that we could observe the dependence of unbinding force on the pulling angle between the two crosslinked actin filaments. This led to the observation that the rupture force significantly decreases when the pulling angle exceeds 45°. While the force at zero angle stretches the cross-linking protein, the force applied with non-zero angle causes a twisting deformation to be applied to the bond (Inset in Fig. 4.4B). Our results suggest that bonds rupture more easily when they are subject to a torque/shear force. Since the same angle-dependent behavior with the similar critical angle ~ 45° was also observed in our previous measurements at low loading rate (17), this implies that the molecular structure of the ABP-actin bond rather than the dynamic loading condition determines the threshold angle. Compared to filamin, the rupture force for α-actinin exhibited a lower dependence on angle except at the largest angles, > 70°. Because both filamin and α-actinin share a similar actin binding-domain, the smaller critical angle for filamin seems to be due to the larger molecular weight and complex structure. Filamin A is a 280kDa protein with an actin binding domain at its N-terminus followed by 24 tandem immunoglobulin-like repeats which are interrupted by two hinge regions; one between repeats 15 and 16 and the other between repeats 23 and 24 (32). Dimerization through the last C-terminal repeat forms a V-shaped homodimer, which is quite different from the short and antiparallel α-actinin dimmer. Tests for filamin mutants such as the hinge-less one will be useful for identifying which subdomain plays a significant role in determining a torsional rigidity.

In vivo ABPs and actin filaments are organized into a three-dimensional actin cytoskeleton. External stress or internal tensions generated by actomyosin contraction can create various types of loading conditions on cross-linking proteins, such as extension, compression, shear, and torsion; these different conditions, as the present results demonstrate, can influence

the force levels for rupture or unfolding. Events associated with network fracture or nonlinear rheology have been suggested to occur at levels force smaller than the plateau value of the single molecule rupture force (6, 45), suggesting that the cross-linking bonds in the network undergo complex deformations. Numerical simulations were useful to help explain how molecular interactions influence the mechanical behavior of the network. The force on the bead exhibited an abrupt decrease when a cross-linking protein unbinds, similar to the transitions observed in the experiments. However, the force at which the force drop occurred was higher compared to the experiments for both single molecule and F-actin network. This difference in force could be caused by discrepancies between the experiment and simulation in terms of system size, filament length, and loading speed.

Combining experiments and computational analysis suggests that unbinding could account for the abrupt transitions observed during bead translation through a cross-linked actin network. However, we can not rule out the possibility that similar transitions might occur as a result of filament buckling or unfolding of ABPs. Small fraction of the measurements exhibits the reversible strain-dependent mechanical properties suggesting the network the network maintain its structure even at larger deformation. Also repeating pattern at a constant force is observed in the network responses implying unfolding of ABPs cause stress relaxation.

4.6 References

1. Bursac, P., Lenormand, G., Fabry, B., Oliver, M., Weitz, D. A., Viasnoff, V., Butler, J. P. & Fredberg, J. J. (2005) Cytoskeletal remodelling and slow dynamics in the living cell *Nat Mater* 4, 557-61.
2. Fabry, B., Maksym, G. N., Butler, J. P., Glogauer, M., Navajas, D. & Fredberg, J. J. (2001) Scaling the microrheology of living cells *Physical Review Letters* 87, 148102.
3. Shin, J. H., Gardel, M. L., Mahadevan, L., Matsudaira, P. & Weitz, D. A. (2004) Relating microstructure to rheology of a bundled and cross-linked F-actin network in vitro *Proc Natl Acad Sci U S A* 101, 9636-9641.
4. Wachsstock, D. H., Schwarz, W. H. & Pollard, T. D. (1994) Cross-linker dynamics determine the mechanical properties of actin gels *Biophys J* 66, 801-9.
5. Xu, J. Y., Wirtz, D. & Pollard, T. D. (1998) Dynamic cross-linking by alpha-actinin determines the mechanical properties of actin filament networks *Journal of Biological Chemistry* 273, 9570-9576.
6. Gardel, M. L., Nakamura, F., Hartwig, J., Crocker, J. C., Stossel, T. P. & Weitz, D. A. (2006) Stress-dependent elasticity of composite actin networks as a model for cell behavior *Physical Review Letters* 96, 088102.
7. Gardel, M. L., Nakamura, F., Hartwig, J. H., Crocker, J. C., Stossel, T. P. & Weitz, D. A. (2006) Prestressed F-actin networks cross-linked by hinged filamins replicate mechanical properties of cells *Proceedings of the National Academy of Sciences of the United States of America* 103, 1762-1767.
8. Kumar, S., Maxwell, I. Z., Heisterkamp, A., Polte, T. R., Lele, T. P., Salanga, M., Mazur, E. & Ingber, D. E. (2006) Viscoelastic retraction of single living stress fibers and its impact on cell shape, cytoskeletal organization, and extracellular matrix mechanics *Biophysical Journal* 90, 3762-3773.
9. Stossel, T. P., Condeelis, J., Cooley, L., Hartwig, J. H., Noegel, A., Schleicher, M. & Shapiro, S. S. (2001) Filamins as integrators of cell mechanics and signalling *Nat Rev Mol Cell Biol* 2, 138-45.
10. Wagner, B., Tharmann, R., Haase, I., Fischer, M. & Bausch, A. R. (2006) Cytoskeletal polymer networks: the molecular structure of cross-linkers determines macroscopic properties *Proc Natl Acad Sci U S A* 103, 13974-8.
11. Ingber, D. E. (1993) Cellular tensegrity: defining new rules of biological design that govern the cytoskeleton *J Cell Sci* 104 (Pt 3), 613-27.
12. Gibson, L. J. & Ashby, M. F. (1982) The Mechanics of 3-Dimensional Cellular Materials *Proceedings of the Royal Society of London Series a-Mathematical Physical and Engineering Sciences* 382, 43-&.
13. Gibson, L. J., Ashby, M. F., Schajer, G. S. & Robertson, C. I. (1982) The Mechanics of Two-Dimensional Cellular Materials *Proceedings of the Royal Society of London Series a-Mathematical Physical and Engineering Sciences* 382, 25-42.
14. Storm, C., Pastore, J. J., MacKintosh, F. C., Lubensky, T. C. & Janmey, P. A. (2005) Nonlinear elasticity in biological gels *Nature* 435, 191-4.
15. Furuike, S., Ito, T. & Yamazaki, M. (2001) Mechanical unfolding of single filamin A (ABP-280) molecules detected by atomic force microscopy *FEBS Letters* 498, 72-75.

16. Yamazaki, M., Furuike, S. & Ito, T. (2002) Mechanical response of single filamin A (ABP-280) molecules and its role in the actin cytoskeleton *Journal of Muscle Research and Cell Motility* 23, 525-534.
17. Ferrer, J. M., Lee, H., Chen, J., Pelz, B., Nakamura, F., Kamm, R. D. & Lang, M. J. (2008) Measuring molecular rupture forces between single actin filaments and actin-binding proteins *Proc Natl Acad Sci U S A* 105, 9221-6.
18. Nakamura, F., Osborn, E., Janmey, P. A. & Stossel, T. P. (2002) Comparison of filamin A-induced cross-linking and Arp2/3 complex-mediated branching on the mechanics of actin filaments *Journal of Biological Chemistry* 277, 9148-9154.
19. Kwiatkowski, D. J., Janmey, P. A. & Yin, H. L. (1989) Identification of Critical Functional and Regulatory Domains in Gelsolin *Journal of Cell Biology* 108, 1717-1726.
20. Suzuki, N., Miyata, H., Ishiwata, S. & Kinosita, J., K. (1996) Preparation of bead-tailed actin filaments: estimation of the torque produced by the sliding force in an in vitro motility assay *Biophys J* 70, 401-408.
21. Lang, M. J., Asbury, C. L., Shaevitz, J. W. & Block, S. M. (2002) An automated two-dimensional optical force clamp for single molecule studies *Biophys J* 83, 491-501.
22. Neuert, G., Albrecht, C., Pamir, E. & Gaub, H. E. (2006) Dynamic force spectroscopy of the digoxigenin-antibody complex *FEBS Lett* 580, 505-9.
23. Bell, G. I. (1978) Models for Specific Adhesion of Cells to Cells *Science* 200, 618-627.
24. Evans, E. & Ritchie, K. (1997) Dynamic strength of molecular adhesion bonds *Biophysical Journal* 72, 1541-1555.
25. Hummer, G. & Szabo, A. (2003) Kinetics from nonequilibrium single-molecule pulling experiments *Biophysical Journal* 85, 5-15.
26. Guo, B. & Guilford, W. H. (2006) Mechanics of actomyosin bonds in different nucleotide states are tuned to muscle contraction *Proceedings of the National Academy of Sciences of the United States of America* 103, 9844-9849.
27. Merkel, R., Nassoy, P., Leung, A., Ritchie, K. & Evans, E. (1999) Energy landscapes of receptor-ligand bonds explored with dynamic force spectroscopy *Nature* 397, 50-53.
28. Tees, D. F. J., Waugh, R. E. & Hammer, D. A. (2001) A microcantilever device to assess the effect of force on the lifetime of selectin-carbohydrate bonds *Biophysical Journal* 80, 668-682.
29. Yuan, C., Chen, A., Kolb, P. & Moy, V. T. (2000) Energy landscape of streptavidin-biotin complexes measured by atomic force microscopy *Biochemistry* 39, 10219-23.
30. Miyata, H., Yasuda, R. & Kinosita, K. (1996) Strength and lifetime of the bond between actin and skeletal muscle alpha-actinin studied with an optical trapping technique *Biochimica Et Biophysica Acta-General Subjects* 1290, 83-88.
31. Dearruda, M. V., Watson, S., Lin, C. S., Leavitt, J. & Matsudaira, P. (1990) Fimbrin Is a Homolog of the Cytoplasmic Phosphoprotein Plastin and Has Domains Homologous with Calmodulin and Actin Gelation Proteins *Journal of Cell Biology* 111, 1069-1079.
32. Gorlin, J. B., Yamin, R., Egan, S., Stewart, M., Stossel, T. P., Kwiatkowski, D. J. & Hartwig, J. H. (1990) Human Endothelial Actin-Binding Protein (Abp-280, Nonmuscle Filamin) - a Molecular Leaf Spring *Journal of Cell Biology* 111, 1089-1105.
33. McGough, A., Way, M. & DeRosier, D. (1994) Determination of the alpha-actinin-binding site on actin filaments by cryoelectron microscopy and image analysis *J Cell Biol* 126, 433-443.

34. Goldmann, W. H. & Isenberg, G. (1993) Analysis of filamin and alpha-actinin binding to actin by the stopped flow method *FEBS Lett* 336, 408-410.
35. Wachsstock, D. H., Schwartz, W. H. & Pollard, T. D. (1993) Affinity of alpha-actinin for actin determines the structure and mechanical properties of actin filament gels *Biophys J* 65, 205-14.
36. Gorlin, J. B., Cunningham, C. C., Yamin, R., Byers, R. H., Stossel, T. P., Kwiatowski, D. J. & Hartwig, J. H. (1990) Human Actin-Binding Protein (Abp) Filamin - a Dystrophin-Like Actin-Binding Domain Linked to 24 B-Sheet Repeats - Abp-Deficient Melanoma Cell-Lines Demonstrate Aberrant Cortical Actin Gelation Invitro and Reduced Virulence Invivo *Clinical Research* 38, A458-A458.
37. Bhasin, N., Carl, P., Harper, S., Feng, G., Lu, H., Speicher, D. W. & Discher, D. E. (2004) Chemistry on a single protein, vascular cell adhesion molecule-1, during forced unfolding *J Biol Chem* 279, 45865-74.
38. Kellermayer, M. S. Z. & Bustamante, C. (1997) Folding-unfolding transitions in single titin molecules characterized with laser tweezers *Science* 277, 1117-1117.
39. Livnah, O., Bayer, E. A., Wilchek, M. & Sussman, J. L. (1993) Three-dimensional structures of avidin and the avidin-biotin complex *Proc Natl Acad Sci U S A* 90, 5076-80.
40. Kellermayer, M. S., Bustamante, C. & Granzier, H. L. (2003) Mechanics and structure of titin oligomers explored with atomic force microscopy *Biochim Biophys Acta* 1604, 105-14.
41. Tskhovrebova, L., Trinick, J., Sleep, J. A. & Simmons, R. M. (1997) Elasticity and unfolding of single molecules of the giant muscle protein titin *Nature* 387, 308-312.
42. Yamazaki, M., Furuike, S. & Ito, T. (2002) Mechanical response of single filamin A (ABP-280) molecules and its role in the actin cytoskeleton *J Muscle Res Cell Motil* 23, 525-34.
43. Kim, T., Hwang, W. & Kamm, R. D. (2009) Computational analysis of a cross-linked actin-like network *Exp. Mech.* 49, 91-104.
44. Chaudhuri, O., Parekh, S. H. & Fletcher, D. A. (2007) Reversible stress softening of actin networks *Nature* 445, 295-298.
45. Tharmann, R., Claessens, M. M. A. E. & Bausch, A. R. (2007) Viscoelasticity of isotropically cross-linked actin networks *Physical Review Letters* 98, 088103.
46. Xu, J. Y., Tseng, Y. & Wirtz, D. (2000) Strain hardening of actin filament networks - Regulation by the dynamic cross-linking protein alpha-actinin *Journal of Biological Chemistry* 275, 35886-35892.
47. Berg, J. M., Tymoczko, J. L. & Stryer, L. (2002) Biochemistry, W. H. Freeman.

5 Studying the Nonlinear Dynamics of F-actin Network under External Stress

5.1 Background

The mechanical properties of the cytoplasm are crucial physical parameters for many cellular processes such as cell motility, cell division, and intracellular transport of vesicles. Previous measurements for *in vivo* cells revealed that the cytoplasm exhibits both elastic and viscous characteristics (1, 2) with an elastic modulus estimated to be on the order of 10-1000Pa. Nonetheless, the complexity and the high degree of heterogeneity of a living cell hinder an accurate characterization of the mechanical properties of the cytoplasm. As the dominant structural constituent of the cell cytoplasm is an F-actin network comprised of individual or bundled filaments, *in vitro* re-constituted F-actin gels polymerized with purified actin and ABP have proven useful as a model system. However, the elasticity of *in vitro* F-actin gels has proven to be smaller than the values measured for *in vivo* cells (3, 4). This discrepancy is not fully understood, but it has been attributed to various factors including prestress of the network and the presence of various cross-linking proteins. For example, entangled actin filaments exhibit elastic moduli of only 0.03-3Pa at an actin concentration of 0.3-3mg/mL (5). Addition of ABP increases the elasticity of an F-actin gel by cross-linking actin filaments. For example, when actin is polymerized with α-actinin, both storage and loss moduli of the F-actin gels increase by factors of 4 and 8, respectively, in measurements using a torsional pendulum (6). Also, an F-actin network cross-linked with filamin exhibits network stiffness an order of magnitude larger than that of pure F-actin (7). However, the mechanical stiffness of an *in vitro* re-constituted F-actin network is still an order of magnitude lower than that observed in cells. Recently,

measurements of F-actin networks under pre-stress have shown that mechanical force plays an important role in determining material properties of an F-actin network, leading to a significant increase in the network elasticity (8). Also it was shown that both internal stress arising from acto-myosin contraction and external adhesion to an extracellular matrix controlled cytoskeletal mechanics (9, 10). F-actin network under further strain exhibited strain-hardening and subsequent softening in which network elasticity decreases as an applied strain increases. F-actin networks are highly nonlinear; under large stress, the elastic modulus increases with applied stress, while under small stress, it is stress-independent.

Recently, computational models of the cytoskeleton consisting of actin filaments and cross-linking ABPs have been reported to help interpret the mechanism behind structural nonlinearities. When a network is highly cross-linked and an external stress deforms the network uniformly or affinely, it has been suggested that network stiffening is caused by the entropic resistance to the extended filaments (11, 12). When a network is weakly cross-linked, its deformation is more complicated including bending as well as extension of actin filaments (11, 12). The mechanical properties of ABPs also play a critical role in determining the dynamic behavior of the network subject to increasing stress. At the same concentrations of actin and ABP, an F-actin network cross-linked with mutant filamin did not exhibit the nonlinear behavior which was observed in the network cross-linked with wild-type filamin (8). The experiments using various cross-linking constructs show that the detailed molecular structure of the ABPs determines the critical stress at which the network modulus decreases (13).

Nonetheless, experimental evidence to test the existing models is lacking and the microscopic origin of the nonlinear behavior of an F-actin network is still unclear. In this chapter, by using a shear device equipped with imaging capabilities, the structural evolution of F-actin

network is visualized while the mechanical properties are simultaneously determined. The microrheology techniques developed in Chapter 2 are used to estimate the mechanical properties of a pre-stressed F-actin network. Relating the change in mechanical properties to the alteration in microstructure provides insight into the origin of the non-linear dynamics of F-actin networks. We also explore how a modification of the ABP alters the mechanical behavior of the cross-linked F-actin network by using a mutant filamin. The methods and techniques in this chapter can be applied to study the dynamic responses of other biological components such as microtubules and intermediate filaments to an external shear stress.

5.2 Methods and Materials

5.2.1 Shear Device

A shear device was designed to apply an external force to a cross-linked F-actin network. The device consists of two metal plates. While the bottom plate is stationary, the top plate can be displaced along two axes by piezo-controlled micromotors. Each plate holds a glass window through which the sample can be visualized.

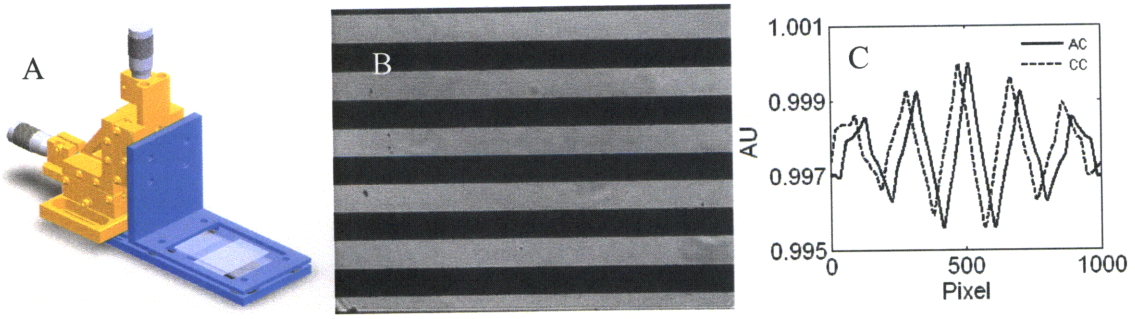

Figure 5.1 Shear device. (A) A 3D drawing of the shear device consisting of a stationary plate for holding a coverglass and a movable plate for holding a glass slide. An F-actin network is polymerized in the space between the two glass surfaces and shear strain is applied by displacing the top plate using a piezo-controlled micromotor. To determine resolution of the device, a standard grooved surface was displaced and imaged by the microscope (B). Auto-correlation (AC) and cross-correlation (CC) analyses for the images determined the resolution of the motor to be 33nm/step (C).

Shear strain applied to a network is determined by the height and the displacement of the top plate. The height of the sample is controlled by the z-axis piezo-micromotor and is calibrated using a height gauge. Another piezo-controlled micromotor determines the displacement of the top surface of the sample. Using a standard silicon surface with 12.5μm-wide grooves, the resolution of the piezo-micromotor is measured to be 33nm per step input.

5.2.2 Estimating Mechanical Properties of a Pre-stressed F-actin Network

One point particle rheology is employed to estimate the mechanical properties of an F-actin network subject to external shear stress. The shear device applies a shear strain to the F-actin network and fluctuations of the microspheres embedded in the network are monitored. The mechanical properties of the sheared F-actin network are obtained by analyzing the time-evolution of the bead fluctuations. As a probe particle, PEG-coated microspheres (see Appendix A.1 for the detailed protocol) are used to minimize non-specific binding between the probe particle and the actin gel. Bead motion is recorded for 30 sec. This time was empirically chosen to meet two conditions: to acquire sufficient data points over short time scales and to minimize the network relaxation over long time scales.

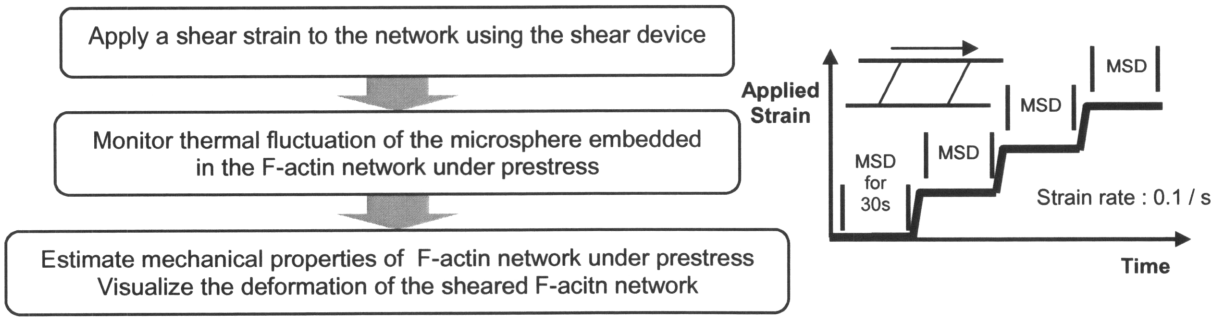

Figure 5.2 Experimental protocol for investigating mechanical behavior of F-actin networks under prestress. Shear strain is applied to the network by displacing the top plate of the shear device at the rate of 0.1/s. Immediately after applying strain, the bead fluctuation is recorded for 30sec to estimate mechanical properties. Deformation of the network structure is also visualized by confocal microscopy. Strain is sequentially increased.

5.2.3 Wild-type and Mutant Filamin

Filamin was discovered as the first family of non-muscle actin binding protein. Filamin in mammals comprises a family of three members: filamin A (FLNa), filamin B (FLNb), and filamin C (FLNc). FLNa is the most widely expressed filamin isoform, but the genomic organization of the three genes is highly conserved.

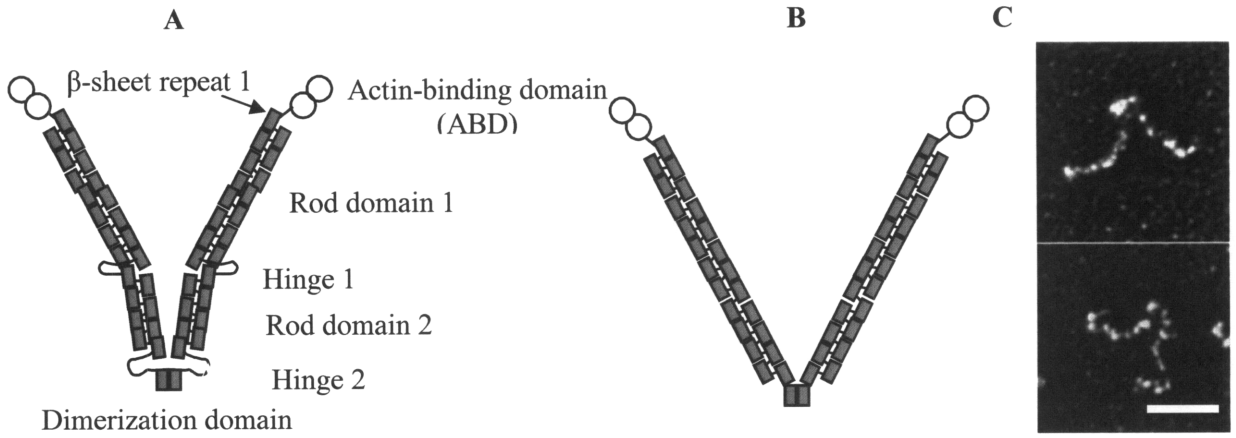

Figure 5.3 The structure of wild-type and mutant FLNa. (A) Filamin is homodimer. Each monomer consists of conserved ABD and 24 β-sheet repeats with two separations of hinge regions. (B) A schematic of mutant filamin with both hinges deleted. (C) Electron micrographs of FLNa dimers adapted from Nakamura et al. (14) (scale bar, 50nm).

Filamin monomers, each with a relative molecular weight of 280kDa, consist of an amino-terminal actin binding domain (ABD) at the N-terminus, long rod-like domain of 24 repeated, antiparallel β-sheets interrupted by two 30-aminoacid loops, and a dimerization domain at C-terminus. The two monomers form a V-shaped dimer with a length of 80nm per subunit and an angle of approximately 80° (15, 16). The ABD encompasses a stretch of 275 amino acids with two tandem calponin homology domains (CHD1 and CHD2), which are conserved in other actin binding proteins such as β-spectrin, dystrophin and α-actinin. The rod domain containing 24 repeats fold into antiparallel β-sheets separated by two hinge regions; hinge-1 between repeats 15 and 16 and hinge-2 between repeats 23 and 24. Over 30 proteins have been reported to interact with filamin rod domains. Three filamin isoforms show 60-80% homology over their entire

sequence with the exception of two hinge regions (45% homology) (17, 18). FLNb is a naturally expressed variant that lacks a hinge 1 domain while FLNa lacks a hingeless variant.

Filamin recruits actin filaments into a three-dimensional gel network. Due to the V-shape geometry and relatively large size, filamin promotes high angle branching of actin filaments, preventing redundant cross-linking of closely aligned filaments. The effective cross-linking of actin filaments facilitates gel formation at low molar ratios relative to actin (19). Filamin binds to various other macromolecules in addition to actin. Anchoring of cortical actin or actin stress fiber to the membrane proteins by filamin provides mechanical stability to the cell membrane and maintains cell-cell adhesion. Also, filamin links transmembrane receptors such as β-integrins to the actin cytoskeleton, and participates in intracellular signaling, serving as a scaffold for several signaling molecules. The impaired locomotion and surface protrusion observed in *Dictyostelium* depleted of filamin suggests that filamin plays a role in cell motility (20, 21).

The first disease linked to filamin mutations in humans was an X-chromosome-linked dominant disorder known as Petroventricular heterotopia (22). It is characterized by an abnormal appearance of neurons, collectioning along the walls of the lateral ventricle, a fetal development site, implying that neurons fail to migrate into the cerebral cortex during early brain development. Recently, a localized mutation in the FLNa gene has been found to cause four other X-linked human disorders including otopalatodigital syndrome type 1(OPD1) and 2(OPD2), frontometaphyseal dysplasia (FMD), and Melnick-Needles syndrome (MNS) (23). Mutation in FLNb has been identified to disrupt bone morphogenesis causing Spondylocarpotarsal syndrome (SCT) and Atelosteogenesis (24). The complexity of phenotype shown in various human diseases suggests that filamin has a more complicated role in mammalian development than being simply an integrator of cell mechanics.

5.3 Results

5.3.1 Structural Evolution of Cross-linked F-actin Network under Shear Stress

As described in Chapters 2 and 3, the cross-linked F-actin network is labeled by polymerizing actin and ABPs with rhodamine-phalloidin. To visualize an alteration of network structure under an external shear stress, the network is formed in the shear device and is imaged by confocal microscopy while strain is applied. In the cross-linking point indicated by arrowhead in Fig. 5.4A, the angle at which actin filaments form varies as the network undergoes shear deformation. Although the cross-link angle increases with applied strain, thermal motion of the actin filaments seems to cause a fluctuation in the measured angle (Fig. 5.4B).

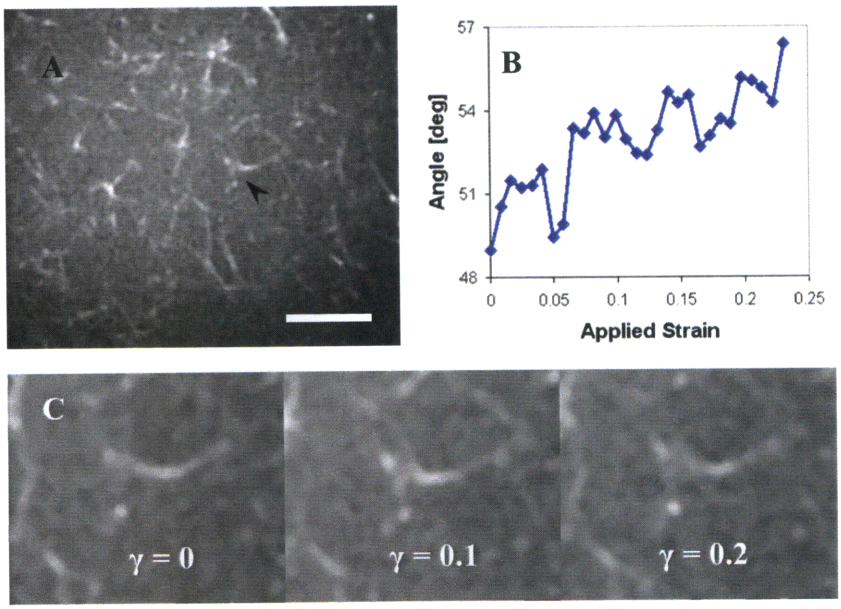

Figure 5.4 Alteration of cross-linking angle. (A) Fluorescent micrograph shows the cross-linked F-actin network polymerized in the shear device. The arrowhead indicates the cross-linking point where an angle between two actin filaments that varies as the external shear stress is imposed on the F-actin network (scale bar, 10μm). (B) The angle increases as the applied strain increases. (C) The magnified images of the region indicated by the arrowhead show the angle as it changes for strains of 0, 0.1, and 0.2.

In another experiment for the cross-linked F-actin network (c_A = 10μM, R_f = 0.01, R_g = 1/1000), shear deformation of the network causes an alignment of filaments and a distortion of the actin mesh. As the network is deformed by external shear, some curved actin filaments are stretched and become progressively aligned. Also, the shape of the mesh is deformed as the distance between the cross-linking points is increased or decreased when the network is sheared.

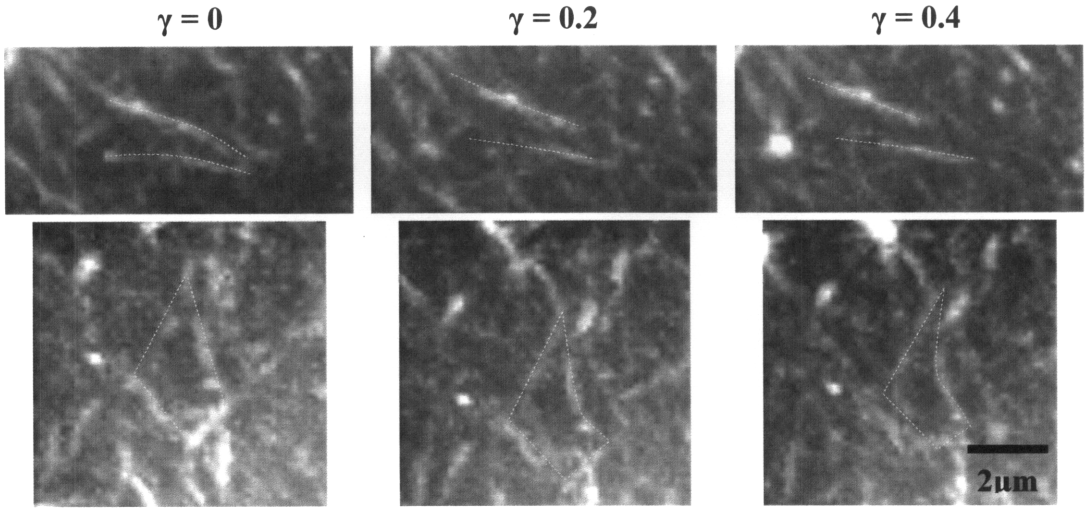

Figure 5.5 Shear-induced alterations of network structures. As the strain applied to the network increases from 0 to 0.4, the curved actin filaments are stretched and become increasingly aligned (Top row). Network deformation sometimes causes a significant bending of the actin filament leading to a distortion of the diamond-shaped mesh formed by the actin filaments (Bottom row).

Also, rupture of the F-actin network is observed at high strain. Networks formed in the absence of external strain exhibit a homogeneous, isotropic structure. At intermediate strains of 0.15-0.3, some actin filaments become aligned along the shear direction. The extended filaments seem to become disconnected as additional strain is applied and heterogeneity of the structure increases. Although it is not easy to identify the cause of the network rupture in these images, the merged image at 3 levels of strain shows local ruptures of network structure more clearly (Fig. 5.7). As the F-actin network increasingly ruptures at higher strains, fewer actin filaments are visualized.

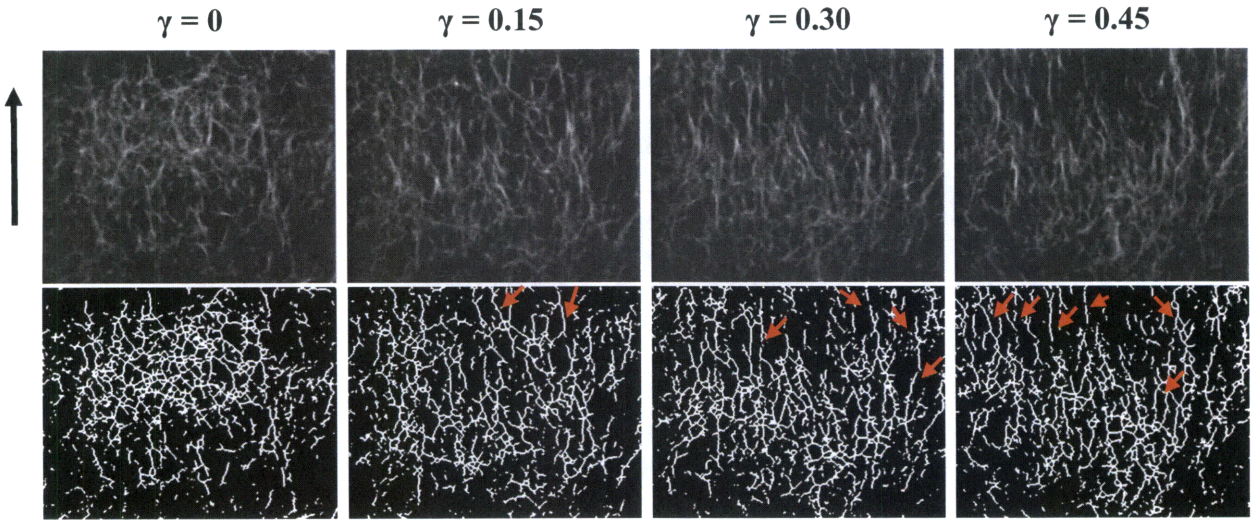

Figure 5.6 Network structure as a function of strain. Strain direction is indicated by the large arrow. Initially ($\gamma = 0$), actin and ABP form a homogeneous network. Applied strain aligned the actin filaments as indicated by the small arrows in the images. As more strain is applied, more ruptures are observed in the network. Increasing strain increases the heterogeneity of the structure.

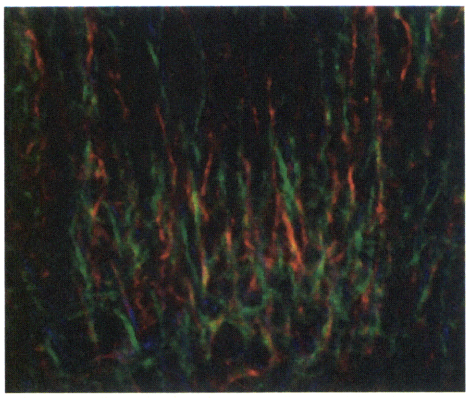

Figure 5.7 Merged image of F-actin network at strains of 0.45 (red), 0.75 (green), and 1(blue). Some of the extended actin filaments are not seen in the image at high strain as the network ruptures.

5.3.2 Mechanical Properties of F-actin Networks under Shear Stress

We also investigate the mechanical properties of cross-linked F-actin networks ($c_A = 20\mu M$, $R_f = 0.01$, $R_g = 1/5000$) subjected to external shear stress by monitoring thermal fluctuation of embedded microspheres. Microspheres in the sheared F-actin network exhibit two different behaviors. For some microspheres, the MSD decreases as the applied strain increases up to a

critical strain and then increases at higher strains. For other microspheres, no significant change is observed in their MSDs for various strains. These results suggest that not all of the network exhibits strain-stiffening and that the nonlinear mechanical behavior of the F-actin network depends on its local structure.

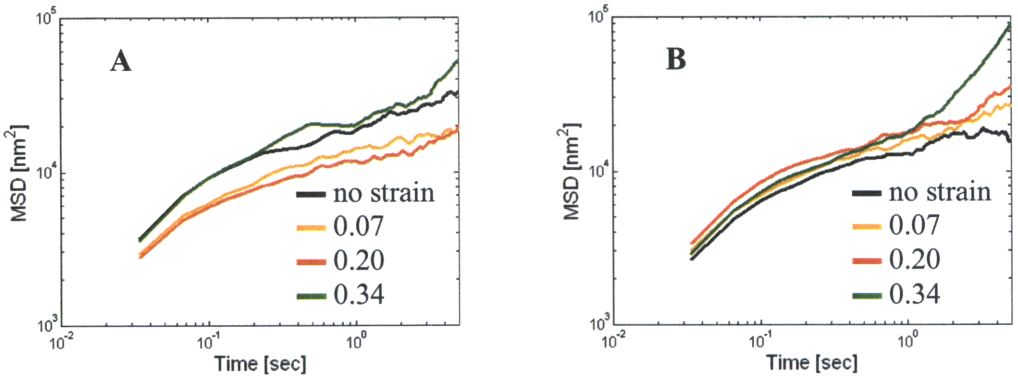

Figure 5.8 Change in MSD at various strains. (A) As the strain increases, MSD decreases over the entire range of time scales suggestive of local strain-hardening. However, the MSD increases at the high strain of 0.34, suggestive of local strain-softening. (B) No significant change in MSD is observed in MSDs for some beads.

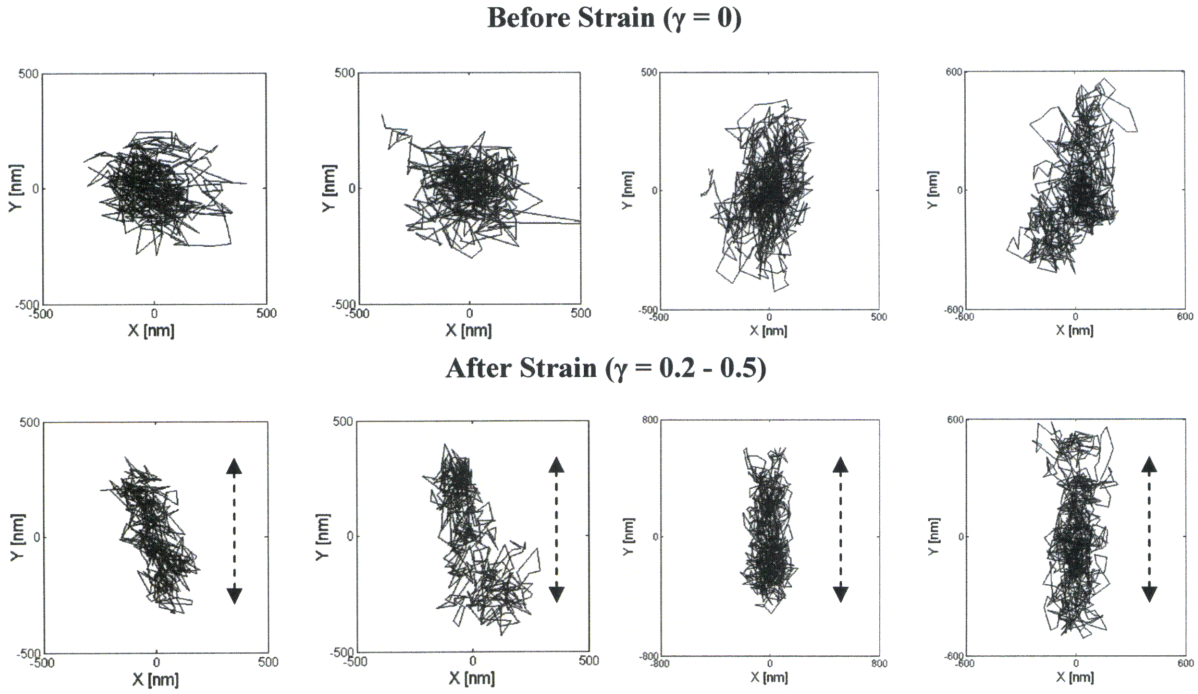

Figure 5.9 Two-dimensional particle trajectories in the presence and absence of external shear. When no strain is applied to the network, the thermal fluctuation of the bead is relatively isotropic exhibiting similar x- and y-axis displacement. However, in the presence of shear strain, the bead fluctuation seems to align along the shear direction (dotted line).

To better understand how the external strain alters internal network structure, the , trajectories of bead movement were also monitored (Fig. 5.9). Before strain is applied, a microsphere embedded in the network exhibits isotropic behavior in which both x- and y-axis displacements are simialr. However, with applied strain, bead fluctuation becomes aligned along the strain direction. This is consistent with the images of the sheared F-actin network in which aligned actin actin filaments were observed at high strain. The aligned network structure seems to constrain thermal motions of the bead in the axis perpendicular to the strain. MSDs in the x- and y-axes were calculated separately and compared to the changes in the network shear modulus. We obtained both MSD and shear modulus as a function of strain at 3Hz; although the lower frequency behavior would reflect more intrinsic mechanical properties of F-actin network, an intermediate frequency of 3Hz was chosen because both MSD and shear modulus are noisy at long time scales as the number of data points decreases. To see if the network exhibits strain-sitffening or strain-softening, both MSD and shear modulus are normalized by the values with no strain is applied.

The shear modulus increases as the applied strain increases at small strain. However, at strains higher than a critical value in the range of 0.3-0.5, the shear modulus decreases indicating an increasing fragility of the network. The increase of shear modulus in the strain-stiffening region is small compared to that observed in the previous bulk measurements (7, 8), but is similar to that in our microscale measurements (Fig. 4.10B). As expected from the particle trajectory with alignment, changes in the shear modulus are more correlated with the MSD along the x-axis, or perpendicular to the shear direction. X-MSD decreases with increasing applied strain up to a critical value and then increases under additional strain. However, not all the probe particles exhibit the same non-linear mechanical behaviors of strain-sitffening and strain-

softening. The results suggest that the degree of non-linearity is specially variable depending on local interaction between a microsphere and actin filaments.

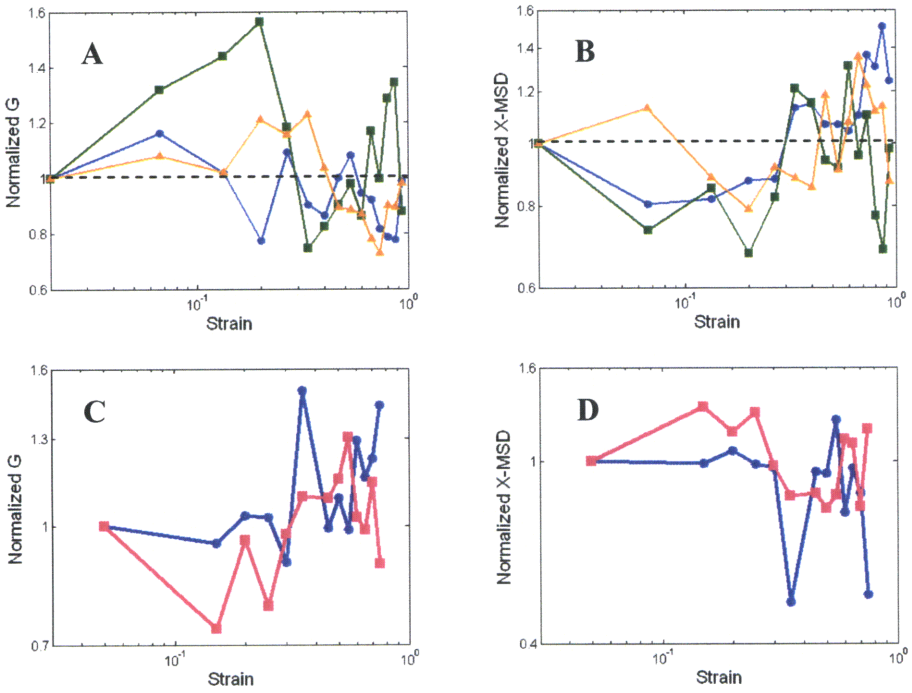

Figure 5.10 Mechanical properties as a function of strain. (A) As indicated by the increase and decrease of shear modulus, strain-stiffening and strain-softening behaviors are observed for some beads embedded in the cross-linked F-actin network. (B) The change in X-MSD is more strongly correlated with the alteration in shear modulus shown in (A). However, this nonlinear behavior exhibits spatial variation. The other beads embedded in the same network do not show a distinct non-linear behavior. Instead, (C) the shear modulus decreases or remains at a constant value with increasing strain up to a critical strain of 0.3-0.5. (D) No significant variation is observed in the corresponding X-MSD as a function of strain.

5.3.3 Effect of Hinge Domain on Mechanical Behavior of F-actin Network

The same experiment was performed for F-actin network cross-linked with mutant filamin to investigate the effect of the hinge domain on the mechanical behavior of F-actin networks. Compared with the results for wild-type filamin/F-actin networks, similar behavior is observed in the mechanical properties as a function of strain for the mutant filamin/F-actin network. While some beads exhibit both strain-stiffening and strain-softening behaviors, others exhibit strain-softening without strain-stiffening. However, both increase and decrease of shear modulus with

increasing strain are more distinct and the data look more consistent between measurements. It seems that the hinge domains in filamin provide more flexibility to the network allowing more complicated deformations.

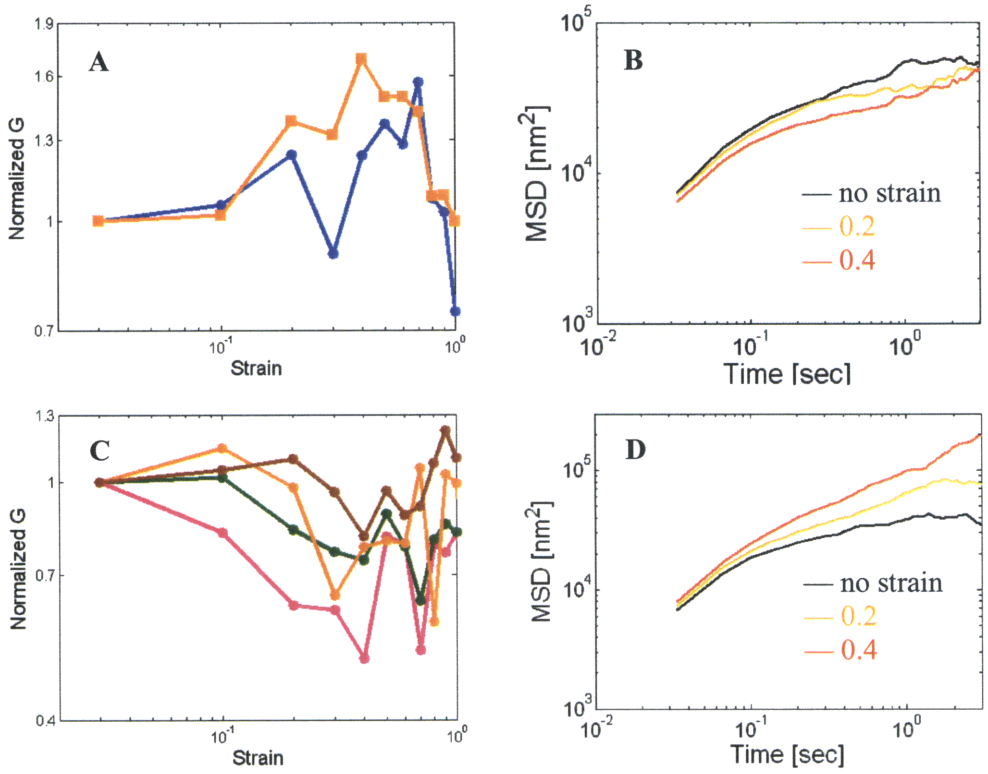

Figure 5.11 Mechanical properties as a function of strain for mutant FLNa/F-actin network. (A) Shear modulus increases as the applied strain increases up to a critical value. With further stain, the stress decreases indicating the local rupture or unfolding of the network. (B) In the strain-stiffening behavior, the MSD decreases as strain increase over the entire period. (C) For beads in another region, the shear modulus decreases with increasing strain suggesting that strain-softening occurs without strain-stiffening. (D) In strain-softening behavior, the MSD increases as strain increases.

We have studied how the local mechanical properties of F-actin network vary when an external shear stress is applied, by obtaining thermal fluctuations of embedded microspheres. We also monitored bead displacements during strain to obtain the global response of the network to an external shear. The displacement is defined as a distance between the average positions of the bead before and after each strain (Fig. 5.12A).

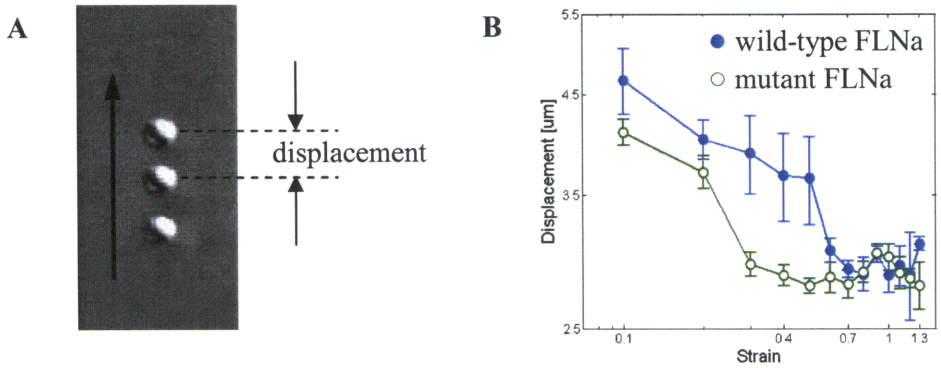

Figure 5.12 Bead displacement as a function of network strain. (A) Stacked images of the bead at the applied strain (thick arrow) moves the average position of bead. (B) The increments in bead displacement decrease as the applied strain increases with a dramatic drop observed at a critical value of strain. The critical strain for wild-type FLNa network is higher than that for mutant FLNa network.

Bead displacement significantly decreases at a critical strain for both wild-type and mutant FLNa networks. However, the critical strain at which bead displacement decreases significantly is higher for the F-actin network cross-linked with wild-type FLNa.

5.3.4 Computational Approach for Network Deformation

In order to investigate further the deformations that occur in a sheared cross-linked F-actin network, a simple model was developed. Actin cross-linking proteins are randomly dispersed in a three-dimensional space of 100 μm(l) x 80 μm (w) x 5 μm (h). The F-actin network is formed by connecting the cross-linking proteins via actin filaments. The minimum and maximum length of actin filaments are constrained to 1 and 8 μm, respectively, to simulate F-actin polymerized in the presence of gelsolin. Therefore, connection by an actin filament is only allowed when the distance between cross-linking proteins is within the limited range. A shear strain is applied to the top surface of the network. In response to the strain, resultant displacements of the cross-linking points are linearly proportional to the height of their positions assuming affine deformation. The network structure after strain is constructed by linking the displaced cross-

linking proteins with actin filaments. When a cross-linking distance exceeds the higher limit after strain, the actin filament is disconnected, simulating force-induced unbinding.

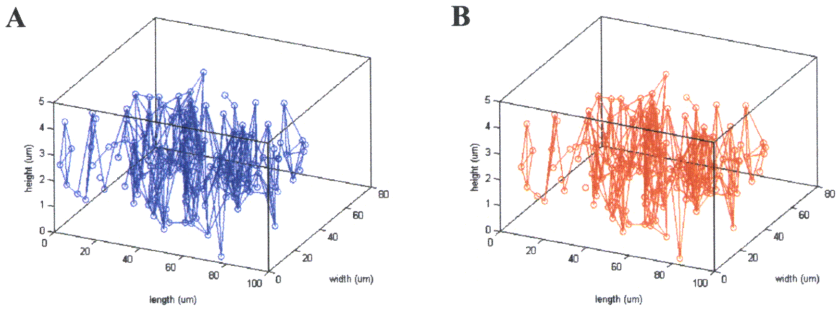

Figure 5.13 Three-dimensional F-actin network consisting of cross-linking proteins (○) and actin filaments (–) before and after strain. Arrow indicates a direction of shear strain. (A) Cross-linking points are randomly distributed in the 3-d space and those are connected by actin filaments when the distance is between limits. (B) The cross-linking points are displaced by the external shear strain assuming affine deformation.

Similarly to visualization using microscope in experiment, we generate projected images of the 3-d F-actin network before and after strain. Comparison of the two images reveals that the applied strain alters the local network structure. For example, mesh geometry is altered as each cross-linking point undergoes a different amount of displacement. When the distance between two cross-linking points is beyond the specified limit, the actin filaments become disconnected. These alterations of local structures are similar to the experimental observations in the F-actin network under external shear stress.

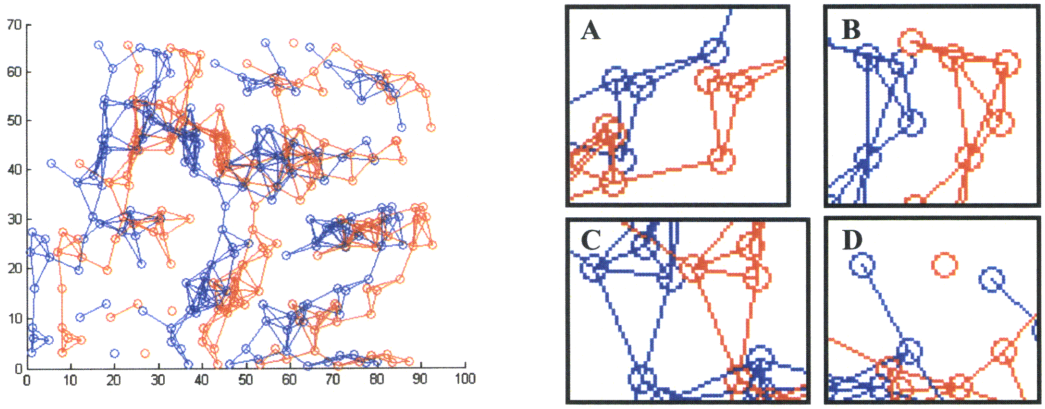

Figure 5.14 Top view of F-actin network before (blue) and after (red) strain. (A,B,C) Depending on local geometry, the size of specific openings can become either smaller or larger with strain. (D) As strain increasingly separates two cross-linking points, the actin filament is disconnected simulating force-induced unbinding.

5.4 Discussion

We directly visualized the structures of cross-linked F-actin networks under shear deformation using a shear device equipped with a confocal microscope. By monitoring the thermal fluctuations of embedded microspheres, we also estimated the mechanical properties of F-actin networks as a function of shear magnitude. Measurements were made in F-actin networks cross-linked with both wild-type and mutant FLNa. Experimental results demonstrate how changes in the molecular structure of the ABP influences the mechanical behavior of the F-actin network.

External shear stress causes significant changes in the micro-architecture of F-actin networks. At small strain (< 0.4), we could observe the deformation of mesh geometry and changes in the cross-link angles. When the F-actin network was subjected to higher strains, actin filaments were stretched and became progressively aligned along the shear direction. The F-actin network often exhibited rupture of the structure at the higher strains. Such events might be associated with rupture of stretched actin filaments or the unbinding and unfolding of cross-linking proteins. To identify the main cause of network rupture at high strain, we tried localizing the cross-links using labeled FLNa. However, the optical resolution of the confocal was not sufficient to detect single molecule fluorescence in 3-d and the background signal from unbound FLNa did not allow an image with sufficient contrast.

Mechanical properties of F-actin network under prestress are obtained using microrheology. In previous studies using a bulk rheometer (7, 8) and AFM (25), prestress was applied to the network and then a small oscillatory strain was superposed to measure differential elastic and loss moduli. We applied a prestress to the F-actin network using shear device and obtained the viscoelasticity of the network by monitoring the thermal motions of embedded microspheres. Compared with the macroscopic measurements, our microscale measurements

also exhibited strain-stiffening and strain-softening of the cross-linked F-actin network. However, the increase in viscoelastic modulus in the strain-stiffening region was significantly smaller and not all the microspheres exhibited strain-stiffening. These discrepancies are probably due to several factors. In the macroscopic measurements, the mechanical properties are estimated by obtaining a global response of the entire F-actin network to an external stress. By contrast, our method probes the mechanical properties by monitoring the passive motion of a microsphere, which is sensitive to the local structure of the network.

The simulation of F-actin networks under shear strain could replicate some of the alterations in structure observed in the experiments. Assuming an affine deformation, displacements of the cross-links by external shear can be expected from their positions in the network. Depending on the change in the separation distance between cross-linking points, some actin filaments are extended while the others are compressed (Fig. 5.15).

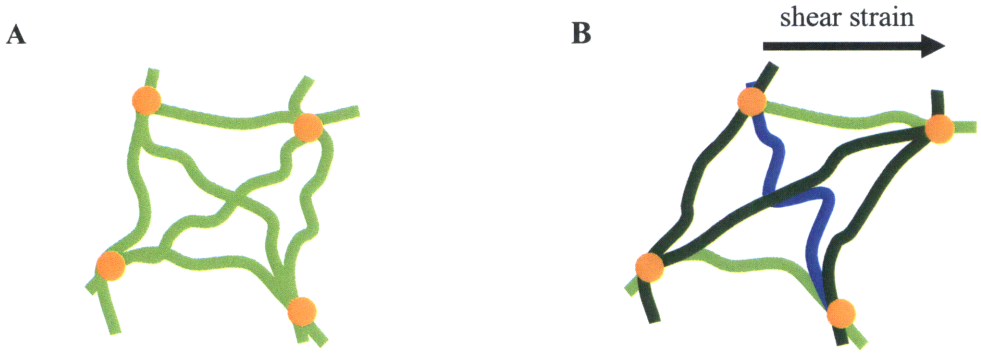

Figure 5.15 Extension of a single actin filament in the network under external shear. (A) For the network without shear strain, no stress is imposed on the filaments (light green) linked with the cross-linking proteins (orange). (B) When the network is subjected to shear strain, some actin filaments are elongated (dark green) and some are compressed (blue)

The experimental observations of elongated actin filament and mesh deformation might be inferred from the affine deformation of the network. The relative concentration of cross-linking protein to actin was 0.01, which was high enough to form a densely cross-linked network. It also increases the possibility that the cross-linked F-actin network deforms affinely rather than non-affinely (11, 12). The F-actin network subject to low strain seems to undergo affine deformation

resulting in mesh deformation and stretching of actin filaments. However, the alignment of actin filament observed at the strain >0.5 suggests that the network deformation become more complicated and non-affine at high strain. It seems that the molecular structure of the cross-linking protein is critical in determining the mechanical behavior of the F-actin network under high strain. As FLNa is a relatively large ABP with two hinge domains, it can provide flexibility for the cross-linked F-actin network to withstand high deformation allowing the actin filaments to be aligned (see the schematics in Fig. 5.16 for wild-type and mutant filamin networks). The alignment of actin filaments makes the network structure heterogeneous and this is consistent with the increase of anisotropy of the bead traces at high strains.

The F-actin network cross-linked with mutant FLNa in which the hinge domains are deleted also exhibits nonlinear behavior such as strain-hardening and strain-softening, but the softening occurs at lower levels of strain. As prestress increases, the mechanical stiffness of the mutant FLNa/F-actin network increases, which is similar to the strain-stiffening behavior observed in the wild-type FLNa/F-actin network. However, average incremental bead displacement decreases significantly at a lower level of macroscopic strain implying that the mutant FLNa network structure collapses earlier than the wild-type FLNa network. Considering these results for both wild-type and mutant FLNa networks, the microscale strain-hardening behavior appears to be initiated by affine stretching of the actin network. However, as strain increases further, the network cross-linked with wild-type FLNa is capable of withstanding larger deformations before undergoing non-affine alignment of filaments, while the F-actin network cross-linked with mutant FLNa ruptures under the high levels of strain (Table 5.1).

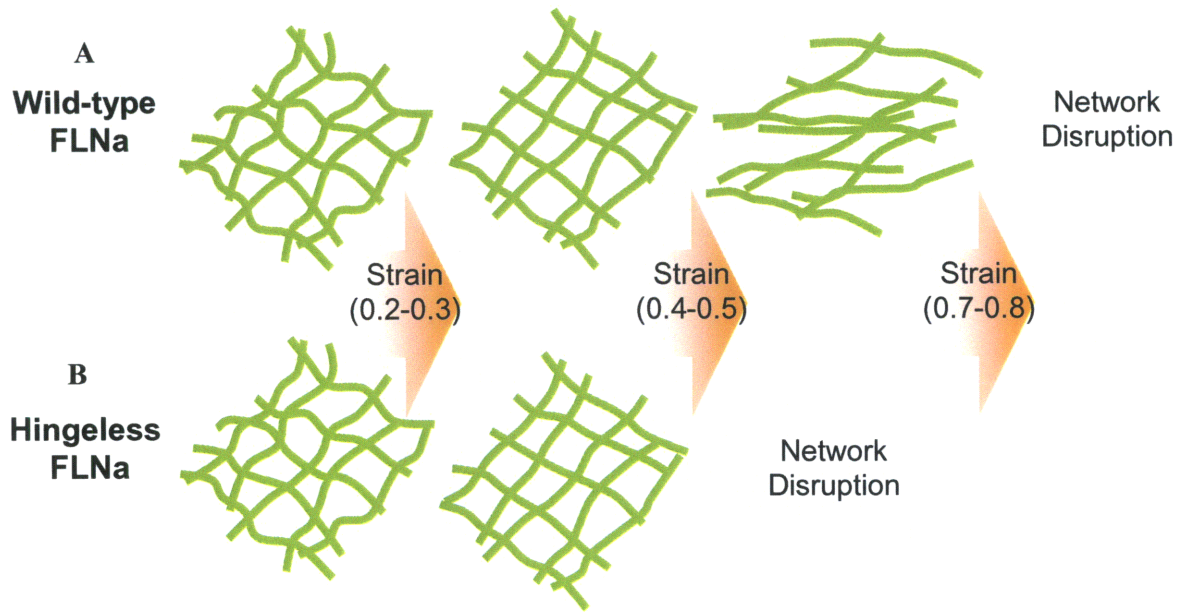

Figure 5.16 Schematic of deformation by external shear strain for wild-type (A) and mutant (B) FLNa networks. In the small applied strain, actin filaments in both networks are stretched as they are sheared. For the intermediate strain, the network cross-linked with mutant FLNa begins to disrupt while that cross-linked with wild-type FLNa exhibits further alignment of the filaments.

Strain	Low		High
Origin of strain-hardening	Extension of filaments		Alignment of filaments
Deformation mode	Affine	Non-affine	Affine
Important component	F-actin		ABP

Table 5.1 Relating structural evolution with network stiffness for the highly cross-linked F-actin. At the low strain, the network deforms in an affine manner and stretched actin filaments cause the non-linear increase of the network elasticity. At the high strain, the strain hardening is originated from the alignment of the stretched actin filaments. Actin binding proteins play a role in sustaining the intermediate strain allowing the transition of the network deformation.

5.5 References

1. Bausch, A. R., Ziemann, F., Boulbitch, A. A., Jacobson, K. & Sackmann, E. (1998) Local measurements of viscoelastic parameters of adherent cell surfaces by magnetic bead microrheometry *Biophysical Journal* 75, 2038-2049.
2. Fabry, B., Maksym, G. N., Butler, J. P., Glogauer, M., Navajas, D. & Fredberg, J. J. (2001) Scaling the microrheology of living cells *Physical Review Letters* 87, 148102.
3. Hinner, B., Tempel, M., Sackmann, E., Kroy, K. & Frey, E. (1998) Entanglement, elasticity, and viscous relaxation of actin solutions *Physical Review Letters* 81, 2614-2617.
4. Xu, J. Y., Wirtz, D. & Pollard, T. D. (1998) Dynamic cross-linking by alpha-actinin determines the mechanical properties of actin filament networks *Journal of Biological Chemistry* 273, 9570-9576.
5. Gardel, M. L., Valentine, M. T., Crocker, J. C., Bausch, A. R. & Weitz, D. A. (2003) Microrheology of entangled F-actin solutions *Physical Review Letters* 91, -.
6. Janssen, K. P., Eichinger, L., Janmey, P. A., Noegel, A. A., Schliwa, M., Witke, W. & Schleicher, M. (1996) Viscoelastic properties of F-actin solutions in the presence of normal and mutated actin-binding proteins *Archives of Biochemistry and Biophysics* 325, 183-189.
7. Gardel, M. L., Nakamura, F., Hartwig, J., Crocker, J. C., Stossel, T. P. & Weitz, D. A. (2006) Stress-dependent elasticity of composite actin networks as a model for cell behavior *Physical Review Letters* 96, 088102.
8. Gardel, M. L., Nakamura, F., Hartwig, J. H., Crocker, J. C., Stossel, T. P. & Weitz, D. A. (2006) Prestressed F-actin networks cross-linked by hinged filamins replicate mechanical properties of cells *Proceedings of the National Academy of Sciences of the United States of America* 103, 1762-1767.
9. Mizuno, D., Tardin, C., Schmidt, C. F. & MacKintosh, F. C. (2007) Nonequilibrium mechanics of active cytoskeletal networks *Science* 315, 370-373.
10. Wang, N., Tolic-Norrelykke, I. M., Chen, J., Mijailovich, S. M., Butler, J. P., Fredberg, J. J. & Stamenovic, D. (2002) Cell prestress. I. Stiffness and prestress are closely associated in adherent contractile cells *Am J Physiol Cell Physiol* 282, C606-16.
11. Head, D. A., Levine, A. J. & MacKintosh, E. C. (2003) Deformation of cross-linked semiflexible polymer networks *Physical Review Letters* 91, 108102.
12. Head, D. A., MacKintosh, F. C. & Levine, A. J. (2003) Nonuniversality of elastic exponents in random bond-bending networks *Physical Review E* 68, -.
13. Wagner, B., Tharmann, R., Haase, I., Fischer, M. & Bausch, A. R. (2006) Cytoskeletal polymer networks: the molecular structure of cross-linkers determines macroscopic properties *Proc Natl Acad Sci U S A* 103, 13974-8.
14. Nakamura, F., Osborn, T. M., Hartemink, C. A., Hartwig, J. H. & Stossel, T. P. (2007) Structural basis of filamin A functions *J Cell Biol* 179, 1011-25.
15. Gorlin, J. B., Yamin, R., Egan, S., Stewart, M., Stossel, T. P., Kwiatkowski, D. J. & Hartwig, J. H. (1990) Human Endothelial Actin-Binding Protein (Abp-280, Nonmuscle Filamin) - a Molecular Leaf Spring *Journal of Cell Biology* 111, 1089-1105.
16. Nakamura, F., Osborn, T., Hartwig, J. H. & Stossel, T. P. (2007) Mechanism of Filamin A (FLNa) actin filament (F-actin) crosslinking *Faseb Journal* 21, A993-a993.

17. Takafuta, T., Wu, G., Murphy, G. F. & Shapiro, S. S. (1998) Human beta-filamin is a new protein that interacts with the cytoplasmic tail of glycoprotein Ibalpha *J Biol Chem* 273, 17531-8.
18. van der Flier, A. & Sonnenberg, A. (2001) Structural and functional aspects of filamins *Biochim Biophys Acta* 1538, 99-117.
19. Stossel, T. P. & Hartwig, J. H. (1976) Interactions of actin, myosin, and a new actin-binding protein of rabbit pulmonary macrophages. II. Role in cytoplasmic movement and phagocytosis *J Cell Biol* 68, 602-19.
20. Cox, D., Ridsdale, J. A., Condeelis, J. & Hartwig, J. (1995) Genetic deletion of ABP-120 alters the three-dimensional organization of actin filaments in Dictyostelium pseudopods *J Cell Biol* 128, 819-35.
21. Cox, D., Wessels, D., Soll, D. R., Hartwig, J. & Condeelis, J. (1996) Re-expression of ABP-120 rescues cytoskeletal, motility, and phagocytosis defects of ABP-120-Dictyostelium mutants *Mol Biol Cell* 7, 803-23.
22. Eksioglu, Y. Z., *et al.* (1996) Periventricular heterotopia: an X-linked dominant epilepsy locus causing aberrant cerebral cortical development *Neuron* 16, 77-87.
23. Robertson, S. P., *et al.* (2003) Localized mutations in the gene encoding the cytoskeletal protein filamin A cause diverse malformations in humans *Nat Genet* 33, 487-91.
24. Krakow, D., *et al.* (2004) Mutations in the gene encoding filamin B disrupt vertebral segmentation, joint formation and skeletogenesis *Nat Genet* 36, 405-10.
25. Chaudhuri, O., Parekh, S. H. & Fletcher, D. A. (2007) Reversible stress softening of actin networks *Nature* 445, 295-298.

6 Conclusions and Future Works

In this thesis, both passive and active microrheology techniques using optical tweezers were developed to estimate the mechanical properties of F-actin networks. Measurements for the F-actin networks cross-linked with various actin binding proteins investigated the effect of filament length, degree of cross-linking, and probe particle size. The active method was modified and applied to obtain the mechanical response of F-actin networks to an external force. The microscale network behaviors were compared with the single molecule binding interactions between F-actin and actin binding protein, which revealed the molecular origin of strain-softening of F-actin networks. The shear device was able to measure the changes in mechanical properties and structural deformation of the sheared F-actin networks simultaneously. These studies provide some insight into the kinetics and dynamics of actin cytoskeletons under strain.

Further study of mechanical properties of actin binding protein will be helpful in establishing a model for cytoskeletal mechanics and rheology. For example, torsional and extensional rigidity of the actin binding proteins can be measured by isolating the protein in using the assay we developed (Ch. 4). Also, the shear device (Ch. 5) can be applied to the study of other biological materials such as polymer networks and cells. Its capacity to simultaneously manipulate and observe the three dimensional matrix is quite helpful considering their unique mechanical characteristics and dimensions. For instance, when biopolymers are encapsulated in a three-dimensional scaffold, the dynamic behavior of the polymers can be investigated.

Appendix

A Protocols

A. 1 Solution T (500mM Tris-HCl, 20mM $CaCl_2$, 1% NaN_3)

1. On a 50-mL Falcon tube, add 3.940 g Tris-HCl and 0.147 g $CaCl_2$.
2. Add ddH_2O to 50 mL and mix well.
3. Add 0.5g per 50mL to make 1% NaN_3 and store at 4°C.

A. 2 TC Buffer

1. Add 40 mL of ddH_2O to a 50mL-Falcon tube and 0.5 mL of Solution T. Mix well.
2. Adjust pH to 8.0 and complete 50 mL with ddH_2O.
3. Filter the buffer using 0.2μm membrane filters store at 4°C.

A. 3 10X FC Buffer

1. Mix 40 mL of ddH_2O with
   - 5 mL of Solution T
   - 1.86 g of KCl
   - 0.0206 g of $MgCl_2$
2. Adjust pH to 8.0 with and complete 50 mL with ddH_2O.
3. Filter the buffer using 0.2μm membrane filters and store at 4°C.

A. 4 General Actin Buffer (GAB)

1. Mix 485 μL of TC buffer, 10 μL of 10 mM ATP and 5 μL of 50 mM DTT.
2. Store at 4°C.

A. 5 Actin Polymerization Buffer (APB)

1. Mix 455 μL of FC buffer, 25 μL of 100 mM ATP and 20 μL of 50 mM DTT.
2. Store at 4°C.

A. 6 Biotin-actin Filaments Labeled with Phalloidin

Actin (Cytoskeleton, AKL99)
Biotinylated actin (Cytoskeleton, AB07)
Rhodamine Phalloidin (or Alexa-488 Phalloidin)

1. Reconstitute actin by adding 100 μL of ddH_2O to 1 mg vial of lyophilized actin. Mix well by pipetting up and down. The solution will have actin concentration of 10 mg/mL. Aliquot 5 μL into vials. Quick freeze the aliquots with liquid nitrogen and store -80°C.

2. Reconstitute biotin/actin by adding 20 μL of ddH_2O. The final concentration is 1mg/mL of biotin/actin. Aliquot into 5 μL vials. Quick freeze the aliquots with liquid nitrogen and store -80°C.
3. Thaw one vial of 10 mg/mL of pure actin and 1 vial of 1.0 mg/mL of biotinylated actin.
4. Prepare fresh GAB.
5. Mix the two actin vials. The ratio is 10:1 (actin:biotinylated actin) with a total actin concentration of 5.5 mg/mL (127.6 μM).
6. Add 90 μL of GAB and mix well by pipetting up and down in a gentle fashion. The solution is 100 μL with a concentration of actin is 0.55 mg/mL (12.8 μM). Mix well by pipetting up and down in a gentle fashion.
7. Place the actin on ice for several hours.
8. Prepare fresh APB.
9. Polymerize actin by adding 10 μL of APB to the actin solution. I like to add 2 μL of 66 μM of labeled phalloidin in order to help polymerization and stabilization of filaments. Mix well by pipetting up and down in a gentle fashion. Actin concentration: 0.435 mg/mL (10 μM).
10. Leave on ice in dark for 1 hour.
11. A concentration of ~20 nM is needed to visualize single filaments. First dilute actin 10 times by mixing 5 μL of 10 μM polymerized actin, 2 μL of 66 μM labeled phalloidin (unlabeled if using labeled monomers) and 90 μL of GAB/APB solution (9GAB:1APB). Further dilutions should be done using GAB/APB.
12. When stored in dark at 4°C, F-actin is stable for at least a couple days.

A. 7 Sodium Carbonate Buffer (0.1 M, pH 9.6)

1. Mix 0.79 g of Na_2CO_3 with 75 mL of ddH_2O. Stir for several minutes until all the solids are dissolved.
2. Mix 0.63 g of $NaHCO_3$ with 75 mL of ddH_2O. Stir for several minutes until all the solids are dissolved.
3. Add Na_2CO_3 to the $NaHCO_3$ solution until pH is ~9.6. The final concentration is 0.1M of sodium carbonate buffer.

A. 8 Sodium Phosphate Buffer (0.02 M, pH 4.5)

1. Mix 0.213 g of Na_2HPO_4 with 75 mL of ddH_2O. Stir for several minutes until all the solids are dissolved.
2. Mix 0.207 g of NaH_2PO_4 with 75 mL of ddH_2O. Stir for several minutes until all the solids are dissolved.
3. Add Na_2HPO_4 to the NaH_2PO_4 solution until pH is ~ 4.5. The final concentration is 0.02M of sodium phosphate buffer.

NOTE: When I prepared NaH_2PO_4, it is at a pH of ~ 4.8, so Na_2HPO_4 will not reduce the pH to 4.5. So I used 1 M HCl to adjust the pH to 4.5 and Na_2HPO_4 if overshoot the pH.

A. 9 Borate Buffer (0.1 M, pH 8.5, 100 mL)

1. Mix 0.618 g of boric acid (H_3BO_3) with 100 mL ddH_2O.
2. Adjust pH to 8.5 with 1 M NaOH.

A. 10 Solution A (0.1 M borate buffer pH 8.5, 0.1 mM $CaCl_2$, 0.1 mM ATP)

1. Prepare a solution of 100 mM $CaCl_2$ by mixing 0.147 g $CaCl_2$ with 10 mL ddH_2O.
2. Mix 10 µL of 100 mM ATP, 10 µL of 100 mM $CaCl_2$ and 10 mL of borate buffer.

A. 11 Solution B (20 mM sodium phosphate buffer pH 7.4, 150 mM NaCl, 10 mg/mL BSA, 0.1 mM $CaCl_2$, 0.1 mM ATP, 5% (v/v) glycerol, 0.1% (w/v) NaN_3)

20 mM sodium phosphate buffer pH 7.4	Glycerol	100 mM $CaCl_2$
20 mM Na_2HPO_4	BSA	100 mM ATP
NaCl	NaN_3	

1. Take 25 mL of 20 mM sodium phosphate buffer, pH 4.5 and adjust pH to 7.4 by adding 20 mM Na_2HPO_4. The volume required to raise the pH to 7.4 will be around 25 mL.
2. Mix 100 mg BSA, 0.5 mL glycerol, 0.01g NaN_3, 10 µL of 100 mM $CaCl_2$, 0.088g NaCl and 9.5 mL of 20 mM sodium phosphate buffer, pH 7.4.

NOTE: ATP will be added to the solution right before use.

A. 12 10X Solution C without ATP and DTT (25 mM imidazole-HCl pH 7.4, 250 mM KCl, 40 mM $MgCl_2$, 1 mM $CaCl_2$, , 0.4% (w/v) NaN_3)

Imidazole	HCl	KCl
$MgCl_2$	100 mM $CaCl_2$	NaN_3

1. Dissolve 680 mg imidazole with 10 mL of ddH_2O for a 1M imidazole solution.
2. Dilute 2.5 mL of 1 M imidazole with 97.5 mL of ddH_20 to obtain 25 mM imidazole solution.
3. Dissolve the following quantities in 10 mL of 25 mM imidazole:
   - 186 mg KCl
   - 81 mg $MgCl_2$
   - 40 mg NaN_3
   - 0.1 mL of 100 mM $CaCl_2$

NOTE: This buffer is required only when the gelsolin-coated beads are mixed with actin filaments. ATP and DTT will be added right before mixing beads with actin filaments.

A. 13 Preparation of Bead Coated with Gelsolin

(Source: Suzuki et al, *Biophys J* 70:401-408 (1996))

2.5% carboxylated microspheres	Sodium carbonate buffer	Sodium phosphate buffer
0.25 M ethanolamine	Solution A	Solution B without ATP
EDC(1-Ethyl-3-[3-dimethylaminopropyl]carbodiimide Hydrochloride)		

1. Place 0.5 mL of 2.5% carboxylated microspheres in an eppendorf centrifuge tube and add 0.5 mL of sodium carbonate buffer.
2. Wash beads 4 times by centrifugation for 5 minutes at 10,000 rpm. After each wash, resuspend by filling half way with sodium carbonate buffer, then vortex, and finally fill the tube with buffer.
3. After last wash, resuspend beads by adding 1 mL of sodium phosphate buffer.
4. Wash 4 times as specified in step 2, but using sodium phosphate buffer.
5. After last wash, resuspend beads with 0.625 mL of sodium phosphate buffer and sonicate for 30 seconds (25% on cup sonicator).
6. Dissolve 20 mg of EDC with 1 mL of sodium phosphate buffer (2% w/v) and add 0.625mL of this solution to the bead suspension. EDC solution should be prepared within 15minutes prior to use.
7. Mix continuously and gently for 3.5 hours at room temperature. Prepare borate buffer and solution A while waiting for incubation.
8. Centrifuge for 7 minutes at 10,000 rpm, and remove supernatant.
9. Resuspend pellet with 1.25 mL of 0.1 M borate buffer and wash beads 4 times (5 minutes at 10,000 rpm) resuspending each time with borate buffer.
10. After last wash, resuspend beads in 0.7 mL of solution A and sonicate for 30 seconds (25% on cup sonicator).
11. Use 0.5 mL of solution A to dissolve 260 μg of BSA, 40 μg of Alexa-labeled BSA, 50μg of G-actin, and 50 μg of gelsolin (400 μg total of proteins).
    a. Protein mix: 5 μL of 10 mg/mL actin, 10 μL of 5 mg/mL gelsolin, 26 μL of 10mg/mL BSA and 40 μL of 1 mg/mL rhodamine-BSA (total 400 μg of protein).
12. Add protein solution to bead solution and mix continuously and gently for 8-10 hours at room temperature in dark.
13. Stop the reaction by adding 50 μL of 0.25 M ethanolamine, and mix gently for 30 minutes at room temperature in dark.
    a. Mix 20 μL of ethalonamine with 1.3 mL of borate buffer to obtain 0.25 M ethalonamine.
14. Centrifuge bead solution for 7 minutes at 10,000 rpm, and resuspend in 1.2 mL of 10mg/mL of BSA in solution A.
    a. Prepare more solution A
    b. Mix 50 mg of BSA with 5 mL of fresh solution A.
15. Sonicate for 30 seconds (25% on cup sonicator), and mix gently for 30 minutes.
16. Wash beads 3 times at 10,000 rpm using 10mg/mL BSA in solution A. During washing, prepare solution B.
17. After last wash, resuspend beads in 1 mL of solution B.
    a. Add 1 mL of solution bead to bead pellet and vortex.
    b. Add 10 μL of 10 mM ATP.
18. Store at 0°C in dark. The coated beads are usable for about 6 months.

A. 14 Attaching Actin Filaments to Gelsolin-coated Beads

(Source: Suzuki et al, *Biophys J* 70:401-408 (1996))

1. Mix 0.1 mL of gelsolin-coated beads stock with 0.1 mL of solution C.
   a. Mix 20 μL of 50 mM DTT, 10 μL of 10 mM ATP, 100 μL of 10X solution C and 870 μL of imidazole pH 7.4.
2. Sonicate for 30 seconds (25% in cup sonicator).
3. Wash beads four times at 6,000 rpm for 4 minutes, and resuspend after each wash with 0.2 mL of solution C except for last wash.
4. Sonicate for 30 seconds (40% in cup sonicator).
5. After last wash resuspend beads in 40 μL of solution C and 5 μL of 10 μM of F-actin labeled with fluorescent dye.
6. Mix gently and incubate overnight at 0°C in the dark.
7. Dilute the suspension 1:50 with 2 mg/mL of BSA in solution C.
8. Incubate for more than 2 hours at 0°C in dark.

A. 15 Preparation of PEG-coated Microsphere

1. Make your own buffer and filter it (0.2 um Durapore membrane).
2. Measure 1mg of PLL-PEG and warm it up at room temperature.
3. Dissolve it in 1ml of your buffer (from step1), so that your final concentration is 1mg/mL. Vortex and filter it again (0.22 um).
4. Make aliquot the solution and store it at -20°C.
5. Dilute the concentration of your beads to be 5mg/mL.
6. Mix same volume of carboxylated-beads and PLL-PEG solution at room temperature for 30 minutes. (I usually use 100 uL of each).
7. Centrifuge the solution at x2000g for 15min (small centrifuge) from step 6 and resuspend the beads pellet with 50 uL of your buffer from step 1.
8. You can keep the beads in 4°C and they should be good for a week.

A. 16 SDS-page for Actin

1. Dilute actin in fresh G-buffer (final concentration: 20μM, 100uL) overnight on ice.
2. Polymerize 50ul of 20uM actin (final concentration: 10uM in 100ul) by adding 10ul 10x buffer (200 mM Tris-HCl, No KCl, 1000mM NaCl, 20 mM $MgCl_2$, 2 mM DTT, 5 mM ATP, 0.1% (w/v) NaN_3, pH 7.5) + water (40ul)
   Note that NaCl is used instead KCl.
   For G-actin (control), dilute 20uM actin to 10uM with G-buffer (final volume 100ul).
3. For F-actin, let them polymerize for a couple hours in room temperature. For G-actin, keep the G-actin on ice.
4. Centrifuge at 300K (or 100K if a lot of actin from G-actin sample goes to pellet at 300K) for 40min at 4C.
5. Take a 100ul supernatant and mix with 50ul of 3x SDS sample buffer in to a 0.5~0.65ml small tube.

6. Add 150ul 1x SDS sample buffer to the pellet, too. Carefully (pellet is sticking at the bottom of the tube) solubilize the pellet with pipette and transfer the entire solution to a 0.5~0.65ml small tube.
7. Heat the samples (both pellet and sup) at 95C for 5min.
8. Cool down the vial at room temperature for 2min, centrifuge briefly, vortex, and then centrifuge briefly.
9. Load 10ul of the samples (both supernatant and pellet) to an SDS-PAGE gel.

A. 17 Negative Staining of Actin Filaments

2% Uranyl Acetate	1X polymerization buffer	Parafilm
Filter paper	Glow-discharged EM grid	

1. On a piece of parafilm, place a couple drops of 20nM polymerized actin in 1X buffer solution.
2. Put one glow-discharged EM grid on top of actin.
3. Wick away excess actin with wedges of filter paper.
4. Place a couple drops of 1X buffer on a piece of parafilm for washing.
5. Put the sample on top of 1X buffer solution.
6. Wick away excess solution with wedges of filter paper.
7. Prepare a couple drop of 2% Uranyl Acetate on a piece of parafilm for staining.
8. Put the sample on top of the staining solution.
9. After ~30s staining, dry grid by wicking away excess solution with wedges of filter paper.